

TECTONIC HISTORY OF THE PROTEROZOIC BASEMENT OF THE
SOUTHERN SANGRE DE CRISTO MOUNTAINS, NEW MEXICO

By
Erwin Adriaan Melis

Department of Earth and Environmental Science
New Mexico Institute of Mining and Technology
Socorro, New Mexico

THESIS
Submitted in Partial Fulfillment of the
Requirements for the Degree of
Masters of Science in Geology

May 2001

“... things are done when Men and Mountains meet”
William Blake (Notebook 1792-1799)

ABSTRACT

The southern Sangre de Cristo Mountains are a N-S elongate uplift underlain by Proterozoic basement and flanking the Rio Grande Rift east of Santa Fe, New Mexico. Mississippian sedimentary rocks unconformably overlie a ca. 1.72 Ga ductily deformed and metamorphosed Proterozoic back arc sequence which retains a partial record of deformation, metamorphism, burial, and uplift from the Proterozoic to the Early Cenozoic. This history has been documented through mapping, structural analysis, and $^{40}\text{Ar}/^{39}\text{Ar}$ thermochronology.

Rock types in the Proterozoic basement include the 1720 Ma Jones Rhyolite Complex, a metavolcanic and metasedimentary sequence, which was intruded by the broadly contemporaneous Windy Bridge tonalite. At 1650 Ma the Indian Creek granite intruded the Windy Bridge tonalite. An isoclinally folded S_1 preserved only in the Windy Bridge tonalite, but not in the Indian Creek granite, suggests that D_1 occurred prior to the Indian Creek granite intrusion and could be related to the Mazatzal orogeny. At 1480 Ma the Macho Creek granite intruded the Jones Rhyolite Complex. It has no magmatic foliation, but locally possesses a mylonitic foliation (S_2). S_2 partially transposes S_1 in the Windy Bridge tonalite, whereas the Jones Rhyolite Complex and the Indian Creek granite solely contain S_2 . Microstructures found in all rock types suggest similar amphibolite grade metamorphic conditions and consistently record dextral strike-slip with a

component of normal south-side-down shearing on an ENE-striking foliation. The age of S_2 is constrained to be between ca. 1480 Ma, the age of crystallization of the locally mylonitized Macho Creek granite, and 1372 Ma, the mean of $^{40}\text{Ar}/^{39}\text{Ar}$ cooling ages of largely post-mylonitic hornblende in the Windy Bridge tonalite. Mineral compositions of feldspar and hornblende in the Windy Bridge tonalite also suggest amphibolite facies metamorphism, which locally outlasted D_2 . Local evidence of retrogression to greenschist facies during D_2 is interpreted to indicate that continued deformation during cooling was locally facilitated by the availability of water. Kinematic indicators argue that D_2 in the study area was a result of transtension, rather than extension or contraction as has been previously suggested.

Following ~1400 Ma ductile deformation, the Proterozoic basement cooled to ~350°C by 1343 Ma at a rate of ~5°C/Ma. After 1343 Ma the basement experienced brittle deformation, metasomatic events, and gradual cooling. Metasomatism in the Windy Bridge tonalite is mostly localized in breccia zones but locally diachronous. The breccia zones are tabular, parallel to the N-NNE striking faults in the area and are interpreted as fault zones; the first precisely dated Proterozoic fault zones at ~800 Ma. One metasomatic event could be associated with the Grenville Orogeny at ~1050 Ma. Brecciation and renewed metasomatism at ~800 Ma as well as accelerated cooling recorded by all samples could be associated with the breakup of Rodinia.

Thermochronologic data indicate that rocks east and west of extensive N-NNE striking faults in the Proterozoic basement had very similar cooling histories from the Proterozoic through the Paleozoic. This suggests that these faults, including the Picuris-Pecos fault, did not accommodate significant dip-slip motion during the Proterozoic.

Dip-slip displacement is constrained by field relations to be post-Carboniferous in age. A previously unidentified north-striking fault within the Pecos River valley displaced Paleozoic strata across the valley as much as 200 m (west-side-down offset). Slow, steady cooling during the Paleozoic implies that the hotter samples remained at elevated temperatures through the Siluro-Devonian and cooled quickly prior to uplift in the Mississippian. K-feldspar samples record no argon loss during Ancestral Rocky Mountain deformation, indicating maximum depths of burial of ~4-5 km at that time. $^{40}\text{Ar}/^{39}\text{Ar}$ thermochronology suggests renewed burial of ~4-5 km during the Mesozoic before rapid uplift at ~70 Ma during the Laramide orogeny.

ACKNOWLEDGEMENTS

First and foremost I would like to thank Laurel Goodwin for scientific guidance, for making me a believer in my own findings, and most important for her editing skills, which were immensely helpful. Paul Bauer I thank for suggesting the project, and STATEMAP funding through the New Mexico Bureau of Mines and Mineral Resources. I thank Matt Heizler for his clear, speedy advice and in keeping me on track. Thanks to Steve Ralser and Andy Campbell for answering the errant questions. I thank Scott Johnson for his understanding and sharing his office space. The New Mexico Geochronology Laboratory staff provided hours of patient help, supplies, and research assistance. I thank Lane Andress for good fieldwork.

During the 1998 field season the following landowners allowed me access to canyons, and critical river outcrops. They are Scottie and the staff of the Brush Ranch Camps, Mr. Shannon, and Eddie Salazar of the Tres Lagunas community. The mapping project benefited from discussions with Paul Bauer and Steve Ralser. Financial support came through a grant from the United States Geological Survey's Educational Mapping Program (EDMAP-Summer 1998) awarded to Laurel Goodwin. Support also came from the New Mexico Tech Graduate Office and the New Mexico Geological Society.

I thank Wendy Melis and Eric Rondeau for their candid advice and their interest in this project. I thank my housemates, Thag, Geff, Peter, and Erik for the countless hours

of discussion and the comradery. Jessie Crain, Kathleen Wright and Chris Gerbi gave their precious time as pinch proofreaders. I thank Walter for the good ride, and superdawg Suske for her loyalty and for making fieldwork fun. Last but not least, I thank my parents for the financial support, and even though thousands of miles away provided the support I needed to see this project to its fruition and ultimate completion. This thesis is dedicated to them.

TABLE OF CONTENTS

	Page
List of Figures	vi
List of Tables	viii
List of Appendices	ix
List of Plates	x

METAMORPHISM AND DEFORMATION OF PROTEROZOIC ROCKS IN THE 7.5 MINUTE ROSILLA PEAK QUADRANGLE, SOUTHERN SANGRE DE CRISTO MOUNTAINS, NORTHERN NEW MEXICO

I.	Introduction	2
II.	Background geology	6
III.	Methods.....	11
	A. Kinematic analysis, and evaluation of metamorphic grade	11
	B. Analytical procedure: geochronology	14
	C. Analytical procedure: electron microprobe	16
IV.	Structure and microstructure in Proterozoic rocks of the Rosilla Peak quadrangle	16
V.	Metamorphism.....	30
VI.	⁴⁰ Ar/ ³⁹ Ar Age spectrum results and discussion	34
VII.	Summary and Discussion	43
VIII.	Conclusions	48

**⁴⁰AR/³⁹AR K-FELDSPAR THERMOCHRONOLOGIC CONSTRAINTS ON THE
BRITTLE TECTONIC AND UPLIFT HISTORY OF THE SOUTHERN SANGRE
DE CRISTO MOUNTAINS, NORTHERN NEW MEXICO SINCE 1100 MA**

IX.	Introduction	52
X.	Geologic setting.....	55
	A. Proterozoic	55
	B. Cambrian to Mississippian	57
	C. Latest Mississippian to Early Permian	57
	D. Late Cretaceous to Tertiary	58
XI.	Methods	61
	A. Sample preparation	61
	B. Analytical procedure: electron microprobe & staining	62
	C. Analytical procedure: geochronology	63
XII.	Brittle deformation and associated metasomatism	64
	A. Faulting and Brecciation	64
	B. Metasomatism	69
XIII.	K-feldspar thermochronology	71
	A. Multi-Diffusion Domain theory	71
	B. Sample descriptions	74
	C. Age spectra & argon kinetic parameter determination	77
	1. Age Spectra	77
	2. Determining the kinetic parameters	81
	D. Thermal History	86
XIV.	Discussion	90
	A. Thermal histories	90
	B. Timing of faulting, brecciation and metasomatism	95
XV.	Conclusions	96
	Combined references	99
	Appendices	108

LIST OF FIGURES

		Page
Figure 1	Proterozoic exposures in New Mexico.....	3
Figure 2	Proterozoic geologic map of the Rosilla Peak 7.5 minute quadrangle	8-9
Figure 3	Typical foliations of all major rock types	17
Figure 4	Photomicrographs of microstructures in rocks of the Jones Rhyolite Complex	19
Figure 5	Foliations plotted on equal area net plots	22
Figure 6	Photomicrographs of microstructures in Windy Bridge tonalite	23
Figure 7	Photomicrograph of microstructures in Macho Creek granite	28
Figure 8	Age spectra of amphiboles from the Windy Bridge tonalite	37
Figure 9	Age spectra of phyllosilicates	40
Figure 10	Proterozoic tectonic history of southern North America	49
Figure 11	Map of north-central New Mexico including Proterozoic basement uplifts	53
Figure 12	Proterozoic geologic map of the Rosilla Peak 7.5 minute quadrangle with a cross-section	59-60
Figure 13	Photo of a tabular breccia ridge parallel to the Picuris-Pecos fault	67
Figure 14	Photo of Windy Bridge tonalite breccia	68

Figure 15	Slabs of K-feldspar altered Windy Bridge tonalite stained with sodium cobaltinitrate.....	70
Figure 16	BSE microprobe images of altered feldspar	72
Figure 17	K-feldspar age spectra and modeled age spectra	78
Figure 18	Corrected isothermal age steps	79
Figure 19	Arrhenius and $\log r/r_0$ plots for K-feldspar step-heating data	82
Figure 20	Cooling histories for samples from three tectonic blocks	88
Figure 21	Summary of the Phanerozoic cooling history of part of the southern Sangre de Cristo Mountains, north-central New Mexico	97

LIST OF TABLES

	Page
Table 1	Compilation of Proterozoic ages from Rosilla Peak
	7.5 minute quadrangle 10
Table 2	Windy Bridge tonalite mylonite amphibole compositions 31
Table 3	Windy Bridge tonalite mylonite feldspar compositions 33
Table 4	K-feldspar sample locations and descriptions 75
Table 5	K-feldspar kinetics and domain size distribution data84-85

LIST OF APPENDICES

	Page
APPENDIX A: Thin section descriptions	108
APPENDIX B: $^{40}\text{Ar}/^{39}\text{Ar}$ data	124

LIST OF PLATES

Page

PLATE 1: Geologic map of part of the
Rosilla Peak Quadrangle in pocket

**METAMORPHISM AND DEFORMATION OF PROTEROZOIC ROCKS IN
THE 7.5 MINUTE ROSILLA PEAK QUADRANGLE, SOUTHERN SANGRE DE
CRISTO MOUNTAINS, NORTHERN NEW MEXICO**

I. INTRODUCTION

Deformed Proterozoic rocks in New Mexico yield U/Pb crystallization ages that range from 1765 to 1400 Ma (Condie, 1982; Reed et al., 1987). Beginning at 1720 Ma, the oldest of these rocks accreted as multiple arc terranes to the Archean Wyoming province causing crustal thickening, manifest in widespread metamorphic assemblages and deformational fabrics in rocks older than 1650 Ma (Bowring and Karlstrom, 1990). A 1.4 Ga tectonic event caused renewed metamorphism and deformation, which in New Mexico overprinted the older fabrics and metamorphic minerals. The regional importance of 1.4 Ga metamorphism and deformation has been demonstrated (e. g. Williams and Karlstrom, 1996; Lanzirotti et al., 1996; Marcoline et al., 2000), however the nature, extent of deformation, and magnitude of overprinting at 1.4 Ga remains controversial (e.g., Williams et al., 1999a).

In the last two decades, two conceptual models have been developed to explain Proterozoic deformation and metamorphism in New Mexico. The most widely accepted model suggests that the dominant structures and mineral assemblages record the ca. 1650 Ma Mazatzal Orogeny (e.g., Pedrick et al., 1998; Read et al., 1999). In this model, plutonism at 1.4 Ga was associated with regional metamorphism, but fabrics developed during contraction were confined to the margins of syntectonic plutons (e.g., Nyman et al., 1994). The timing of Mazatzal-age deformation has been constrained largely by evaluating the timing and development of foliations relative to intrusion of precisely dated granitoids (cf. Paterson et al., 1989). The timing of initial deformation is arguably best constrained in the Magdalena and San Andres Mountains (Figure 1). In the

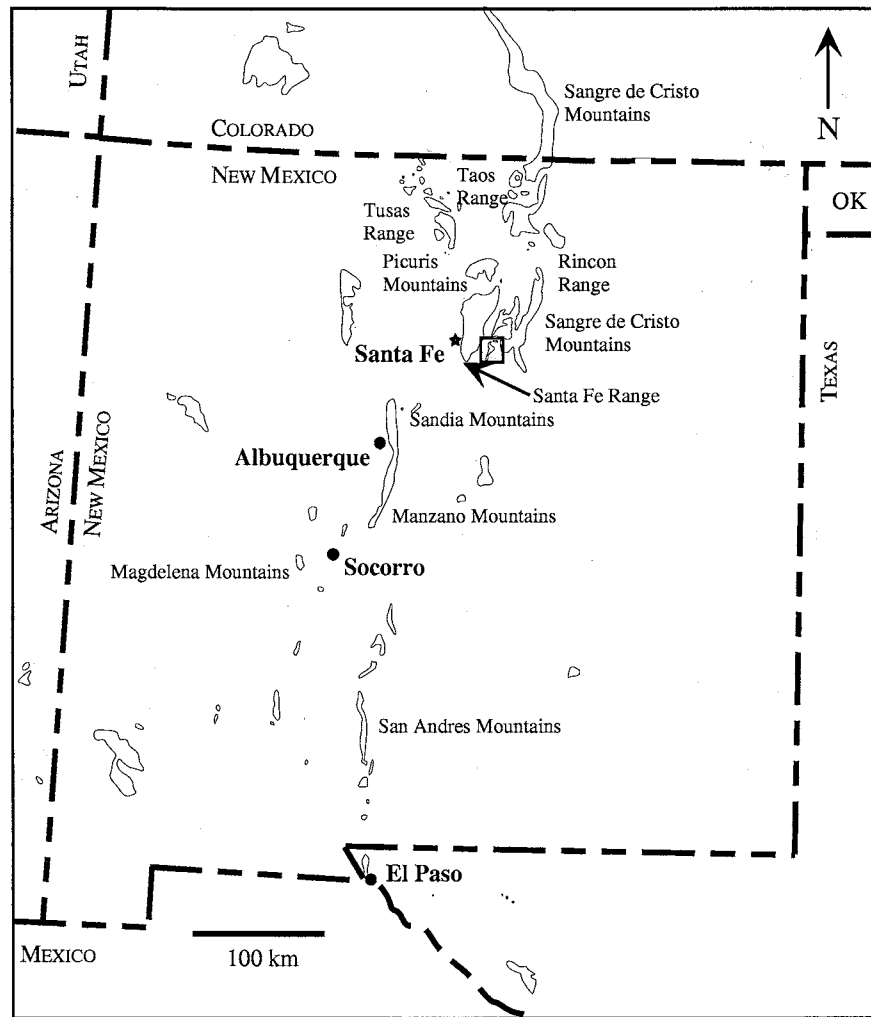


Figure 1. State map of New Mexico with outlines of the mountain ranges that mostly include Proterozoic rocks. Study area is highlighted in yellow. Compiled after map by Bauer and Pollock (1993).

Magdalena Mountains, crosscutting relationships and U/Pb zircon ages of undeformed plutons were used to date a regional NE-striking foliation and associated upper greenschist – lower amphibolite facies metamorphism at 1664 to 1654 Ma (Bauer and Williams, 1994). Similar techniques were used to constrain the ages of folded NE- and NW-striking foliation and associated upper greenschist – lower amphibolite facies metamorphic minerals to between 1650 to 1630 Ma in the San Andres Mountains (Vollbrecht, 1997). In both of these cases, the quality of the age determinations depends on the accuracy of the interpreted timing of intrusion relative to deformation and metamorphism.

The kinematics of ca. 1650 Ma shear zones vary. Deformation has been generally interpreted to be characterized by north-directed thrusting within accreted terranes from the Cheyenne Belt south to New Mexico (Karlstrom and Houston, 1984; Grambling et al., 1988). However, recent documentation of strike-slip shear in New Mexico suggests that the accretionary process may not have involved solely thrusting. Structures in the San Andres Mountains and the Ladron Mountains record strike-slip shear and transpression, respectively (Pollock, 1994; Vollbrecht, 1997), consistent with structures of similar age in northern Colorado (Selverstone et al., 1997), provoking questions about the nature of the Mazatzal Orogeny in New Mexico.

$^{40}\text{Ar}/^{39}\text{Ar}$ ages record the time at which metamorphic minerals either crystallized or cooled below their closure temperature (T_c). In New Mexico, 1.4 Ga $^{40}\text{Ar}/^{39}\text{Ar}$ ages of hornblende and micas have been used as evidence of crustal reheating without regional deformation (Karlstrom et al., 1997; Pedrick et al., 1998; Read et al., 1999). This interpretation is based on two fundamental assumptions. The first is that 1.4 Ga

deformation was confined to pluton margins and the second is that $^{40}\text{Ar}/^{39}\text{Ar}$ ages of minerals that grew at ca. 1650 Ma were reset during 1.4 Ga metamorphism. In contrast, 1.4 Ga $^{40}\text{Ar}/^{39}\text{Ar}$ ages in the Manzano Mountains (Figure 1) have been interpreted to date amphibolite facies metamorphism and associated regional deformation (Marcoline, 1996). Microstructural analysis and in situ U-Pb dating of monazite have been utilized to discriminate between these hypotheses in a few key areas (Williams et al., 1999b). Monazites aligned with the regional foliation (S_2) yield ages of 1410 Ma in the southern Tusas Mountains (Williams et al., 1999b). This foliation was originally thought to have formed at 1650 Ma (Williams, 1991). Other metamorphic minerals in northern New Mexico, such as staurolite and garnet, yield U-Pb ages of ca. 1455 Ma (Lanzirotti et al., 1996; Lanzirotti and Hanson, 1997). These data lend support to the second conceptual model, which suggests that 1.4 Ga plutonism and metamorphism were associated with regional deformation and extensively overprinted structural and metamorphic evidence of the ca. 1650 Ma Mazatzal event. This model is supported by the observation that microstructures within rocks of the Manzano Mountains do not show evidence of annealing as they would if they had formed at ca. 1650 Ma and experienced prolonged residency in the middle crust and reheating at 1400 Ma (Ralser, 2000). Both regional extension (Grambling et al., 1988; 1989) and contraction (Nyman et al., 1994) have been proposed to have occurred at 1.4 Ga in northern New Mexico, underscoring our lack of understanding about the processes and nature of tectonism.

Proterozoic rocks exposed east of the Neogene Rio Grande rift in the southern Sangre de Cristo Mountains (Figure 1) are typical of rocks in northern New Mexico in that they have been multiply deformed (e.g., Grambling and Coddling, 1982). The research

reported in this paper focused on an evaluation of the character and age of structures within the Pecos Complex, an area of the southern Sangre de Cristo Mountains not previously addressed by detailed metamorphic and structural studies. This area is particularly appropriate for evaluating the relative impact of ca. 1650 Ma versus 1.4 Ga events as it contains three plutons with U/Pb crystallization ages between 1720 ± 15 Ma and ca. 1480 Ma (Bowring and Condie, 1982). $^{40}\text{Ar}/^{39}\text{Ar}$ step heating of syntectonic metamorphic minerals was used along with mapping, field structural analysis, microstructural analysis and the study of co-existing mineral phases to establish the timing and grade of metamorphism and the timing, extent and character of deformation. I have found that amphibolite facies metamorphism, locally followed by retrogression to greenschist facies, occurred during the period ca. 1480 - 1370 Ma. Metamorphism was accompanied by dextral strike-slip with a component of normal, south-side-down shearing on an E-striking foliation. Structures developed during this deformation extensively overprinted older, presumably ca. 1650 Ma structures.

II. BACKGROUND GEOLOGY

Proterozoic rocks of northern New Mexico are exposed in mountain ranges flanking the Neogene Rio Grande rift. East of Santa Fe, the southern Sangre de Cristo Mountains include the Pecos Complex, exposed in the Rosilla Peak 7.5-minute quadrangle (Figure 1). The Pecos Complex, one of the oldest bimodal volcanic-sedimentary sequences in New Mexico, includes amphibolites, quartz-mica schists, and deformed metasedimentary/metavolcanic rocks (Robertson and Moench, 1979; Robertson

and Condie, 1989; Robertson et al., 1993). Geochemically, the mafic rocks have a back-arc signature, whereas the felsic igneous rocks have an arc signature (Robertson and Condie, 1989). In the Rosilla Peak quadrangle, the Pecos Complex was intruded by three granitoids (Figure 2). U/Pb ages were initially reported by Bowring and Condie (1982), who interpreted them to record volcanism and contemporaneous plutonism both at 1720 ± 15 Ma and ca. 1650 Ma (for all ages see Table 1). The foliated 1718 ± 5 Ma (U-Pb zircon; reported in Robertson and Condie, 1989) Windy Bridge tonalite was intruded by the largely nonfoliated ca. 1650 Ma (no reported uncertainty) Indian Creek granite (U-Pb zircon; Bowring and Condie, 1982). The megacrystic ca. 1480 Ma (no reported uncertainty) Macho Creek granite intruded the 1720 ± 15 Ma Jones Rhyolite Complex (U-Pb zircon; both reported in Robertson and Condie, 1989). Model lead ages of metavolcanic ore-bearing rocks along the Pecos River just west of Tres Lagunas are ca. 1720 Ma (no reported uncertainty), as are ages of rocks from the Jones mine (Stacey et al., 1976). Rocks from the southern Sangre de Cristo Mountains have $^{40}\text{Ar}/^{39}\text{Ar}$ ages of 1422 – 1393 Ma for hornblende and 1337 Ma for muscovite (Karlstrom et al., 1997).

The only detailed structural investigation in this area was performed north of the Pecos Complex. There, rocks of the Pecos Complex overlie younger Proterozoic sedimentary rocks of the Hondo and Vadito groups along the Pecos thrust (Grambling and Ward, 1987). The Hondo and Vadito group rocks experienced three deformation events (Grambling and Coddling, 1982). Rootless isoclinal folds with axial planes dip to the south, parallel to the regional foliation (S_1). S_1 was deformed into open folds with axial planes parallel to S_2 , which also dips to the south, albeit steeper than S_1 . Grambling and Coddling (1982) concluded that F_1 and F_2 were coaxial and could have developed

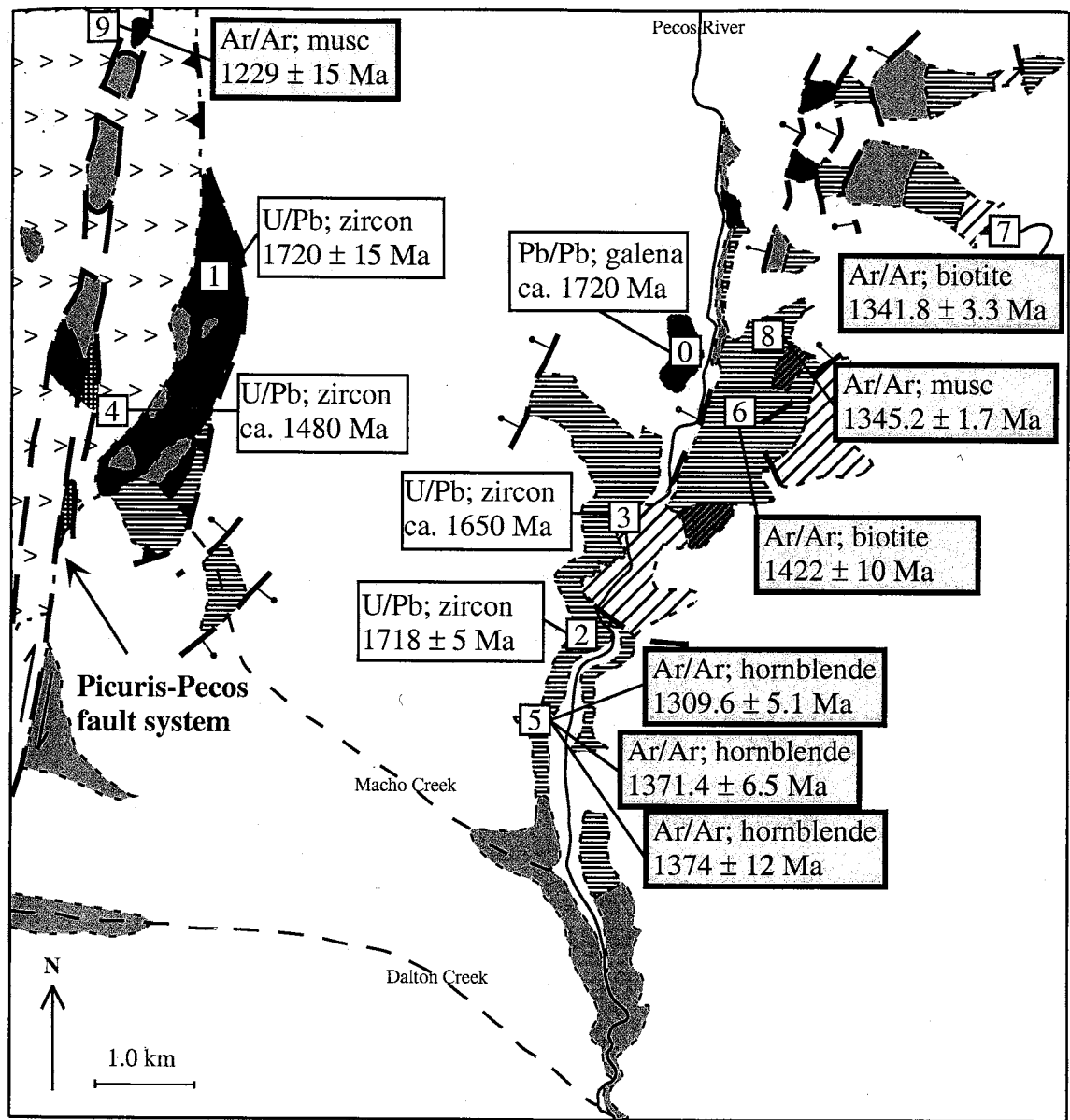


Figure 2. Proterozoic bedrock geologic map of part of the Rosilla Peak 7.5 minute quadrangle, San Miguel and Santa Fe counties. Numbers in squares refer to ages mentioned in the text (compiled and referenced in Table 1).

Explanation

Paleozoic



Undifferentiated



Madera limestone

Proterozoic



Macho Creek granite



Pecos granodiorite



Indian Creek granite



Windy Bridge tonalite

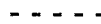
Pecos
Complex



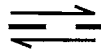
Jones Rhyolite Complex
amphibolite



Jones Rhyolite Complex
metasedimentary and metavolcanic rocks



Lithologic contact, dashed where
inferred



Fault, dashed where inferred



Strike-slip component of movement
shown with arrow. Normal compo-
nent of motion indicated by bar and
ball on the hanging wall

Figure 2 (continued). Explanation of map units.

Table 1. Compilation of Proterozoic ages from the Rosilla Peak 7.5 minute quadrangle

No.	Age Ma	Method	mineral	age type	Tc °C	grain size µm	rock - map unit	Sample #/ location	type	UTM	approx. elevation m	Ref.
0	1720	Pb-Pb	galena	model 207/206	?	-	Tres Lagunas metavolcanic/JRC	MA-25/RP-86	felsic metavolcanic	3952539	2330	a
1	1720 ± 15	U/Pb	zircon	concordia	700	-	Jones Rhyolite Complex	PR-1	qtz-eye porphyry	3954417	2800	b
2	1718 ± 5	U/Pb	zircon	concordia	700	-	Windy Bridge tonalite	WB-6	coarse tonalite	3950693	2310	c
3	1650	U/Pb	zircon	?	700	-	granite	WB-6	granite	3951200	2290	d
3	1650	U/Pb	zircon	concordia	700	-	Indian Creek granite	WB-6	granite	3951153	2292	e
4	1480	U/Pb	zircon	concordia	700	-	Macho Creek granite	RP-70	megacrystic granite	3951743	2545	e
5	1374 ± 12	Ar/Ar	hornblende	plateau	500	700	Windy Bridge tonalite	WB-23	tonalite	3949400	2260	this study
5	1371.4 ± 6.5	Ar/Ar	hornblende	plateau	500	200	Foliated enclave in tonalite	WB-15B	amph. enclave in ton.	3949900	2290	this study
5	1309.6 ± 5.1	Ar/Ar	hornblende	plateau	500	200	Windy Bridge tonalite	WB-10	mafic layer in tonalite	3949300	2270	this study
6	1422 ± 10	Ar/Ar	biotite	plateau	<300	200	Windy Bridge tonalite	RP-36B	fol. tonalite	3952400	2410	this study
7	1341.8 ± 3.3	Ar/Ar	biotite	plateau	<300	250	Pecos GD	RP-28B	Pecos GD	3953850	2710	this study
8	1345.2 ± 1.7	Ar/Ar	muscovite	plateau	350	1500	Windy Bridge tonalite	RP-34	pegmatite	3953100	2633	this study
9	1229 ± 15	Ar/Ar	muscovite	plateau	350	500	Macho Creek granite	RP-87	MC gneiss	3955900	2830	this study

References:

- general Bauer, P. W., and Pollock, T. R., 1992. Compilation of Precambrian isotopic ages in New Mexico, NM Bureau of Mines and Mineral Resources, Open-file Report 389, 130 pgs.
- a Stacey et al. (1977)
- b Bowring (personal communication, 1987) in Robertson and Condie (1989)
- c Bowring and Condie (1982) quoted in Robertson and Condie (1989)
- d Silver unpublished data in Stacey et al. (1977)
- e Bowring (personal communication, 1984) in Robertson and Condie (1989).

during continuous north-directed thrusting. S_3 is a variably developed weak crenulation cleavage. In the southern Picuris Mountains to the north of the study area (Figure 1), the same S_3 (Grambling, 1979) is well developed, dips steeply to the south, and has been U/Pb dated at ca. 1450 Ma using electron microprobe in-situ monazite and isotopic dating of garnet and staurolite (Wingsted et al., 1996; Lanzirotti and Hanson, 1997; Williams et al., 1999a). The grade of metamorphism in the Santa Fe Range, west of the Pecos Complex was first constrained by the coexistence of garnet and biotite and the absence of staurolite. These coexisting minerals were used to estimate metamorphic conditions at 525°C and 4 kbar (Fulp, 1982). Daniel (1995) used new thermobarometric constraints to revise this estimate to 600 - 680°C and 5 - 6 kbar.

III. METHODS

A. Kinematic analysis and evaluation of metamorphic grade

Over 100 samples were collected from the study area, of which 52 were chosen for petrographic analysis. Samples collected were oriented, facilitating later reconstruction of the kinematic framework. Where both a foliation and lineation were evident in the field, samples were cut perpendicular to the foliation and parallel to the lineation. Selected samples were also cut at a high angle to the lineation to determine relative components of coaxial and noncoaxial deformation and whether or not the lineation accurately tracked the transport direction, as well as to evaluate shear sense. These goals were accomplished by evaluating the asymmetry of the fabric (fabrics produced by coaxial flow are symmetrical) and whether or not the maximum asymmetry

is evident in sections cut parallel to the lineation, which is expected if the lineation records the transport direction (e.g., Goodwin and Williams, 1996; Tikoff and Greene, 1997).

Metamorphic grade was estimated by evaluating stable mineral assemblages, determining the chemistry of coexisting minerals, and evaluating microstructures indicative of metamorphic grade. For example, the calcium content of plagioclase feldspar and the aluminum content of amphibole have been used to delineate the boundary between the greenschist and the amphibolite facies in basic rocks and granitoids (e.g., Apter and Liou, 1983; Anderson, 1983). Albite is characteristic of the greenschist facies, and becomes more calcic with increasing metamorphic grade. At the boundary between the greenschist and amphibolite facies, albite and oligoclase coexist, whereas in the amphibolite facies the sole plagioclase is oligoclase (Crawford, 1966). The existence of the peristerite gap ($An_3 - An_{18}$) prevents the formation of plagioclase feldspar of intermediate compositions between albite and oligoclase (e.g., Spear, 1993).

The dominant microstructures in feldspar and quartz were used to estimate the temperature during deformation (cf. Boullier and Bouchez, 1978; Simpson, 1985; Hirth and Tullis, 1992). Although strain rate, water content, and temperature all influence the microstructures found in these minerals (e.g., Lister et al., 1978), temperature is the most regionally consistent variable. High strain rates favors grain size reduction, whereas water content makes rocks weaker; both are generally more important locally. K-feldspar commonly displays undulose extinction and elongate, fractured 'bookshelf' subgrains at lower greenschist facies temperatures (300 – 400°C; Pryer, 1993). Deformation typically occurs by fracturing at these conditions. At temperatures of 400 – 500°C feldspars

recrystallize, forming 'neocrystals' along grain boundaries, resulting in core and mantle structures (White, 1976). Linear arrays of recrystallized grains may also traverse larger porphyroclasts in micro-shear zones (Passchier and Trouw, 1996), and deformation twins and myrmekites are ubiquitous in K-feldspar at these conditions (Pryer, 1993). At amphibolite facies and above, deformed plagioclase grains are typically strain-free and of uniform size (Passchier and Trouw, 1996). A shape-preferred orientation (SPO) of feldspar grains is common at metamorphic conditions above 500°C. Myrmekites are very common in K-feldspars in the amphibolite facies (Simpson and Wintsch, 1989; Vernon, 1991).

The use of microstructures in quartz to estimate temperatures during deformation has increased since Boullier and Bouchez introduced the concept in 1978. Work by Hirth and Tullis (1992) clarified the effect of temperature on quartz microstructures through the identification of particular dislocation creep regimes. Quartz forms well-defined monocrystalline ribbons at lower greenschist facies temperatures (<350°C). At higher temperatures (350 – 400°C), deformation bands within quartz grains are visible. These deformation bands lead to subgrain formation and are recognized as a Type 1 quartz microstructure (Boullier and Bouchez, 1978). At temperatures between 400°C and 500°C (mid-upper greenschist facies) quartz forms flattened, relatively strain-free new grains (Type 2; Boullier and Bouchez, 1978; Hirth and Tullis, 1992). At temperatures typical of the amphibolite facies (>500°C), type 3 ribbons consist of strain-free elongate grains with straight grain boundaries, whereas at even higher metamorphic grades these grains are further modified to form a compositional layering (type 4 ribbons) consisting of entirely

recrystallized quartz with bulging grain boundaries (Boullier and Bouchez, 1978; Hirth and Tullis, 1992).

B. Analytical procedure: geochronology

Samples with visible hornblende and mica from selected locations were used for $^{40}\text{Ar}/^{39}\text{Ar}$ age spectrum analysis. Proterozoic granitoids and a pegmatite yielded suitable mineral separates. Samples were crushed, washed and sieved in the laboratory. Magnetic material was separated using a Franz magnetic separator and amphiboles and micas were concentrated by floatation using heavy liquids, and purified by handpicking under a binocular microscope. Size fractions analyzed were all greater than 200 μm (Appendix A). Samples weighing 1-2 mg were loaded into individual holes in aluminum trays along with flux monitor Fish Canyon tuff (FC-1) 27.84 Ma relative to 520.4 Ma for sample Mmhb-1 (Cebula et al., 1986; Samson and Alexander, 1987). The trays were irradiated at the University of Michigan Ford reactor in two irradiation packages (NM-84 and NM-102) for 50 and 100 hours, respectively.

Samples were step-heated in a double-vacuum molybdenum resistance furnace at the New Mexico Geochronology Research Laboratory (NMGRL). A tungsten filament heated the samples and the temperature was monitored by a W-Re thermocouple. The furnace temperature was calibrated to $\pm 10^\circ\text{C}$ by melting copper foil at 1083°C . Within the NMGRL system the gas extracted enters a two-stage vacuum cleanup line, with a SAES GP-50 getter (450°C) on the first stage reacting with the evolved gas during heating. The second stage is gettered by two SAES getters (one at room temperature, and one at 450°C) and a tungsten filament (2000°C) for a total of two minutes. Heating

duration for all steps was 8 minutes per step. Samples were heated in 13 or fewer steps until 1300°C (muscovite - 1650°C).

The gas is then expanded into a MAP 215-50 mass spectrometer operated in static mode. The mass spectrometer has a resolution of ~450 at mass 40 and isotopes are measured with an electron multiplier. Final isotopic intensities are determined by linear regression to time zero of the peak height plotted against analysis time. Each mass intensity is corrected for mass spectrometer baseline, background and system blank. The electron multiplier sensitivity was $\sim 2 \times 10^{-16}$ mol/pA. The total ^{40}Ar system blank ranged from 4.5×10^{-16} to 6.3×10^{-15} moles, while the average blank was 2.5×10^{-15} moles. The plateau ages were determined by weighting each step within the plateau by the inverse of the variance, while the error is calculated after Taylor (1982). A Mean Square Weighted Deviates (MSWD) value is determined by dividing the Chi-squared value by $n-1$ degrees of freedom for the plateau ages. If the MSWD is outside the 95% confidence window (cf. Mahon, 1996; Table 1), the plateau or preferred age error is multiplied by the square root of the MSWD. Uncertainties for each of the heating steps and the total gas age are quoted at one-sigma (1σ), while the plateau ages are quoted at two-sigma (2σ). Both do not include the error in the J-factor. The variable J is a measure of the dosage of fast neutrons a sample receives during irradiation. The J-factor was determined with a precision of 0.10% by the total fusion analysis of four flux monitors per hole and four monitors per tray using either a 10 or 50W Synrad CO_2 laser.

C. Analytical procedure: electron microprobe

Compositions of amphibole in one whole-rock separate of an enclave in the Windy Bridge tonalite, mica and amphibole separates from the Windy Bridge tonalite, and plagioclase and amphibole from two key thin sections were determined with a Cameca SX-100 electron microprobe to help evaluate $^{40}\text{Ar}/^{39}\text{Ar}$ ages and to constrain metamorphic grade. Back-scattered electron (BSE) images were checked for grain-shape, alteration, and potassium-bearing contaminants in dated phases. Quantitative analyses were performed on at least seven points on several grains from each sample to obtain a statistically significant average. For most quantitative analysis, the beam diameter was 5 μm ; for sodic samples the beam was defocussed over an area of 20 μm to minimize volatilization. The accelerating voltage was 15 kV, and probe current was set at 20 nA.

IV. STRUCTURES AND MICROSTRUCTURES IN PROTEROZOIC ROCKS OF THE ROSILLA PEAK QUADRANGLE

Rocks of all rock types vary from nonfoliated to very well foliated in the study area (Plate 1). Large-scale folds are absent and outcrops generally exhibit a single, macroscopically visible, solid-state foliation (Figure 3). In thin section, all rock types also display a wide variety of strain states, from coarse-grained little-deformed igneous rocks to fine-grained ultramylonites. To facilitate evaluation of evidence for multiple deformation events, structures will be discussed in units of different age, from

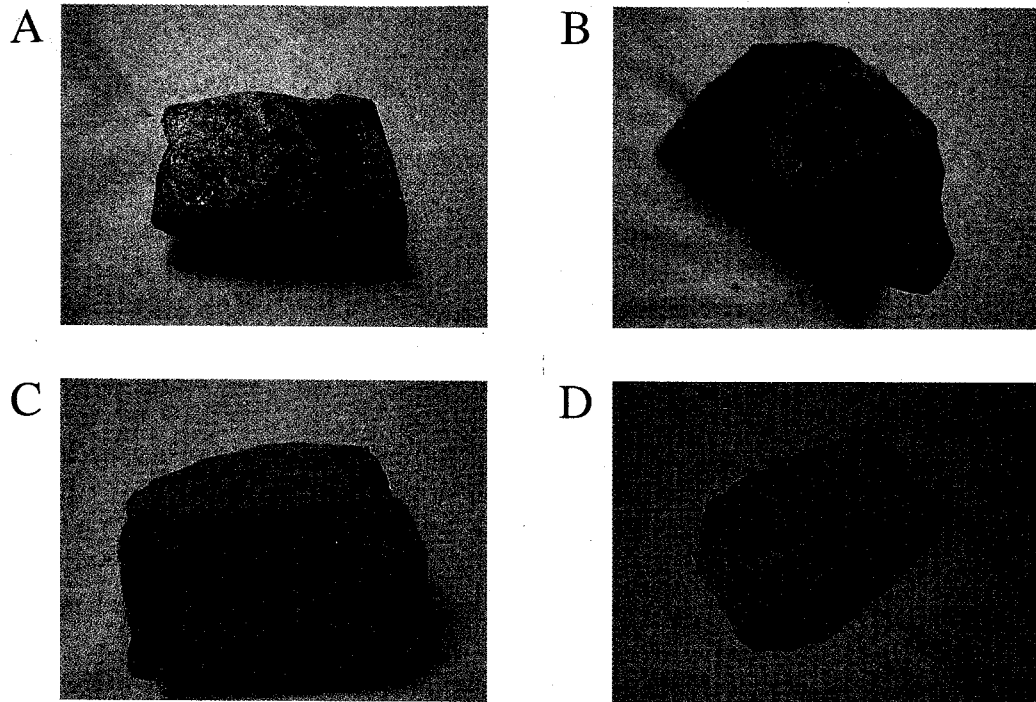


Figure 3. Typical foliations in each of the four major rock types studied. A) Quartz-muscovite schist of the Jones Rhyolite Complex. Light is reflecting off the foliation surface defined by muscovite mica and chlorite. B) Windy Bridge tonalite mylonite, with foliation defined by biotite; also note lineation. C) Indian Creek granite mylonite, in which foliation is defined by strong quartz and biotite alignment. D) Macho Creek granite mylonite, in which the foliation is defined by recrystallized plagioclase feldspar and discontinuous bands of mica. In all photographs the long direction of the red rectangle is 4.5 cm.

oldest to youngest, in the following paragraphs. Similar magnitudes of high strain are present regardless of the age of the protolith (Figure 3).

The Jones Rhyolite Complex is composed of a variety of rock types, including amphibolites, quartz-chlorite schists and quartz-mica-feldspar mylonites. Coarser-grained micas are found in schists, whereas mylonites have a recrystallized, fine-grained texture. The stable mineral assemblage in the amphibolites consists of plagioclase + hornblende + quartz \pm titanite \pm garnet, whereas quartz-chlorite schists (Figure 4a) contain quartz + chlorite \pm feldspar \pm muscovite. Metasedimentary rocks of the Jones Rhyolite Complex consist of quartz + biotite + feldspar \pm muscovite \pm garnet. The least deformed rocks of the Jones Rhyolite Complex are non-foliated, coarse-grained gabbros, which contain igneous features such as concentric zoning in feldspar and amphibole glomerocrysts that are several millimeters in size. Relict pillow basalts have been observed (Riesmeyer, 1978). Less-deformed samples are foliated, but not lineated, and have a symmetrical fabric. Fine-grained micas most commonly define the foliation in these samples. Amphibolites are mostly massive, but locally exhibit a poor to well-developed foliation. More intense foliation in amphibolites is defined by aligned pleochroic green to brown-green hornblende and a subhorizontal mineral lineation. In some amphibolites, chlorite is aligned along conjugate shear bands. Schists within the Jones Rhyolite Complex have a single macroscopically visible foliation that is defined by a well-developed compositional layering, with alternating quartz-(feldspar) and phyllosilicate-rich domains (Figure 4a). Asymmetry parallel to the mineral lineation in these schists is manifested as a SPO of quartz defining a foliation (S-surfaces; Figure 4a)

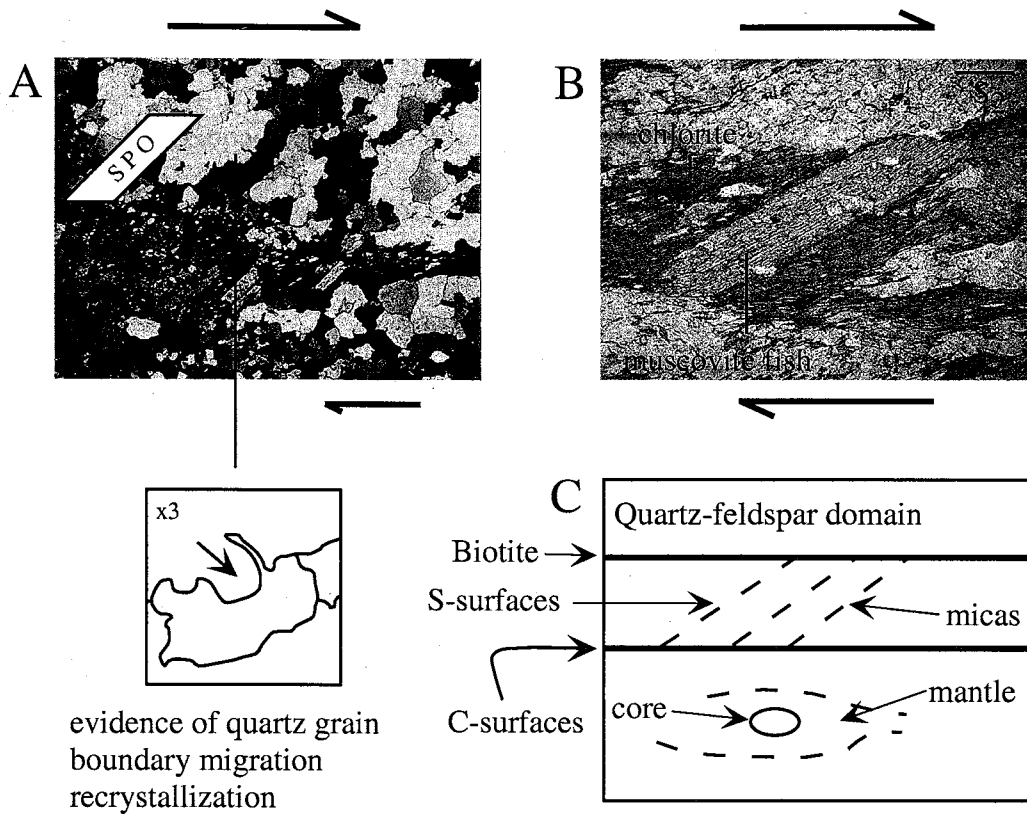


Figure 4. Photomicrographs and sketches of microstructures in metasedimentary and metavolcanic rocks of the Jones Rhyolite Complex. Both sections were cut perpendicular to the foliation and parallel to the lineation. A) Foliation defined by chlorite parallel to the long side of the photomicrograph. Quartz has a shape preferred orientation, which is parallel to the 'imbricated' micas in the mica-rich domains and records top-to-the-right (dextral strike-slip) shear (arrows). Crossed nicols. Long axis of photo is 4 mm. Close-up sketch shows bulging grain boundaries in quartz, which record grain-boundary migration recrystallization. B) Muscovite fish in a quartz-muscovite-chlorite schist record dextral strike-slip shearing (arrows). Muscovite grain is overgrown with chlorite, which helps define the main foliation. Plane light. Long axis of the photo is 1.5 mm. C) Sketch of structural elements present in sample RP-80 (mylonite). C-surfaces of aligned biotite are indicated by bold lines. S-surfaces, which anastomose around feldspar porphyroclast systems, are indicated by dashed lines. See text for further explanation.

oblique to the main foliation. Muscovite is present as mica fish, with orientations that record dextral strike-slip shearing (Figure 4b).

Where best developed, the foliation in the Jones Rhyolite Complex units is mylonitic and is defined by foliation-parallel recrystallized mineral segregations: fine-grained quartz-(feldspar) domains alternate with micaceous domains (Figure 4a). As in the schists, S-C fabrics indicate asymmetry; kinematic indicators consistently show dextral shear. In the mylonites, recrystallized plagioclase has a uniform grain size (~0.02 mm) and a SPO which defines S-surfaces. In mylonite RP-80, garnet is present and preserves an internal foliation (S_i). The external foliation (S_e) is deflected around the garnet. The continuity between S_i and S_e could not be resolved.

Microstructures of individual minerals provide additional information about deformation and metamorphic grade. In the Jones Rhyolite Complex, fine-grained quartz is mostly anhedral with many promontories and embayments (Figure 4a) suggestive of grain boundary migration recrystallization (cf. Urai et al., 1986). Coarser-grained, polygonal quartz also appears in up to 1-cm-wide, foliation-parallel, recrystallized domains. Plagioclase feldspar porphyroclasts are locally present in mylonites. The foliation is deflected around these porphyroclasts (Figure 4c) as well as around polycrystalline feldspar augen, which are believed to have formed by recrystallization of feldspar porphyroclasts. Reaction relationships record the syndeformational retrogression from muscovite and biotite to chlorite in schists, and amphibole to biotite and chlorite in amphibolites.

Mineral lineations are only observed in the mylonite and are mostly defined by elongate domains of micas or amphiboles. The dominant foliation strikes NE and dips

moderately to steeply NW or SE (Figure 5a). Mylonites are neither common nor clearly geographically defined, and there is a large variation in the orientation of the few lineations measured from near horizontal to steeply plunging. All the lineations, except one, are confined to steeply south-dipping foliation planes.

The Windy Bridge tonalite, geographically the most extensive and the oldest pluton, intruded the Jones Rhyolite Complex. It exhibits the greatest variation in foliation development. The continuity of the foliation across the contact between the Jones Rhyolite Complex and the Windy Bridge tonalite could not be established.

Mineralogically, the tonalite consists of plagioclase + quartz + biotite \pm hornblende \pm titanite. Where least deformed, it is coarsely crystalline and nonfoliated. These nonfoliated tonalites are recrystallized, macroscopically undeformed, and occur most notably near the contact with the Indian Creek granite. However, this 'undeformed' tonalite has non-equilibrium microstructures (Figure 6a). Plagioclase porphyroclasts, up to 1 cm in the longest dimension, show concentric igneous zoning in the interior of crystals and subgrain formation closer to their edges. The recrystallized mantles are equigranular and fine-grained.

The dominant tonalite foliation is a gneissic fabric (S_1) in some places and a mylonitic foliation (S_2) elsewhere. Narrow, chlorite-rich shear zones (S_3), locally several centimeters wide, crosscut the dominant foliation. Within these shear zones chlorite has replaced all the biotite, and the plagioclase feldspar is extensively sausseritized. These S_3 shear zones will not be discussed. The majority of the foliated Windy Bridge tonalite has orthorhombic symmetry, is not lineated, and is coarse-grained. The S_1 foliation in the gneiss is defined by recrystallized quartz-rich domains, rimmed by anastomosing

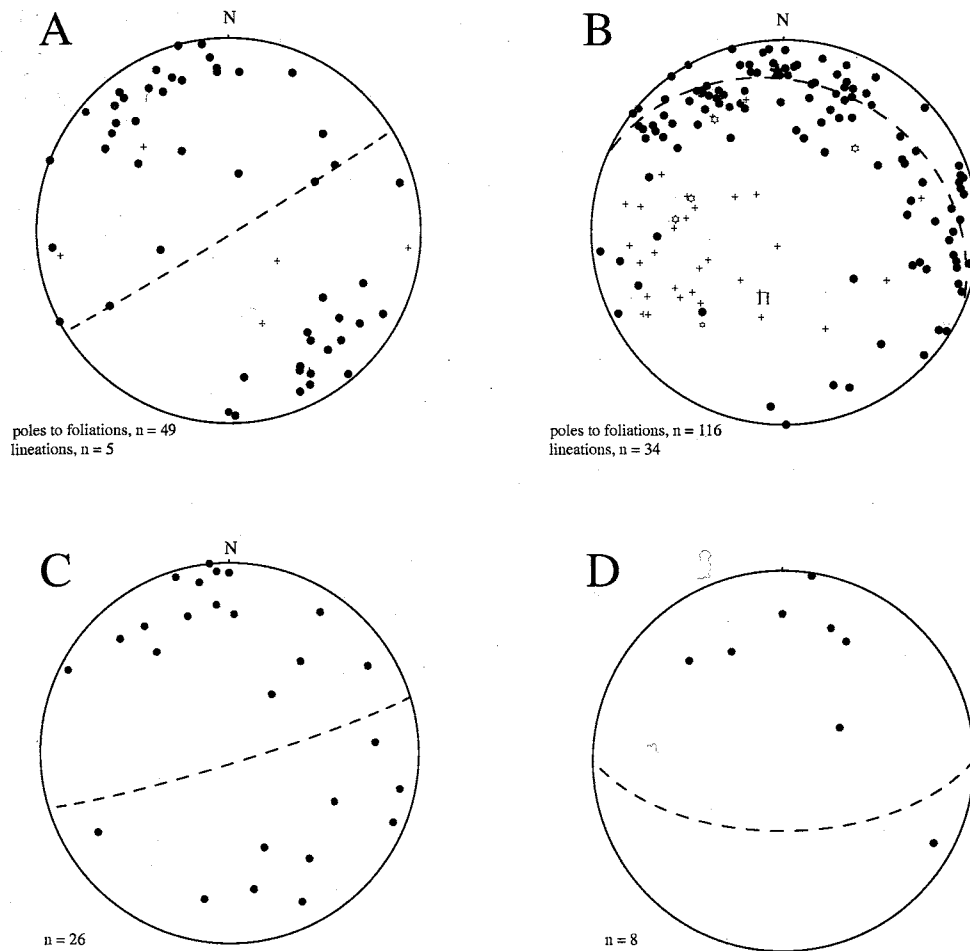


Figure 5. Lower hemisphere, equal area net plots of lineations (crosses), poles to S_1 and S_2 (red dots, where mylonitic) and fold hinges (yellow stars). Dashed line in A, C, and D is the mean orientation of the foliation. In B, the great circle girdle containing poles to the foliation is shown as a dashed line. The number of data points is shown at the lower left of each diagram. Orientations of foliations reoriented near the Picuris-Pecos fault are not included in plots. A) Jones Rhyolite Complex B) Windy Bridge tonalite. Red Π shows the orientation of the fold axis. C) Indian Creek granite. D) Macho Creek granite.

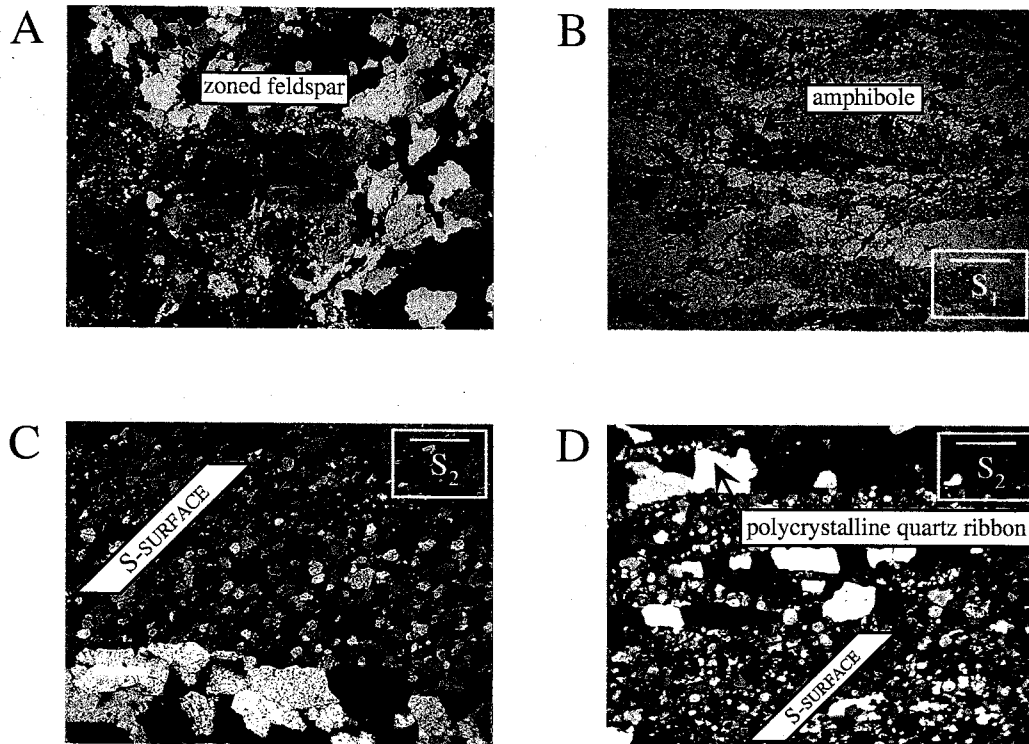


Figure 6. Photomicrographs of variably deformed samples of the Windy Bridge tonalite. Sections shown in B), C), and D) were cut perpendicular to the foliation; sections shown in C) and D) were also cut parallel to the lineation. A) Macroscopically undeformed plagioclase feldspar porphyroblast with undulose extinction. Note smaller recrystallized grains forming a mantle around the porphyroblast and bulging quartz grain boundaries. Crossed nicols. Long axis of image is 4.5 mm. B) Hornblende aligned parallel to S_1 . Quartz is white and drab colors are recrystallized, sausseritized plagioclase feldspar. Plane light. Long axis of image is 2.5 mm. C) S-C fabric developed in tonalite ultramylonite, recording dextral strike-slip shear with a normal, top-to-the SW component. C-surfaces are defined by boundaries between compositional bands. S-surfaces are defined by the SPO of plagioclase feldspar. Crossed nicols. Long axis of image is about 1.5 mm. D) Recumbent, isoclinally folded, polycrystalline quartz ribbon in tonalite mylonite. Note elongate quartz in quartz domain and straight grain boundaries. Fabric records dextral strike-slip shear with a normal, top-to-the SW component. Long axis of the image is about 1.5 mm.

phyllonites, recrystallized feldspar, and large, locally poikilitic hornblende (Figure 6b). Amphibolite enclaves and xenoliths are common in the tonalite and have finer grain sizes than the host tonalite. These amphibolite enclaves and xenoliths are locally aligned parallel to the dominant gneissic foliation. Margins of bigger amphibolite dikes that crosscut the tonalite commonly have an intense schistosity parallel to the gneissic foliation in the tonalite.

Kinematic indicators cannot be resolved in the field; an orthorhombic symmetry is present throughout the Windy Bridge tonalite gneiss, which is possible evidence for coaxial flow. In thin section, it is evident that recrystallized feldspar grains are strain-free, anhedral, and locally elongate. Core and mantle structures are rare. In contrast, quartz has bulging grain boundaries and widespread undulose extinction. Most quartz grains are inequigranular, interlobate and subhedral; some grains are elongate. Locally quartz has achieved stable triple-junction grain boundaries within polycrystalline ribbons. Undulose extinction and deformation lamellae are also locally present. Hornblende grains are mostly foliation-parallel but locally crosscut the fabric. They preserve an internal foliation defined by plagioclase inclusions (S_i). S_i is parallel to S_e , which in turn is parallel to the feldspar SPO that defines S-surfaces outside the crystal.

In mylonitic tonalites, compositional layering defines the main foliation, which consist of C-surfaces (S_2) (Figure 6b). Individual grains are not visible to the naked eye and all grains have been recrystallized, making these rocks ultramylonites (cf. Sibson, 1977). In the field, the ultramylonites appear dark and glassy; only on weathered surfaces can white streaks of plagioclase be recognized. Mafic domains are thin, wispy, and undulose. Aligned biotite locally defines a mineral lineation. Extended quartz

domains define a stretching lineation on some foliation planes. In these rocks, the maximum asymmetry is evident in sections cut perpendicular to the foliation and parallel to the stretching lineation. In thin sections of this orientation, large plagioclase porphyroclasts show evidence of progressive recrystallization to equigranular, anhedral ~0.05 mm large grains with a well-developed SPO in progressively more deformed samples (Figure 6c). This SPO defines S-surfaces, which are oblique to the main foliation, the C-surfaces. Aligned biotite, or locally chlorite, also defines S-surfaces. The angle between S- and C-surfaces varies between 30° and 45°. The S-C fabric consistently records dextral strike-slip shear with a component of normal, southeast down motion. Winged, several-millimeter-large, recrystallized, quartz porphyroclast systems are present locally, and also record dextral strike-slip shear. Mylonites with a well-developed mineral lineation constitute less than 10% of the outcrops surveyed, and have monoclinic symmetry, indicating that they experienced a significant component of noncoaxial flow. An apparently geographically random distribution of this monoclinic fabric is found.

Poles to the gneissic foliation plot on a shallowly dipping great-circle girdle, indicating that S_1 was folded about a steeply dipping, southwest-plunging fold axis (Figure 5b). The fold axis plunges steeply to the southwest: 66° toward 205° azimuth. In contrast, mylonites exhibit an ENE-striking foliation that dips steeply to the SSW (Figure 5b – red dots). Lineations (measured exclusively in Windy Bridge tonalite ultramylonites) define a broad cluster with a mean of 285°, 36°NE. Folded compositional layering in mylonites, isoclinally folded recrystallized polycrystalline quartz ribbons, and rootless intrafolial folds are also found throughout the Windy Bridge tonalite (Figure 6d).

Fold hinges vary in orientation, but most fall within the range of orientations exhibited by the lineation.

The contact between the Indian Creek granite and the Windy Bridge tonalite is a modified intrusive contact. In places it is a brittlely reactivated ductile shear zone, with tonalite foliations bent into parallelism with the contact (Bauer et al., 1995). No intensification of the fabric was noted at the pluton boundary and no lineations were observed. The stable mineral assemblage in the Indian Creek granite is plagioclase + K-feldspar + biotite + quartz \pm muscovite.

The Pecos granodiorite (new informal name) is related to, and interfingers with, the Indian Creek granite. Compositionally, it has more plagioclase feldspar and up to 20% biotite. Locally, it has a mylonitic fabric. The Indian Creek granite is generally undeformed and non-foliated but locally exhibits a solid-state mylonitic foliation. Where undeformed, the granite has a roughly equigranular igneous texture with megacrysts of K-feldspar. Mylonitized granites occur in unevenly distributed zones tens of meters wide. In these areas, compositional banding and lens-shaped mineralogical domains define the foliation. Mineralogical domains consist of elongate recrystallized quartz grains with a maximum aspect ratios of 1:10 and decussate biotite. Mantles of recrystallized K-feldspar grains approximately 0.1 mm are present around relict K-feldspar cores. Myrmekites exist in some K-feldspar porphyroclasts, and anhedral plagioclase feldspar grains (0.05 – 0.1 mm) are fractured and have bent albite twins. Chlorite has replaced the foliation-parallel biotite in some samples. White mica locally replaced K-feldspar. The foliation dips steeply to the SSE and NNW, and has a mean orientation of 073°, 85°SE (Figure 5c). The rock is not lineated.

The contact between the Macho Creek granite and the Jones Rhyolite Complex is intrusive, and the mylonitic foliation in the granite is continuous across the contact, indicating that the dominant foliation in the study area is at least partly younger than the ca. 1480 Ma Macho Creek granite. The mean foliation is oriented $090^{\circ}, 60^{\circ}\text{S}$ (Figure 5d). The Macho Creek granite is a two-mica, megacrystic K-feldspar granite, which is only locally deformed. It is composed of K-feldspar + quartz + plagioclase feldspar + muscovite + biotite \pm garnet. The foliation, which typically dips steeply to the south, grades from granite mylonite to largely undeformed granite over tens of meters (Figure 5d). Foliations in these mylonites are defined by mineralogical segregations of recrystallized quartz, recrystallized feldspar and biotite (Figure 3d), whereas K-feldspar megacrysts remain as porphyroclasts. Aligned biotite domains define a shear band foliation as well as a nearly horizontal mineral lineation. Macroscopic kinematic indicators include both these shear bands and σ -type porphyroclast systems, both of which record dextral strike-slip shear. Microscopically, SPO in plagioclase and some of the K-feldspar define S-surfaces, which also record dextral strike-slip shear.

In general, the microstructures of the Macho Creek granite are similar to those of the Indian Creek granite. Muscovite, biotite and quartz ribbons anastomose around partially recrystallized K-feldspar megacryst domains (Figure 7a), whereas recrystallized quartz and plagioclase feldspar domains parallel C-surfaces. In the most deformed samples, K-feldspar porphyroclasts with undulose extinction possess linear arrays of neocrystals, equigranular to grains in the recrystallized mantles of porphyroclasts. Some K-feldspar porphyroclasts have been completely recrystallized (Figure 7a). Less deformed K-feldspar grains exhibit myrmekite and deformation twins (Figure 7b). Some grains in

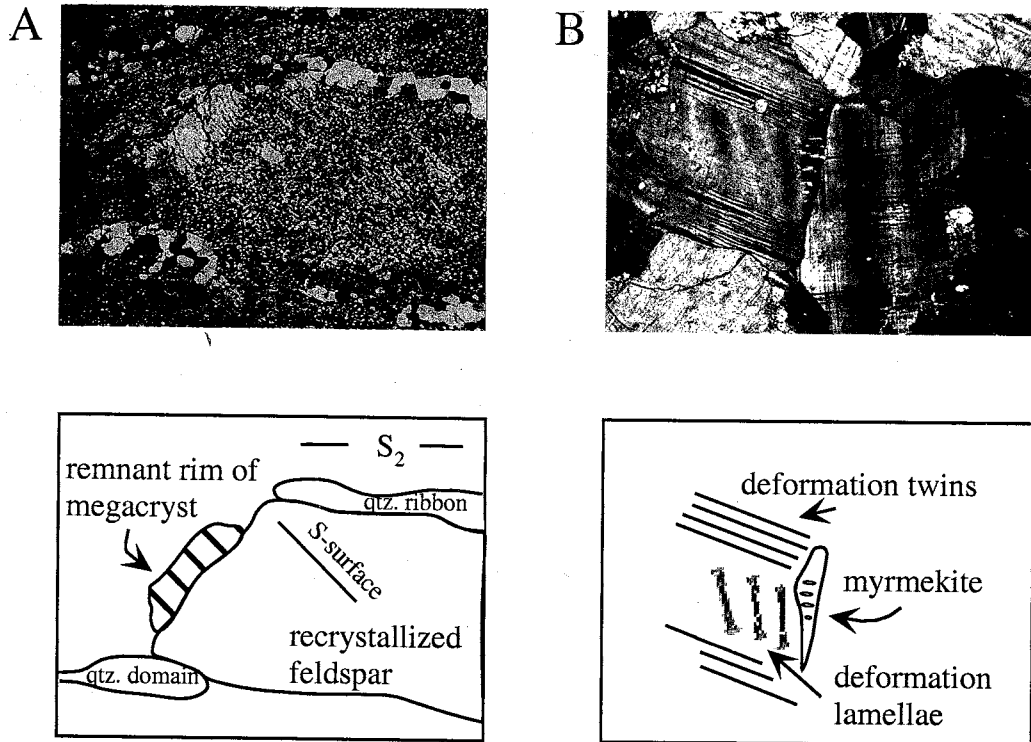


Figure 7. Photomicrographs of the Macho Creek granite. Both sections were cut perpendicular to the foliation; Figure 7A is also parallel to the lineation. A) Megacryst of K-feldspar, mostly recrystallized except for the rim. Note grain-shape preferred orientation of the recrystallized grains. Polycrystalline quartz ribbon parallels the C-surfaces. Angle between S_2 and the S-surfaces is 45° . Crossed nicols. Long axis of image is 4.5 mm. B) Myrmekite, deformation twins and deformation lamellae in K-feldspar. Long axis of image is 1.5 mm.

quartz domains have aspect ratios of 1:5, but most quartz grains display an equigranular foam texture. Some of the micas exhibit undulose extinction and evidence for intracrystalline cataclasis (cf. Goodwin and Wenk, 1990). Locally, muscovite and biotite have reaction rims of biotite and muscovite, respectively. Biotite is locally altered to chlorite along cleavage planes. Epidote rims both micas and some oxides. Garnet is locally altered to aggregates of white mica.

In summary, all three plutons in the Rosilla Peak quadrangle include macroscopically undeformed rocks as well as solid-state foliations that vary in development from gneissic to mylonitic (e.g. Figure 6). All mylonitic foliations are defined by strong compositional layering, except within the Macho Creek granite, where they are characterized by an anastomosing foliation in part due to incompletely recrystallized K-feldspar porphyroclasts. Most of the samples with K-feldspar display myrmekitic intergrowths. Plagioclase feldspar in most of the deformed samples has recrystallized to a fine grain size and in tonalite ultramylonite and rocks of the Jones Rhyolite Complex has a grain-shape-preferred orientation defining S-surfaces. Quartz has recrystallized, but mostly does not have a stable microstructure. Undulose extinction and bulging grain boundaries in quartz are common in most undeformed samples. Where quartz does exhibit a stable microstructure, it is a foam texture within polycrystalline quartz ribbons. Micas mostly define the main foliation. Evidence of an older folded foliation has been found in the Windy Bridge tonalite, suggesting that it possessed a foliation (S_1) that was partially transposed into the dominant, mainly south-dipping foliation (S_2). By inference, the older Jones Rhyolite Complex must also have been deformed prior to formation of the dominant foliation (S_2), which is continuous across the contact between the Jones

Rhyolite Complex and the ca. 1480 Ma Macho Creek granite. Kinematic indicators in the Macho Creek granite, Jones Rhyolite Complex, and the Windy Bridge tonalite mylonites record dextral strike-slip and normal shearing in a roughly E-striking, steeply south-dipping shear zone. There is evidence of local chlorite, epidote and sericite alteration in some rocks, as well as locally pervasive epidote veining. The sense of shear of narrow, chloritic shear zones that cut S_2 in the Windy Bridge tonalite has not been established.

V. METAMORPHISM

The compositions of plagioclase feldspar and amphibole from the Windy Bridge tonalite ultramylonite were determined with the electron microprobe to evaluate metamorphic grade. Amphiboles analyzed from all samples of the Windy Bridge tonalite mylonite and an enclave within the tonalite are calcic, with varying aluminum + sodium + potassium \pm magnesium substituting for silica \pm iron (tschermak ($MgSi = Al^{IV}Al^{VI}$) and edenite ($NaAl = \square Si$) exchange (Table 2). All of the amphiboles analyzed have compositions characteristic of the amphibolite facies. Syntectonic, acicular aluminoferro-tschermakite (WB-10) grains occur in a folded, nearly monomineralic amphibole layer within the ultramylonite. Amphibole from enclave WB-15 are classified as magnesio-hornblende (cf. Yavuz, 1999). Amphibole cores within this enclave are more aluminous and alkalic than the margins. Rims are richer in Si and Mg. The cores are characteristic of amphibolite facies conditions, whereas the rims are characteristic of lower amphibolite facies conditions. Compositionally homogenous ferro-pargasite ($Al +$

Table 2. Compilation of average oxide weight percent and site occupancy (after Yavuz, 1999) of amphibole from electron microprobe analyses

	WB-23 average tonalite mylonite	WB-10 average tonalite mylonite	WB-15b enclave core remnants	WB-15b enclave complete shell
name #	ferro pargasite	aluminio ferro- tschermakite	magnesio hornblende	magnesio hornblende
Oxides				
SiO ₂	40.69 ± 0.39	39.86 ± 0.60	46.46 ± 1.47	51.11 ± 1.14
TiO ₂	0.35 ± 0.05	0.30 ± 0.05	0.38 ± 0.13	0.21 ± 0.08
Al ₂ O ₃	13.56 ± 0.65	15.99 ± 0.52	9.46 ± 1.48	5.22 ± 1.10
MgO	6.74 ± 0.24	5.85 ± 0.27	11.03 ± 0.95	13.71 ± 0.73
CaO	11.32 ± 0.13	11.18 ± 0.15	12.06 ± 0.14	12.15 ± 0.16
MnO	0.56 ± 0.04	0.36 ± 0.03	0.30 ± 0.02	0.30 ± 0.03
FeO	21.74 ± 0.27	21.30 ± 0.21	16.55 ± 0.72	14.34 ± 0.59
Na ₂ O	1.37 ± 0.13	1.20 ± 0.17	0.82 ± 0.08	0.47 ± 0.10
K ₂ O	0.72 ± 0.22	0.41 ± 0.03	0.64 ± 0.22	0.23 ± 0.09
H ₂ O	1.94 ± 0.01	1.94 ± 0.01	2.02 ± 0.02	2.06 ± 0.01
Total	99.00 ± 0.39	98.39 ± 0.51	99.73 ± 0.47	99.79 ± 0.36
No. of analyses	n=43	n=17	n=6	n=10

Cations	23	23	23	23
---------	----	----	----	----

T 1	SiO ₂	4.000	4.000	4.000	4.000
T 2	SiO ₂	2.240	2.120	2.880	3.430
	Al ₂ O ₃	1.760	1.880	1.120	0.570
	Total	4.000	4.000	4.000	4.000
C site	Al ₂ O ₃	0.700	1.010	0.530	0.330
	TiO ₂	0.040	0.033	0.043	0.023
	Fe ₂ O ₃	0.430	0.370	0.160	0.010
	Cr ₂ O ₃	na	na	na	na
	FM †	3.830	3.590	4.270	4.630
	Total	5.000	5.003	5.003	4.993
B site	FM †	0.140	0.160	0.090	0.110
	CaO	1.874	1.853	1.919	1.895
	Na ₂ O				
	Total	2.014	2.013	2.009	2.005
A site	K ₂ O	0.140	0.214	0.122	0.042
	Na ₂ O	0.413	0.227	0.237	0.134
	Total	0.553	0.441	0.359	0.176
	Vacancy	0.447	0.559	0.641	0.824

na = not analyzed

* average contains all data of next two columns

= named using conventions of Yavuz (1999)

† = FeO, MgO, MnO

Fe + Na hornblende) cross-cuts S_2 in sample WB-23, and is therefore post-kinematic. Hornblende in WB-23 could also be syntectonic if S_2 was localized away from hornblende growth. Petrographically similar hornblende from other samples has recrystallized plagioclase feldspar inclusions characteristic of S_2 , which suggests that hornblende generally overgrew S_2 .

Plagioclase feldspar from tonalite ultramylonite sample WB-23 is oligoclase (An_{23-29} ; Table 3) within the plagioclase compositional range suggested for tonalites from Finland (Arth et al., 1978). Feldspar from altered tonalite ultramylonite sample RP-36 is compositionally similar. No co-existing albite was found, indicating that a peristerite solvus did not exist, and suggesting that metamorphic conditions were above the greenschist facies. Oligoclase is in equilibrium with temperatures indicative of the amphibolite facies (Crawford, 1966). As indicated previously, the feldspars in both rocks define a SPO. The Windy Bridge tonalite thus preserves evidence for amphibolite facies metamorphism in both syntectonically recrystallized and post-tectonic minerals, suggesting that D_2 deformation occurred during amphibolite facies metamorphism. The experimental thermometer of Liou and Apter (determined at $P_{H_2O} = 7$ kbar using Ca versus Al and Na partitioning; 1983) can be applied to co-existing amphibole and plagioclase feldspar in the WB-23 tonalite ultramylonite sample. This yields M_2 temperatures of 610 – 700°C, which agrees with Daniel's (1995) calculated temperatures of 600 – 680°C at 5-6 kbar.

Microstructural evidence also helps to constrain metamorphic grade during D_2 deformation. Recrystallized feldspar with a SPO is characteristic of metamorphic conditions above 500°C (Passchier and Trouw, 1996). Such microstructures are in the

Table 3. Oxide weight percent of feldspars from electron microprobe analysis of Windy Bridge tonalite. Feldspars are oligoclase. Values are averages of all analyses, while the uncertainty is the mean of the standard deviation.

Oxide Wt. %	RP-36xz	WB-23
	tonalite	tonalite
	matrix plag.	matrix plag.
SiO ₂	61.97 ± 0.62	60.59 ± 0.50
Al ₂ O ₃	24.46 ± 0.37	25.74 ± 0.28
CaO	4.91 ± 0.40	6.17 ± 0.29
FeO	0.06 ± 0.02	0.08 ± 0.05
SrO	0.05 ± 0.02	0.07 ± 0.02
BaO	0.01 ± 0.01	0.02 ± 0.01
Na ₂ O	8.80 ± 0.22	8.12 ± 0.17
K ₂ O	0.17 ± 0.03	0.14 ± 0.09
Total	100.42 ± 0.36	100.94 ± 0.37
Cations	8	8
% An	23.31	29.35
No. of analyses	23	33

Windy Bridge tonalite, metavolcanic rocks of the Jones Rhyolite Complex, and the Macho Creek granite. The Macho Creek and Indian Creek granites commonly have both myrmekite intergrowths, typical of amphibolite facies and deformation twins in K-feldspar, indicative of either temperatures less than 500°C (Pryer, 1993) or relatively high strain rates. Quartz behaved ductilely, forming elongate domains and polycrystalline ribbons (Figure 6d). Evidence for quartz grain-boundary migration recrystallization is present in all rock types (e.g. Figure 4a). Locally, quartz displays a foam texture (Figures 4a, 6c, 6d, and 7a). These observations are consistent with compositional data indicating that deformation occurred largely under amphibolite facies conditions, but locally continued during cooling to greenschist facies conditions.

Garnet and andalusite appear as minor phases in amphibolites and plagioclase-mica-quartz mylonites of the Jones Rhyolite Complex. Garnet commonly has a reaction rim of biotite and quartz with biotite locally altered to foliation-parallel chlorite. Garnet is more common in relatively plagioclase-rich areas within the amphibolite. Relict andalusite in aluminous rocks shows evidence of reaction to biotite and quartz. In some samples, deformation continued at lower temperatures, as indicated by the presence of chlorite parallel to S_2 , which commonly replaces biotite and hornblende. Hornblende also locally reacted to biotite and epidote. In some rocks, replacement of biotite by chlorite is complete. Few of these chlorites are pseudomorphs of chlorite after biotite. Titanite in these rocks has overgrowths of epidote. Localized alteration includes the sausseritization of plagioclase feldspar in some samples. Sericite is also common in these sections. Epidote and quartz veins, including tourmaline, crosscut the main fabric,

indicating that vein formation postdated development of S₂. All reactants and their products, except epidote, are synkinematic with respect to mylonitization.

VI. ⁴⁰Ar/³⁹Ar AGE SPECTRUM RESULTS AND DISCUSSION

⁴⁰Ar/³⁹Ar dating yields the time at which minerals crystallize or cool below their closure temperature. Above the mineral-specific closure temperature argon escapes by volume diffusion (Dodson, 1973). In some cases, ⁴⁰Ar/³⁹Ar ages indicate the time at which the system was reset during reheating. Below the closure temperature, radiogenic daughter product (⁴⁰Ar*) can accumulate in the mineral lattice and not be lost by volume diffusion. Closure to ⁴⁰Ar* however, typically occurs over a range of temperatures which is determined by a number of variables, including composition, cooling rate, and grain size (Harrison, 1981; Goodwin and Renne, 1991; Cosca and O'Nions, 1994; Hodges et al., 1994; Dahl, 1996). For this study, the closure temperature for hornblende is taken to be ~500°C (Harrison, 1981). The closure temperature for muscovite is between 350° and 400°C (Hames and Bowring, 1994). For biotite, the typical closure temperature is ~325°C, but it can vary by ±50°C or more depending on composition and other factors (e.g. grainsize) (Goodwin and Renne, 1991; McDougall and Harrison, 1999).

Three amphibole separates were obtained from different rock-types contained within the Windy Bridge tonalite. All of the rock samples were foliated, but the three amphiboles are compositionally different (Table 2). The amphibole from sample WB-23 is large (1-3 mm crystals), has good crystal faces and cross-cuts the foliation. The amphibole is a blue-green ferro-pargasite. Amphibole from sample WB-15b was

separated from a foliation-parallel mafic enclave within the tonalite. Amphibole from this sample is fine-grained (< 0.5 mm) magnesio-hornblende. This amphibole is zoned with an irregular, non-concentric core with more Al, K, Na, and Fe, and a rim higher in Si and Mg. In sample WB-10, acicular, large (~1 mm) amphibole crystals were separated from a folded compositional band of nearly pure amphibole within the tonalite. These alumino-ferrotschermakite grains are aligned parallel to the foliation and are green-brown in thin section.

Two of the three amphiboles, WB-23 and WB-15b, yield similar flat age spectra, whereas the third, WB-10 has a younger, complex age spectrum (Figure 8; data tables of all $^{40}\text{Ar}/^{39}\text{Ar}$ analytical results are given in Appendix B). WB-15b has a well-defined plateau (MSWD=1.2) for 95% of the spectrum and yields an age of 1371.4 ± 6.5 Ma (Figure 8a). The initial steps are anomalously young, but the K/Ca spectrum, an indicator of contamination (e.g. Harrison and Fitz Gerald, 1986), is flat. WB-23 is slightly more disturbed than WB-15b, however it has several steps equal to the plateau age given by WB-15b. The minor disturbance in the middle of the spectrum is correlated with a slight increase in K/Ca, as are the initial young age steps. A weighted mean age calculated for steps G, H, J, K is 1374 ± 12 Ma and is the preferred age for this sample. Step I, omitted from the calculation, is thought to be anomalously young due to minor contamination by a high-K/Ca phase with a lower argon retentivity than the amphibole. The third sample, WB-10, has a disturbed spectrum with an overall age gradient from ~40 - 1310 Ma (Figure 8b). The final three heating steps, comprising 32% of the total ^{39}Ar released, are concordant and have a weighted mean age of 1309.6 ± 5.1 Ma. The initial very young

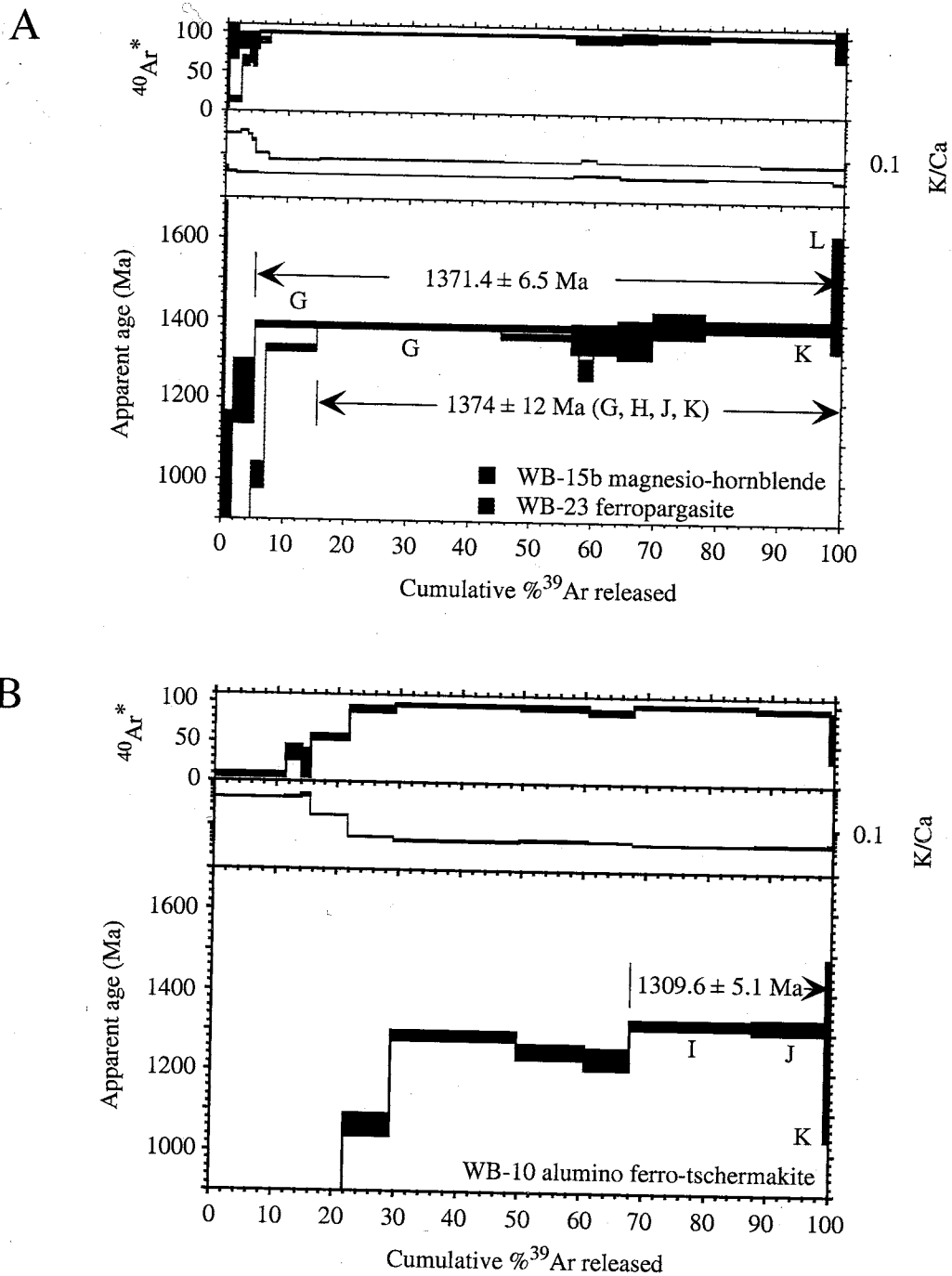


Figure 8. Age spectra, K/Ca, and radiogenic yield diagrams for amphibole from the Windy Bridge tonalite. A) Samples WB-15B and WB-23 display similar plateau ages. B) Plateau age of sample WB-10 is significantly younger than those shown in A). Plateau ages shown for all samples are the preferred ages. Plateau errors are two sigma. Samples were collected from location 5 (Figure 2).

steps have higher K/Ca and lower radiogenic yields than other steps, and are believed to reflect contamination by a less retentive K-bearing phase(s).

The amphibole samples were expected to yield similar ages because of their proximity to one another (Fig. 2); however, WB-10 yields an apparent age significantly younger than both WB-15b and WB-23. Although the first heating steps of the WB-10 amphibole are marked by a high K/Ca ratio, characteristic of contamination by phyllosilicates, such alteration could not be found in thin section or back-scattered electron images. Comparison of the K/Ca ratio obtained with the electron microprobe and K/Ca determined for the plateau segment of the spectrum from argon isotopes show good agreement, indicating that the probe sample is representative of the bulk sample used for dating (Table 2). Other reasons for the anomalous age spectrum could be lab contamination or amphibole composition. The relationship between amphibole chemistry and argon retentivity was addressed by Dahl (1996), who noted that samples that were either aluminous (tschermakitic) or had full A-site occupancy exhibited a 40°C higher closure temperature than other amphiboles. Based on the criteria of Dahl (1996), WB-10 would have a higher T_c than the other amphiboles (Table 2) and thus amphibole composition does not explain the age discordance. Harrison and Fitz Gerald (1986) reported an anomalously young hornblende age and very complex spectrum from a New Hampshire amphibolite, which they interpreted to result from low argon retentivity caused by cummingtonite exsolution in hornblende. No evidence of exsolution was observed in either thin sections or back-scattered electron images. This leaves the young age of sample WB-10 unexplained.

Four mica separates were obtained from four different rock types. Average mica compositions determined from electron microprobe analyses are given in Appendix C. RP-34 muscovite was separated from a slightly foliated pegmatite. The muscovite is euhedral, 0.5 - 2 mm in size, and free of impurities. Biotite of RP-28B is from the Pecos granodiorite (new informal name), is anhedral, and has inclusions of quartz, epidote, and apatite. In thin section it is evident that cleavage planes in biotite are bent and some chlorite alteration is present along the cleavage planes. Biotite grains separated from RP-36, a sample of metasomatized Windy Bridge tonalite ultramylonite is 0.1-0.2 mm, anhedral, and locally kinked. The biotite includes chlorite and epidote. RP-87 muscovite, separated from foliated Macho Creek granite, is anhedral and large (up to 1 mm in diameter). In thin section, muscovite exhibits undulose extinction, kinks, and cleavage-parallel zones of deformation. The material within these zones exhibits no change in color with rotation of the microscope stage. These zones are interpreted to be regions of intracrystalline cataclasis (cf. Goodwin and Wenk, 1990). Biotite, chlorite, and quartz are inclusions within the muscovite grains.

One biotite and one muscovite yielded similar plateau ages (RP-28B and RP-34; Figure 9a) whereas the other micas have complex argon release patterns (RP-87 and RP-36; Figure 9b). The well-defined plateau ages for RP-34 muscovite and RP-28B biotite are 1345.2 ± 1.7 Ma (MSWD=0.9) and 1341.8 ± 3.3 Ma (MSWD=3.0), respectively. The RP-34 muscovite plateau has eight steps, comprising ~91% of the total ^{39}Ar released, with similar K/Ca for each step of the plateau. The first 7% of the ^{39}Ar released from the biotite of RP-28B yields young ages corresponding to a variation in the K/Ca ratio. However, six of the remaining nine steps are within 1σ error of the plateau age of the

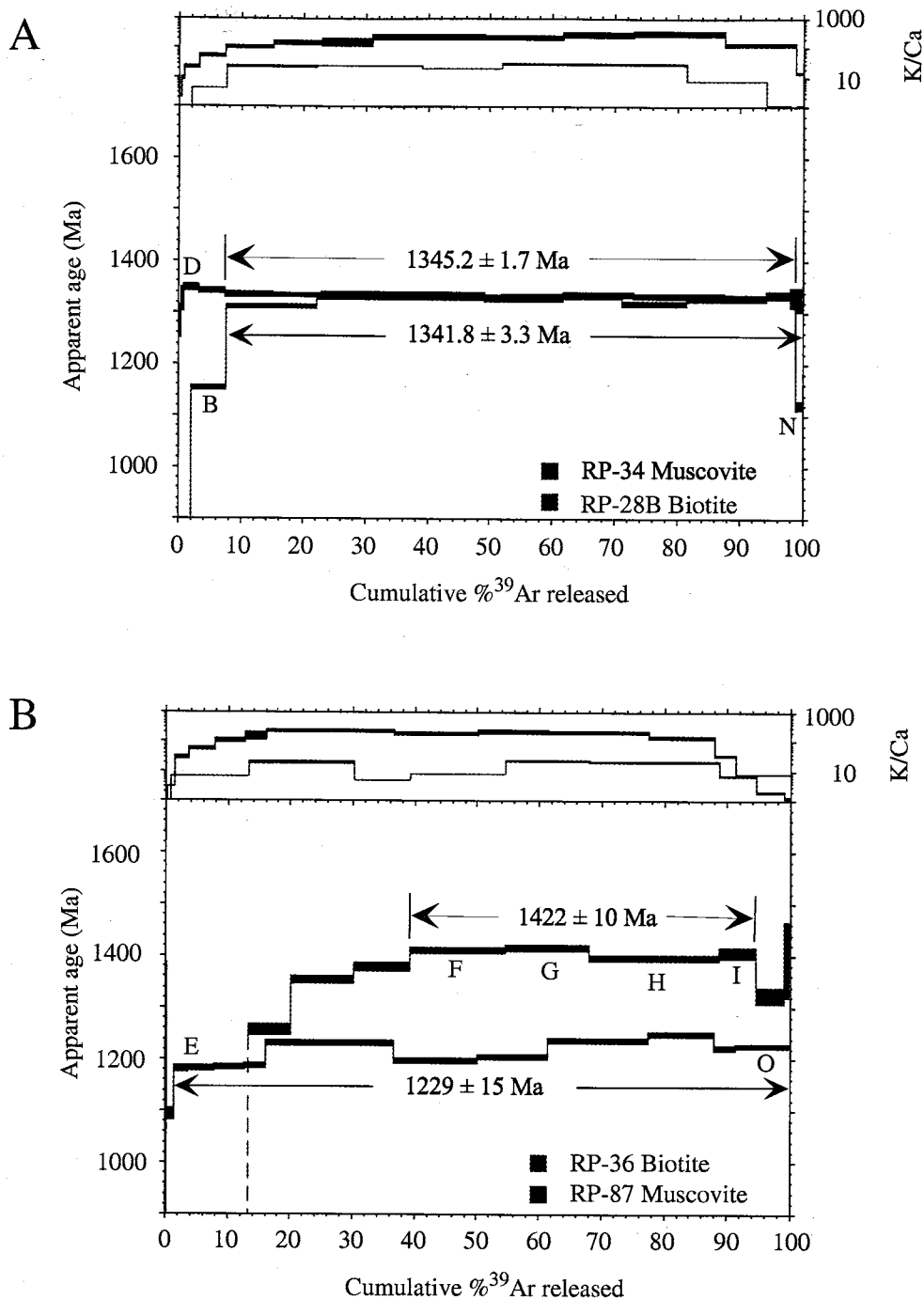


Figure 9. Age spectra and K/Ca ratios for muscovite (blue) and biotite (red). A) Samples RP-34 and RP-28B show well defined plateaus. Plateau ages shown are the preferred ages, which correspond to samples 7 and 8, respectively, both in Figure 2 and Table 1. B) Samples RP-36 and RP-87 display complex age spectra. The K/Ca variation in sample RP-36 correlates with age. Separates are from samples 6 and 9, respectively, (Figure 2 and Table 1).

muscovite from RP-34. These concordant mica ages are 28 Ma younger than the concordant amphibole ages shown in Figure 8a.

The apparent ages of the remaining micas differ almost 200 Ma from each other (Figure 9b). Although the closure temperature of biotite is reported to be less than that of muscovite, the biotite from RP-36 yields an apparent age that is oldest than all of the other micas analyzed. The spectrum obtained from RP-36 biotite is hump-shaped, with ages varying from 300 Ma to 1433 Ma. Hump-shaped spectra for biotite are common (e.g., Heizler et al., 1988), and the maximum age recorded by the hump has in many cases been shown to be anomalously old. Six of the steps from RP-36 yield ages older than the preferred ages of hornblende, which has a higher closure temperature, supporting the idea that the biotite age is inaccurate. Back-scattered electron images show that the biotite from sample RP-36 has intergrown chlorite. Lo and Onstott (1989) reported complex age spectra similar to those shown in Figure 9b from chloritized biotite. In accord with Lo and Onstott's (1989) model, the anomalously old age for the intermediate steps from RP-36 biotite probably reflects recoil of ^{39}Ar into chlorite, which during step heating is released first, leaving the sample enriched in $^{40}\text{Ar}^*$. The $^{40}\text{Ar}^*$ is released at intermediate temperatures steps, yielding old apparent age. Lo and Onstott (1989) advocate the use of total gas ages for recoil-affected biotite; however, the total gas age for RP-36 is ~1270 Ma, younger than the other mica ages, and may reflect partial argon loss during metasomatism.

Ages vary between 1199 and 1267 Ma for 11 heating steps of RP-87 muscovite and yield a calculated weighted mean age of 1229 ± 15 Ma. The high MSWD of ~98 emphasizes the high degree of scatter observed in the age spectrum. All of the steps have

high radiogenic yields and relatively constant K/Ca. The muscovite from RP-87 yields a younger age than any other mica in this study. Previous in-situ laser analysis of muscovite from slowly cooled terranes and samples affected by multiple events have yielded complex ages, due to a non-uniform spatial distribution of $^{40}\text{Ar}^*$ (Hames and Hodges, 1993; Hodges et al., 1994). During step-heating analysis, the complex argon distribution is often variably homogenized resulting in age spectra that could range from nearly flat (Hodges et al., 1994) to approximately representative of the true gradient (Heizler and Ralser, 1994; Heizler et al., 1997). The undulatory age spectrum of RP-87 is believed to be caused by partial homogenization of spatially varying concentrations of argon. Spatially constrained younger ages could be the result of partial argon loss during reheating or fluid flux. Other reasons for its complex age spectrum could be recoil artifacts caused by impurities, or intergrowths of chlorite or biotite. The muscovite from RP-87 appeared free of impurities under the binocular microscope after separation. In thin section, however, it displays undulose extinction, remains locally extinct and possesses intergrown biotite and chlorite. The age spectrum does not seem to show the effects of these mixed phases, as the K/Ca is similar to muscovite from sample RP-34. As mentioned above, zones where muscovite stays extinct with rotation of the microscope stage are interpreted to be zones of intracrystalline cataclasis, causing changes in crystallographic orientation. Goodwin and Renne (1991) reported anomalously old biotite $^{40}\text{Ar}/^{39}\text{Ar}$ ages where recoil redistribution had taken place between undeformed biotite and zones of intracrystalline cataclasis. Older ages within the age spectrum could result from the release of argon from ^{39}Ar -depleted sites. The low overall age of sample RP-87 could be a combination of recoil redistribution, biotite

degassing and a spatially heterogeneous argon distribution, which is homogenized during furnace step heating. RP-87's $^{40}\text{Ar}/^{39}\text{Ar}$ age is therefore not considered further.

VII. DISCUSSION AND SUMMARY

Different lithologic units in the Rosilla Peak 7.5-minute quadrangle have a mylonitic foliation (S_2) that is similar in both intensity and orientation. It extends across the contact between the oldest unit, the 1720 Ma Jones Rhyolite Complex, and the youngest unit, the 1480 Ma Macho Creek granite, indicating that it is younger than the granite. In the Windy Bridge tonalite, S_2 contains intrafolial folds and isoclinally folded and transposed S_1 foliations, which either record progressive deformation or overprinting of a pre-existing foliation. Variations in orientation of gneissic foliation, however, record folding at a larger scale, indicating that the overprinting interpretation is correct (Figure 5b). This relict foliation is not preserved in the other rock units, but I infer that it was present and was transposed into the younger S_2 foliation, whereas it was never present in the Indian Creek granite. The reason that the metavolcanic and metasedimentary rocks of the Jones Rhyolite Complex did not preserve S_1 is unclear. A difference in degree of development of S_2 between these rocks and the Windy Bridge tonalite could be due to differences in rheology. The tonalite is 40-50% plagioclase feldspar and should be relatively strong; the finer grained rocks of the Jones Rhyolite Complex might be weaker. The sole fabric preserved in the ca. 1650 Ma Indian Creek granite is interpreted to be S_2 , suggesting that S_1 formed after crystallization of the Windy Bridge tonalite at 1718 ± 5 Ma but prior to ca. 1650 Ma. This is similar to Bauer and Williams' (1994) interpretation

of relationships in the Magdalena Mountains, which suggest 1664 – 1654 Ma Mazatzal age deformation. Several possibilities in addition to post-tectonic intrusion could explain the absence of the gneissic S_1 foliation in the Indian Creek granite. During the younger deformation strain was perhaps partitioned into discrete zones in the tonalite, preserving the older foliation in the mechanically strong regions, but not in the Jones Rhyolite and the Indian Creek granite. A third alternative is that more detailed mapping in the Windy Bridge tonalite allowed me to distinguish folds at different scales, whereas less detailed mapping elsewhere, including poor outcrop exposure in the eastern map area, caused them to be missed.

The extension lineation associated with the mylonitic foliation trends southwest with kinematic indicators recording a component of extension as well as a component of right-lateral strike-slip shear parallel to that lineation. The timing of this transtension is bracketed between the crystallization age of the deformed ca. 1480 Ma Macho Creek granite and the 1372 Ma $^{40}\text{Ar}/^{39}\text{Ar}$ age of late syn- to post-kinematic hornblende.

Several authors have speculated on the nature of 1.4 Ga deformation and metamorphism; nearly all have concluded that NNE-SSW extension occurred during 1.4 Ga deformation (e.g. Nyman et al., 1994). Using three plutons in the southwestern U.S., Nyman et al. (1994) showed N-S extension on SW-striking foliation planes, recorded by NNE plunging extension lineations. Kinematic indicators in Nyman et al. (1994) show dextral movement, consistent with transtension. In New Mexico, Kirby et al. (1995) reported top-to-the-NW extension using sinistral, normal kinematic indicators in the 1420 Ma Sandia pluton. Both a magmatic foliation in the pluton and a crenulation cleavage in the metamorphic aureole strike moderately to steeply NE with a stretching lineation that

plunges steeply to the NW and undeformed dikes that strike both NE and NW. This is similar to Grambling and Dallmeyer (1993), who proposed top-to-the-southeast extension, with dextral motion on a NE-striking decollement in northern New Mexico. Each of these studies presented kinematic histories that are consistent with regional transtension. In contrast, ca. 1450-1400 Ma, top-to-the-west reverse shearing with a small sinistral component on NNE-striking foliation planes, as reported by Marcoline et al. (1999) in the Manzano Mountains of central New Mexico, suggests north-directed contraction.

The current data are compatible with Grambling and Dallmeyer's (1993) idea of regional extension at 1.4 Ga, but suggest a component of top-to-the-southwest normal, and dextral strike-slip shearing on south-dipping foliation planes. The variation in kinematics might be an expression of transtension on variably oriented shear zones and foliation planes. Regional dextral transtension could be resolved into northeast-directed extension.

Minerals indicative of metamorphic grade are rare in granitoids, but petrographically distinct amphiboles both parallel to, and locally cross-cutting, the S_2 foliation in the Windy Bridge tonalite (e.g., Figure 6b) are Na-Al-Mg hornblendes, which were in equilibrium during amphibolite facies conditions. It is significant that the amphibole locally crosscuts the foliation, indicating that metamorphism outlasted deformation. The composition of recrystallized feldspars in equilibrium with the hornblende suggests temperatures close to 610 – 700°C (at $P_{H_2O} = 7$ kbar; Apter and Liou, 1983), very similar to conditions of metamorphism calculated by Daniel (1995) for the Santa Fe Range to the west, across the Picuris-Pecos fault (see part II). K-feldspar grains are locally bordered

by myrmekite, which are also consistent with amphibolite facies conditions.

Temperatures were therefore high enough ($>500^{\circ}\text{C}$) during 1.4 Ga deformation in the study area that feldspar recrystallized to smaller, aligned grains, locally forming S-C structures that record dextral strike-slip shear (Figures 4a, 6c, 6d, and 7a). Retrograde metamorphism followed deformation as indicated by local epidote and chlorite alteration. Since amphiboles provide evidence that prograde metamorphism outlasted deformation it is puzzling that retrograde chlorite is locally aligned within S_2 (Figure 6b). Perhaps deformation was possible in local, relatively fluid-rich areas, but not in fluid-poorer areas.

$^{40}\text{Ar}/^{39}\text{Ar}$ hornblende ages record cooling through $\sim 500^{\circ}\text{C}$ at ca. 1373 Ma. Well-defined plateau ages for RP-34 muscovite and RP-28B biotite of 1345.2 ± 1.7 Ma and 1341.8 ± 3.3 Ma, respectively, record the time of cooling through $325 - 400^{\circ}\text{C}$. The concordance probably reflects the similarity of the muscovite and biotite T_c 's rather than rapid cooling at 1345 Ma. The muscovite and biotite ages are indistinguishable within error, and since the closure temperature for muscovite is higher than biotite, the closeness of the ages suggests rapid cooling. The cooling rate estimated from these hornblende and mica ages is $\sim 5^{\circ}\text{C}/\text{Ma}$, faster than the $<1^{\circ}\text{C}/\text{Ma}$ estimated by Hodges et al. (1994) for the same time period in Arizona. However, Hodges et al. (1994) noted that micas can have large age gradients, which, when homogenized during $^{40}\text{Ar}/^{39}\text{Ar}$ step heating, can yield a meaningless flat plateau. Laser spot-fusion analyses were not performed for this study, but might detect such age gradients, especially in the large muscovite from RP-34.

$^{40}\text{Ar}/^{39}\text{Ar}$ ages of 1.4 Ga in New Mexico have been interpreted to be evidence for either reheating at 1.4 Ga (e.g., Brown et al., 1999) or amphibolite facies metamorphism

associated with regional deformation (e.g., Marcoline et al., 1999). This is because $^{40}\text{Ar}/^{39}\text{Ar}$ ages cannot be used to distinguish between relict minerals that were 'reset' above their closure temperature and new metamorphic minerals. However, the 1.4 Ga U-Pb monazite electron microprobe ages from aligned inclusions in metamorphic minerals (Williams et al., 1999a) as well as U-Pb ages from synkinematic metamorphic minerals (Lanzirotti and Hanson, 1997) suggest contemporaneous metamorphism and regional deformation in New Mexico. The occurrence of ca. 1650 Ma $^{40}\text{Ar}/^{39}\text{Ar}$ ages (Grambling and Dallmeyer, 1993; Brown et al., 1999) suggests that 1400 Ma metamorphic temperatures were locally less than the argon closure temperature of hornblende. $^{40}\text{Ar}/^{39}\text{Ar}$ hornblende and mica ages determined in this study are comparable to ages obtained by Karlstrom et al. (1997), but are taken to record cooling after 1.4 Ga metamorphism and deformation. Hornblende from sample WB-23 crosscuts the S_2 mylonitic foliation, indicating post-tectonic mineral growth. The 1374 ± 12 Ma age of this sample thus dates post-tectonic cooling.

Delicate microstructures have survived cooling from amphibolite facies after 1.4 Ga. Cooling at a rate of $\sim 5^\circ\text{C}/\text{Ma}$ to $\sim 325^\circ\text{C}$ could potentially preserve the microstructures found in these rocks. This is independent evidence of 1.4 Ga deformation as opposed to Mazatzal age deformation. Microstructures produced during ca. 1650 Ma Mazatzal deformation and metamorphism could not have survived mid-crustal residence followed by renewed amphibolite facies deformation and metamorphism at 1.4 Ga (cf. Ralser, 2000).

VIII. CONCLUSIONS

Proterozoic basement rocks of the southern Sangre de Cristo Mountains have experienced two ductile tectonic events, D₁ and D₂ (see Figure 10). The oldest basement rocks are the 1720 ± 15 Ma Jones Rhyolite Complex, consisting of locally mylonitic Proterozoic metasedimentary and metavolcanic rocks that were intruded by the 1718 ± 5 Ma Windy Bridge tonalite. Geochemical studies suggest that the rocks coevolved in a back-arc setting (Robertson and Condie, 1989). The tectonic setting for D₁ deformation was probably in the collisional belt between the arc and the southern North American margin prior to intrusion of the 1650 Ma Indian Creek granite. An isoclinally folded and transposed S₁ foliation is observed only in the Windy Bridge tonalite, but is inferred to have originally existed in the rocks of the Jones Rhyolite Complex. Intrusion of the Indian Creek granite occurred post-D₁, as the only fabric preserved in the Indian Creek granite is mylonitic and is interpreted to be S₂.

The 1480 Ma Macho Creek granite does not have a magmatic foliation, suggesting it did not intrude during deformation. However, in some areas it possesses a mylonitic S₂ foliation characterized by the layering of ductily deformed feldspar, domains of recrystallized quartz, and aligned mica. Locally, hornblende cross-cuts S₂. Similar mylonitic fabrics with consistent kinematic indicators are found in the Jones Rhyolite Complex, the Windy Bridge tonalite, and the Indian Creek granite. D₂ records dextral strike-slip shearing with a component of normal, south-down shearing on ENE-striking foliation planes. It is constrained to be younger than the 1480 Ma mylonitized Macho Creek granite, but older than 1372 Ma, the ⁴⁰Ar/³⁹Ar cooling age of post-tectonic

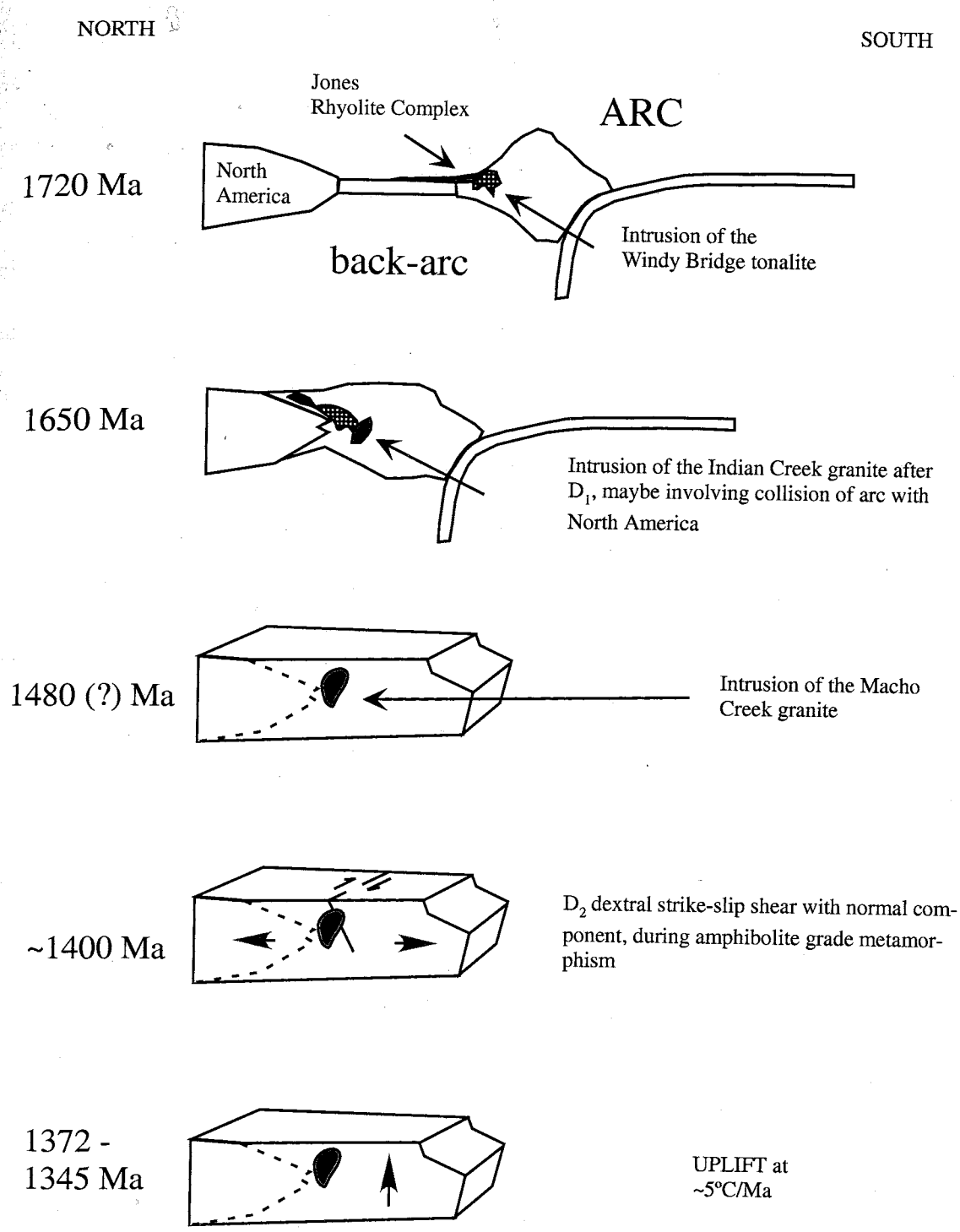


Figure 10. Schematic cross section of part of the Proterozoic southern North American crust affected by deformation, metamorphism and plutonism. Arrows show sense of motion on faults and relative motion of the crustal block.

hornblende in the Windy Bridge tonalite. Kinematic indicators suggest that dextral transtension could be resolved into a component of NE-SW extension in the study area, consistent with other studies in Proterozoic rocks of New Mexico. Metamorphism at 1400 Ma reached amphibolite facies and generally outlasted D₂ deformation, but was followed locally by retrogression to greenschist facies and local ductile deformation. Based on mineral cooling ages from ⁴⁰Ar/³⁹Ar analyses, cooling from 500°C at 1372 Ma to ~350°C at 1343 Ma occurred at a rate of approximately 5°C/Ma.

**$^{40}\text{Ar}/^{39}\text{Ar}$ K-FELDSPAR THERMOCHRONOLOGIC CONSTRAINTS ON THE
BRITTLE TECTONIC AND UPLIFT HISTORY OF THE SOUTHERN SANGRE
DE CRISTO MOUNTAINS, NORTHERN NEW MEXICO SINCE 1100 MA**

IX. INTRODUCTION

The Neogene Rio Grande rift in New Mexico exposes north-trending uplifts of Proterozoic basement (Figure 11) capped by Carboniferous sedimentary sequences; the uplifts preserve as much as ca. 1.7 billion years of Earth history. Studies of the basement geology in the uplifts north and east of Santa Fe, including the Sangre de Cristo Mountains, have focused on the record of three Early and Middle Proterozoic orogenies (e.g., Williams et al., 1999a), but the Late Proterozoic through Phanerozoic record is limited. Thus this period of time has been informally referred to as a “thermochronological void” (Heizler, 1998). Our lack of knowledge of this time period is unfortunate because numerous north-striking faults, including the Picuris-Pecos fault, are believed to have been episodically active since the Late Proterozoic (Sutherland, 1963b; Bauer and Ralser, 1995; Karlstrom and Humpreys, 1998). The purpose of this paper is to document brecciation, metasomatism and exhumation that took place during this “thermochronological void” in the southern Sangre de Cristo Mountains using a combination of structural analysis and $^{40}\text{Ar}/^{39}\text{Ar}$ analysis of K-feldspar.

Thermochronology allows rock cooling histories to be determined, and can therefore be used to identify differences in the timing of exhumation of fault blocks and provide constraints on the timing of vertical movement (e.g. Fillipone et al., 1995; Dunlap and Fossen, 1998). K-feldspar $^{40}\text{Ar}/^{39}\text{Ar}$ thermochronology can resolve a significant portion of the low-temperature thermal history. Multi-diffusion domain theory (MDD; Lovera et al., 1989) is based on the assumption that K-feldspar grains consist of discrete diffusion domains. From the laboratory heating schedule and measured loss of ^{39}Ar , the kinetic

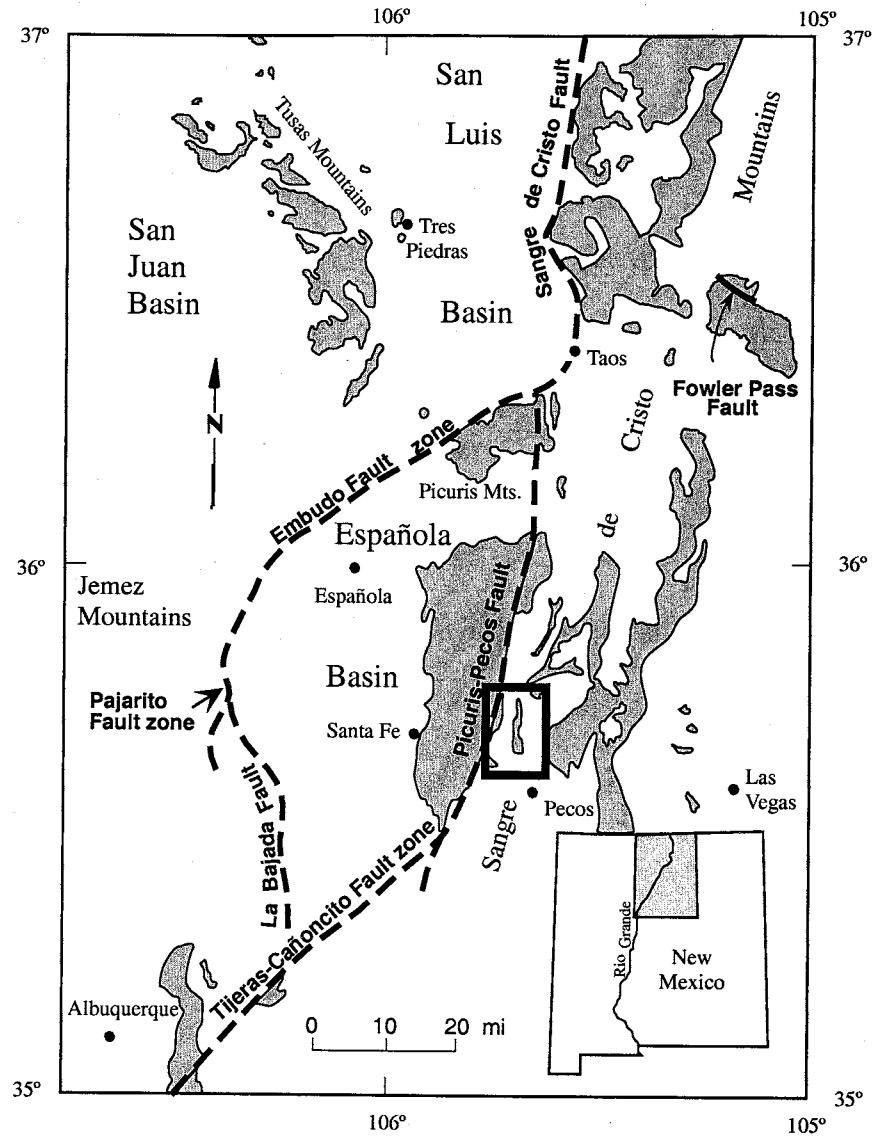


Figure 11. Map of north-central New Mexico showing the location of key faults and Proterozoic basement uplifts flanking the Neogene basins of the Rio Grande rift (adapted from Bauer and Ralser, 1995). Thick-lined box contains area shown in Figure 2.

parameters of each domain can be estimated. This information together with the age spectrum allows retrieval of the thermal history.

The domains of different sizes have a range in closure temperatures (T_c) and thus can typically provide constraints on the temperature evolution of a K-feldspar sample from 350 – 125°C (e.g. Richter et al., 1991). The temperature for volume diffusion in K-feldspar thus lies between the closure temperature of micas (~350°C; McDougall and Harrison, 1999) and the annealing temperature for apatite fission tracks (AFT; 60-120°C; Naesar, 1979). The ages of the youngest micas and the oldest AFTs in the southern Sangre de Cristo Mountains are a billion years apart (Heizler, 1998). The thermal history of MDD modeling of K-feldspar $^{40}\text{Ar}/^{39}\text{Ar}$ step heating data can potentially resolve exhumation from ca. 1000 Ma (youngest $^{40}\text{Ar}/^{39}\text{Ar}$ mica ages; Karlstrom et al., 1997) to uplift in the Cenozoic (AFT thermochronology; Kelley et al., 1992; Kelley and Chapin, 1995).

My research shows that contemporaneous brecciation and potassium metasomatism occurred within subvertical, north-striking fault zones between 1345 and 1050 Ma. The timing of faulting and alteration is bracketed by $^{40}\text{Ar}/^{39}\text{Ar}$ mica and K-feldspar cooling ages, suggesting that deformation was associated with ca. 1100 Ma Grenville tectonism. K-feldspar growth and rapid uplift at ca. 800 Ma could relate to rifting during the breakup of Rodinia. The thermal histories across three structural blocks, which are separated by north-striking faults show both similarities and differences. MDD modeling of K-feldspar $^{40}\text{Ar}/^{39}\text{Ar}$ step-heating data constrained by geology indicate that during the Late Proterozoic, all basement rocks cooled at a similar, accelerated rate between 1050 and 800 Ma. Samples show differences in their timing of exhumation prior to sedimentation

in the Early Mississippian as well as possible argon loss during Mesozoic burial before exhumation at 70 Ma.

X. GEOLOGIC SETTING

Parts of the Phanerozoic and Proterozoic geologic history and sedimentary record of northern New Mexico and, in particular, the southern Sangre de Cristo Mountains are well understood (e.g. Grambling and Coddling, 1982; Armstrong and Mamet, 1990; Baltz and Myers, 1999). Post-1400 Ma tectonically active periods can potentially be recognized in the thermal history and are therefore summarized below. Particular attention is given to studies concerning the movement history of the Picuris-Pecos fault, a major brittle fault in the study area (e.g. Sutherland, 1963b; Bauer and Ralser, 1995).

A. Proterozoic

$^{40}\text{Ar}/^{39}\text{Ar}$ age gradients measured in muscovite from rocks in central Arizona suggest slow cooling following equilibration to temperatures of $\sim 325^\circ\text{C}$ after the last major Proterozoic ductile deformational event at 1400 Ma (Hodges et al., 1994). Slow cooling of the Proterozoic basement is also suggested for areas that have been dated in New Mexico, where $^{40}\text{Ar}/^{39}\text{Ar}$ mica ages range from 1350 to 960 Ma and indicate closure to radiogenic argon over a long time period (Karlstrom et al., 1997).

During the Grenville Orogeny, ca. 1100 Ma, New Mexico underwent E-W extension (Grambling and Dallmeyer, 1993; Heizler et al., 1997; Karlstrom and Humphreys, 1998; Karlstrom et al., 1999). K-feldspars with age maxima of 1100 – 1000 Ma have been

reported from New Mexico Proterozoic basement rocks (Harrison et al., 1986; Harrison and Burke, 1989). Basement exhumation at 800 – 850 Ma is recorded by $^{40}\text{Ar}/^{39}\text{Ar}$ K-feldspar thermochronology, which shows either terminal ages or argon loss at this time (Harrison et al., 1986; Harrison and Burke, 1989; Heizler, 1998). This suggests either rapid cooling following re-heating or accelerated cooling, possibly related to the breakup of Rodinia (Heizler, 1998).

The breakup of Rodinia is interpreted to be characterized by the development of N-striking faults (Timmons et al., in press). Faulting may have occurred on the approximately 1-km-wide, north-to northeast-striking Picuris-Pecos fault zone at this time. The Picuris-Pecos fault has a complex history, recorded by evidence for both significant strike-slip and dip-slip displacement. Extensive, elongate breccia ridges in Proterozoic rocks locally flank the fault, and were taken to be evidence for Proterozoic brittle deformation by Bauer and Ralser (1995). Montgomery (1963) proposed pre-Carboniferous motion, but preferred Proterozoic fault motion on the basis of reorientation of Proterozoic ductile foliation into parallelism with the fault.

Regional hydrothermal alteration, characterized by potassium metasomatism, local tourmalinization, and the emplacement of pegmatites and quartz veins, post-dates the last Proterozoic ductile deformation and metamorphic event (Montgomery, 1963). Alteration did not affect Carboniferous rocks however, indicating that it possibly occurred in the Proterozoic. The exact timing of this event had not been determined prior to this study.

B. Cambrian to Mississippian

The rock record from the Cambrian to the Mississippian is limited. Cambrian syenite intrusions are believed to be related to the development of a failed continental rift in New Mexico (Loring and Armstrong, 1980; McLemore et al., 1999), and are the only evidence of Early Paleozoic igneous activity. Throughout the southwest, alkalic intrusives suggest Cambrian NNE extension (McLemore et al., 1999; McMillan and McLemore, 1999). Cambrian (?) syenite intruded Proterozoic basement about 10 km north of the study area (Klich, 1983).

Proterozoic rocks of the southern Sangre de Cristo Mountains were at the surface during the Mississippian. The Mississippian Arroyo Penasco Group lies unconformably on an Early Mississippian peneplain developed on Proterozoic basement (Armstrong and Mamet, 1990). Varying thicknesses of the Arroyo Penasco Group have been attributed to deposition along fault scarps and in valleys adjacent to the Picuris-Pecos fault (Sutherland, 1963a). East-side-down motion on the Picuris-Pecos fault was inferred from this thickness variation.

C. Latest Mississippian – Early Permian

Latest Mississippian to early Permian sedimentation in the Taos trough (Rowe-Mora basin of Read and Wood, 1947; Kluth and Coney, 1981) occurred during the development of the Ancestral Rocky Mountains (Baltz and Myers, 1999), when deformation was characterized by contractional uplifts associated with basins far inboard of a plate margin (e.g. Ye et al., 1996). Representative of one of these uplifts is the

Uncompahgre uplift in northern New Mexico (Ancestral Brazos uplift of Baltz and Myers, 1999), which was bound on the east by the Picuris-Pecos fault (Sutherland, 1963a). Depths to Proterozoic basement after burial may have exceeded 5 km in the Taos trough (Dickerson, 1984). Sutherland (1963a) envisioned three dip-slip events on the Picuris-Pecos fault during the Carboniferous based on the depositional history of the area, as well as at least 500 m of east-side-down slip since Carboniferous time. Sediments from the Uncompahgre uplift were also shed south onto a limestone platform, named the Pecos shelf. Situated between the Uncompahgre uplift to the north and the Pedernal uplift to the south, the Pecos shelf received about 3 km of Madera Formation sediments before possible erosion, followed by deposition of the Pennsylvanian-Permian Sangre de Cristo Formation (Sutherland, 1963a).

D. Late Cretaceous – Tertiary

The Late Cretaceous – Early Tertiary Laramide Orogeny produced both uplifts and basins (e.g., Coney, 1987). Movement of the relatively rigid Colorado Plateau during the Laramide Orogeny has been interpreted by some workers to have produced right-lateral strike-slip faults in northern New Mexico (e.g. Cather, 1999). The Picuris-Pecos fault is believed by a number of workers to have accommodated from 26 to 37 km of dextral strike-slip displacement at this time (Chapin and Cather, 1981; Karlstrom and Daniel, 1993; Cather, 1999). The fault has been interpreted as the center of a positive flower structure (Figure 12; Bauer and Ralser, 1995), and juxtaposes many different lithologies along strike. The proposed dip-slip motion and associated uplift along the Picuris-Pecos fault has never been rigorously investigated. However, dip-slip movement must account

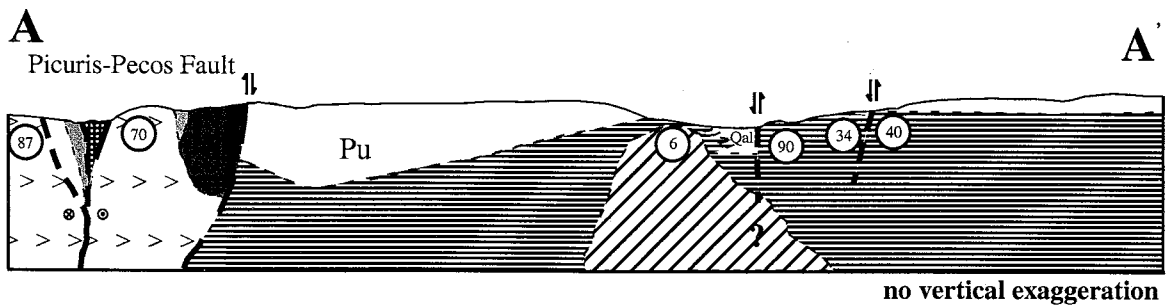
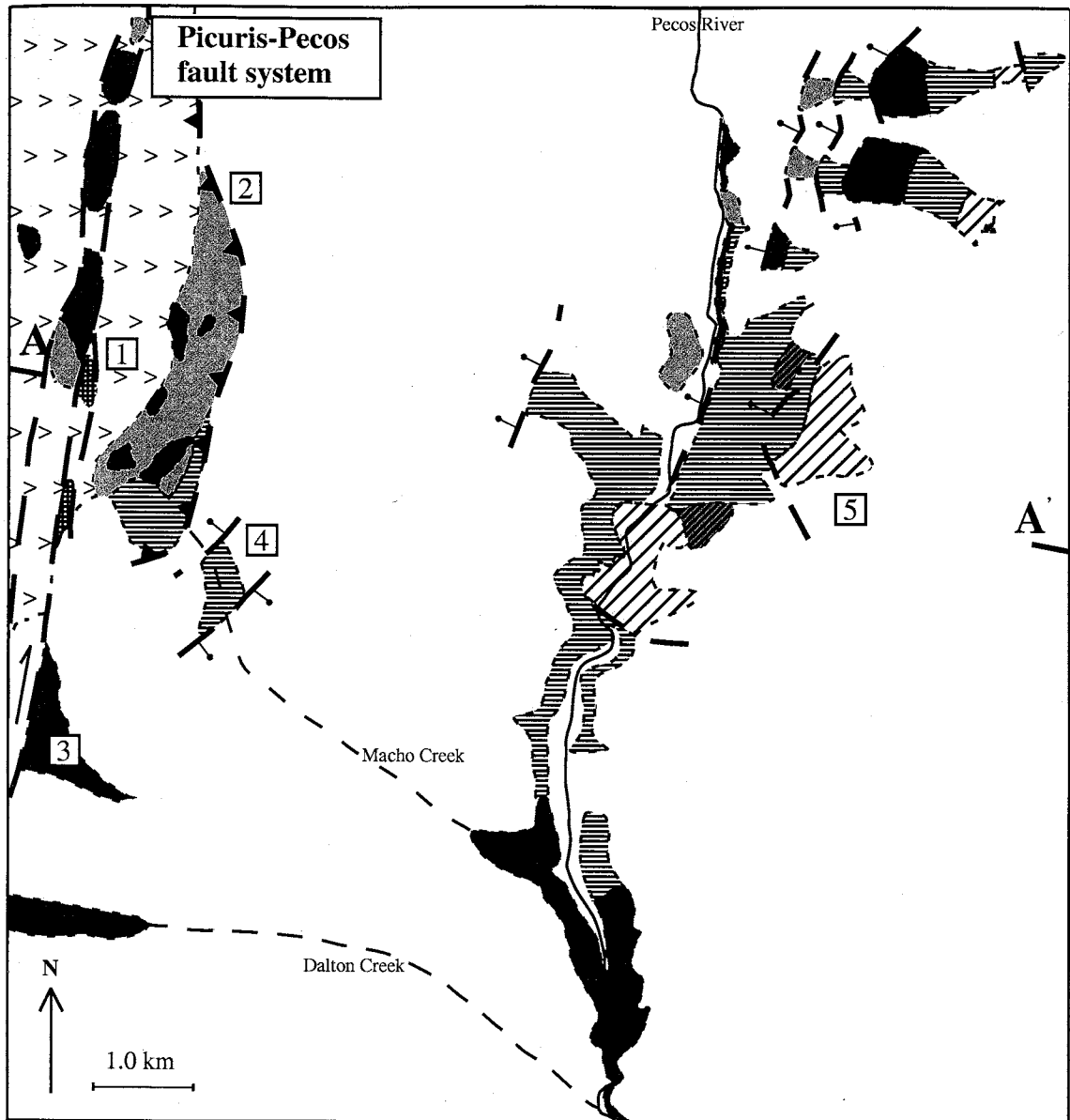


Figure 12. Proterozoic bedrock map of part of the Rosilla Peak 7.5' quadrangle, San Miguel and Santa Fe counties. Cross-section shows locations of the six analyzed K-feldspar samples by number. Subsurface control is by projection and some borehole data. No vertical exaggeration. Numbers in squares indicate locations referred to in the text.

Explanation

Paleozoic



Undifferentiated



Madera limestone

Proterozoic



Macho Creek granite



Pecos granodiorite



Indian Creek granite



Windy Bridge tonalite

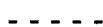
Pecos
Complex



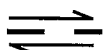
Jones Rhyolite Complex
amphibolite



Jones Rhyolite Complex
metasedimentary and metavolcanic rocks



Lithologic contact, dashed where
inferred



Fault, dashed where inferred



Strike-slip component of movement
shown with arrow. Normal compo-
nent of motion indicated by bar and
ball on the hanging wall

Figure 12 (continued). Explanation of map units.

for the juxtaposition of Carboniferous sedimentary rocks east of the fault against Proterozoic granites on the west (Sutherland, 1963b). At least 500 m of post-Paleozoic west-side-up motion is suggested (Sutherland, 1963b; Bauer and Ralser, 1995). Kelley et al. (1992) documented AFT cooling ages of 70 Ma, suggesting that the southern Sangre de Cristo Mountains were uplifted during the Laramide Orogeny. Two kilometers of Late Cretaceous denudation west of the Picuris-Pecos fault is probable, which translates to a cooling rate of 3-4°C/Ma (Kelley, 1990).

The local preservation of some Laramide AFT cooling ages in the southern Sangre de Cristo Mountains suggests that the rocks dated have not been above the annealing temperature for AFT (60-120°C) since the Late Cretaceous (Kelley, 1990). Younger AFT ages of 30-40 Ma within the Rosilla Peak 7.5 minute quadrangle (Kelley and Chapin, 1995) could have been caused by local elevated heat flow adjacent to dikes intruded during initiation of the Rio Grande rift (Melis et al., 2000).

XI. METHODS

A. Sample preparation

Six rock samples spanning structural boundaries, including the Picuris-Pecos fault, were selected for $^{40}\text{Ar}/^{39}\text{Ar}$ age spectrum analysis. These samples, collected from three Proterozoic plutons and a pegmatite, were crushed, washed and sieved. Felsic material was separated using a Franz magnetic separator. K-feldspars were first concentrated by floatation using heavy liquids, then purified by handpicking under a binocular microscope. Size fractions of separates varied from greater than 1000 μm for

the pegmatite (RP-34) to less than 100 μm for metasomatized tonalite samples (RP-40B and RP-90).

Samples weighing 1-2 mg were loaded in individual holes in aluminum trays along with flux monitor Fish Canyon tuff (FC-1) 27.84 Ma relative to 520.4 Ma for sample MMhb-1 (Cebula et al., 1986; Samson and Alexander, 1987). The trays were irradiated at the University of Michigan Ford Reactor in two irradiation packages (NM-84 and NM-102) for 50 and 100 hours, respectively.

B. Analytical procedure: staining and electron microprobe

To aid in $^{40}\text{Ar}/^{39}\text{Ar}$ age interpretation, K-feldspars were carefully checked for compositional homogeneity and inclusions with a Cameca SX-100 electron microprobe. Back-scattered electron (BSE) images were checked for grain shape, compositional variation, alteration, and incorporation of other potassium-bearing phases. A potassium X-ray map of grains of sample RP-90 was made over an area of 100 μm using a fixed 20nA beam current. After BSE imaging, samples were analyzed quantitatively. At least seven points were quantitatively analyzed on several grains from the same feldspar separate to obtain a statistically significant average. For quantitative analysis the beam diameter was 5 μm , accelerating voltage was 15 kV, and probe current was set at 20 nA. The degree of potassium metasomatism of tonalite samples RP-40 and RP-90 was also evaluated by exposing a polished thin-section chip to sodium cobaltinitrate, a process that highlights K-feldspar.

C. Analytical procedure: geochronology

Samples were step-heated in a double-vacuum molybdenum resistance furnace at the New Mexico Geochronology Research Laboratory (NMGRL). A tungsten filament heated the samples and the temperature was monitored by a W-Re thermocouple. The furnace temperature was calibrated to $\pm 10^\circ\text{C}$ by melting copper foil at 1083°C . Heating duration ranged from 10 minutes to 8 hours. Samples were heated in pairs of isothermal steps from 450°C until 700°C (RP-40 until 750°C) in 50°C increments, and then further step heated until 1650°C (Appendix B). Within the NMGRL system, the gas extracted enters a two-stage cleanup line. During heating in the first stage, the evolved gas is exposed to a 450°C SAES GP-50 getter. In the second stage the gas is exposed to two SAES getters, one at room temperature and one at 450°C , and a tungsten filament (at 2000°C) for a total of two minutes.

The gas is then expanded into a MAP 215-50 mass spectrometer operated in static mode. The mass spectrometer has a resolution of ~ 450 at mass 40 and isotopes are measured with an electron multiplier. Final isotopic intensities are determined by linear regression to time zero of the peak height plotted against analysis time. Each mass intensity is corrected for mass spectrometer baseline, background and system blank. The electron multiplier sensitivity was $\sim 2 \times 10^{-16}$ mol/pA. The total ^{40}Ar system blank ranged from 6.4×10^{-17} to 1.7×10^{-15} moles (3.4×10^{-16} moles average) during the K-feldspar runs. Uncertainties for the age determinations are quoted at one-sigma (1σ) and do not include the error in the J-factor. J is a measure of the fast neutrons dosage a sample receives during irradiation, which is necessary for $^{40}\text{Ar}/^{39}\text{Ar}$ age calculations. The J-

factor was determined to a precision of 0.10% by the total fusion analysis of four flux monitors per hole and four monitors per tray using either a 10 or 50W Synrad CO₂ laser.

XII. BRITTLE DEFORMATION AND ASSOCIATED METASOMATISM

A. Faulting and brecciation

In the Rosilla Peak 7.5 minute quadrangle, the Picuris-Pecos fault is exposed in Macho and Dalton Creek canyons (Figure 12). Parallel faults form splays and separate widely different lithologic units within the fault zone. Horizontal slickenlines locally record strike-slip motion. Several hundred meters of a vertical component of motion are also recorded by the juxtaposition of Paleozoic limestone with Proterozoic gneiss.

Fault splays, marked by topographic lows and poor outcrop, bound blocks of Proterozoic metasedimentary rocks and amphibolite belonging to the Jones Rhyolite complex, as well as the Pennsylvanian Madera Formation (Figure 12) over much of the exposure of the Picuris-Pecos fault. In Macho Creek canyon, for example, a Madera Group limestone block is down-dropped in a graben (Figure 12, locality 1). Bounding faults are thought to be nearly vertical, based on outcrop pattern. A Picuris-Pecos fault splay near the Jones Mine (Figure 12, locality 2) marks the eastern edge of the fault system. A reverse fault at this locality juxtaposes Proterozoic metasedimentary rocks (west) over shales of the Madera group (east). The reverse fault dips to the west, toward the main trace of the Picuris-Pecos fault. Further east, two faults bound a tonalite horst, which has been uplifted relative to adjacent Paleozoic limestone (Figure 12; locality 4). To the south, in Dalton Creek canyon, Proterozoic amphibolite is juxtaposed against

down-dropped undifferentiated Paleozoic limestones (Figure 12, locality 3). Different Proterozoic units are also in fault contact. For example, amphibolite is present as both fault blocks and country rock that was intruded by the Proterozoic Macho Creek granite in Macho Creek canyon.

Faults east of the Pecos River, which are largely parallel to the Picuris-Pecos fault, have a dominantly down-to-the-west sense of slip. These normal faults cut Paleozoic rocks (Figure 12 cross section; locality 5), and are probably associated with Rio Grande rifting. Paleozoic strata east of the Pecos River are structurally higher than west of the river; an inferred fault within the Pecos River valley must in places, have accommodated 200 m of down-to-the-west slip. A minimum post-Pennsylvanian dip-slip separation of 430 m across one of the faults in the field area (between localities 2 and 4; Figure 12) is estimated from elevation differences between the maximum topographic high of the Proterozoic outcrop and the topographic low at the base of Macho Creek, which preserves the unconformity between Paleozoic units and Proterozoic basement. In Paleozoic units east of the main trace of the Picuris-Pecos fault, bedding is locally vertical and strikes parallel to the fault, suggesting reorientation of bedding during dip-slip motion on these high-angle faults. Paleozoic rocks are absent west of the Picuris-Pecos fault in the field area and were presumably eroded away after post-Paleozoic west-side-up motion.

The only evidence for strike-slip motion in the study area is the presence of the nearly horizontal slickenlines mentioned earlier. Slickensides suggest that motion on the Picuris-Pecos fault was dextral strike-slip shear. Minor faults in both Madera Formation rocks and Proterozoic granites adjacent to and within the Picuris-Pecos fault zone also

have sub-horizontal slickenlines suggesting post-Paleozoic strike-slip motion. The timing of strike-slip movement is otherwise unconstrained. The amount of strike-slip separation is unconstrained, as rocks juxtaposed by the Picuris-Pecos fault are typically different and piercing points are absent. The best field constraint on the timing of dip-slip fault movement is the juxtaposition of the Pennsylvanian Madera Formation against Proterozoic granites and metasediments since the Pennsylvanian.

Breccia zones in Proterozoic granites, similar to those described by Bauer and Ralser (1995), parallel the Picuris-Pecos fault and are present throughout the map area. These fault zones do not continue into the Paleozoic section, and thus represent pre-Mississippian faults. The ridges (Figure 13) stand out as conspicuously rounded, erosional remnants consisting of locally silicified and always K-feldspar metasomatized, variably brecciated country rock. East of the Pecos River, the ridges cut foliated Windy Bridge tonalite, and are especially prevalent. There the brecciated rocks (Figure 14) consist of a pinkish to white matrix of roughly sand-sized angular particles supporting poorly sorted, angular rock fragments of Windy Bridge tonalite. Angular clasts of foliated Windy Bridge tonalite up to several tens of centimeters in longest dimension are locally present. These clasts are also metasomatized. Vugs are locally present in the breccia zones, as are epidote veins. The brecciation post-dates the foliation, since foliated pieces of the Windy Bridge tonalite comprise breccia clasts. Alteration is associated with zones of fractures.

Metasomatized zones are up to hundreds of meters wide. Metasomatism is not limited to the breccia zones, but the degree of metasomatism increases with proximity to the breccias, which are consistently intensely metasomatized. This indicates that

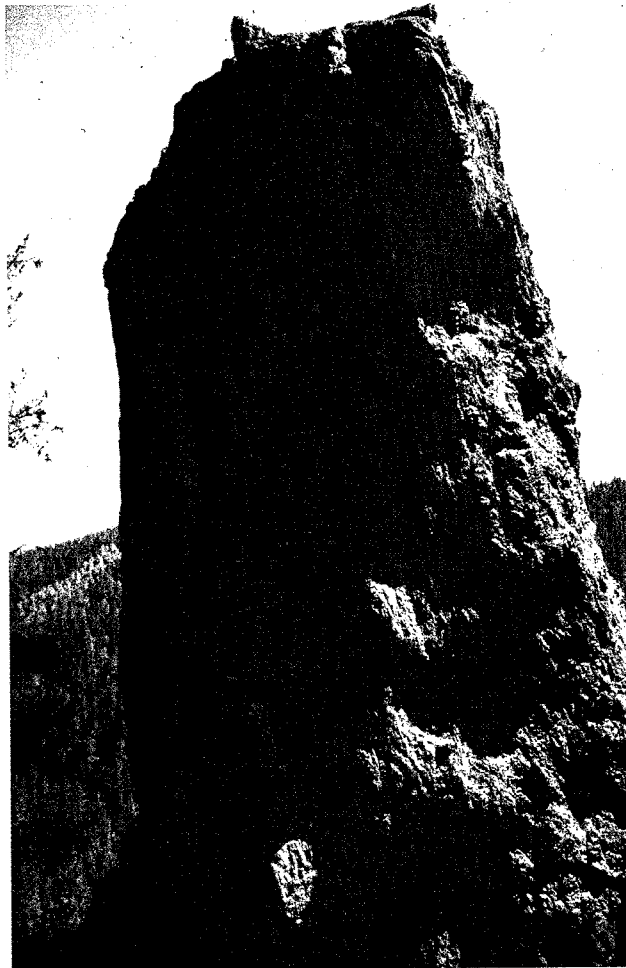


Figure 13. Tabular breccia ridge west of and parallel to the Picuris-Pecos fault. Ridge is a ~10 m tall erosional remnant, and consists of metasomatized and brecciated country rock.



Figure 14. Breccia in Windy Bridge tonalite. Pencil is about ~15 cm long.

metasomatism post-dated or was locally associated with brecciation. However, brecciation locally post-dated or outlasted metasomatism, since metasomatic K-feldspar is locally fractured and associated tourmaline is locally boudinaged. Brecciation and metasomatism were thus locally contemporaneous, but also independent of each other.

B. Metasomatism

In the Windy Bridge tonalite, metasomatic zones are irregularly developed but sub-parallel to the northeast-striking regional foliation. A gradient from slightly to completely altered tonalite can be seen with increasing proximity to breccia zones (Figure 15 a-c). Metasomatism, like brecciation, does not extend into the Carboniferous rocks that unconformably overlie the Proterozoic basement. In metasomatized rock, oligoclase has altered to orange-pink orthoclase. Regardless of the degree of metasomatism, a foliation defined by distinct elongate quartz eyes and ribbons makes identification of the parent tonalite possible. One-to-three-meter-wide aplite dikes are present within some ridges (Figure 15d). These fine-grained dikes consist of K-feldspar, quartz and plagioclase feldspar. They locally crosscut the dominant foliation in the country rock, but are also locally foliated.

Metasomatic K-feldspar is difficult to distinguish petrographically from plagioclase. K-feldspar staining was therefore used to determine the degree of metasomatism and evaluate structural controls on metasomatism within selected samples. Even tonalite that appears macroscopically to be unaltered has up to 10% K-feldspar localized along foliation planes. Strongly metasomatized tonalite consists of aphanitic K-feldspar, which has replaced most of the biotite and quartz, as well as plagioclase feldspar (Figure 15c).

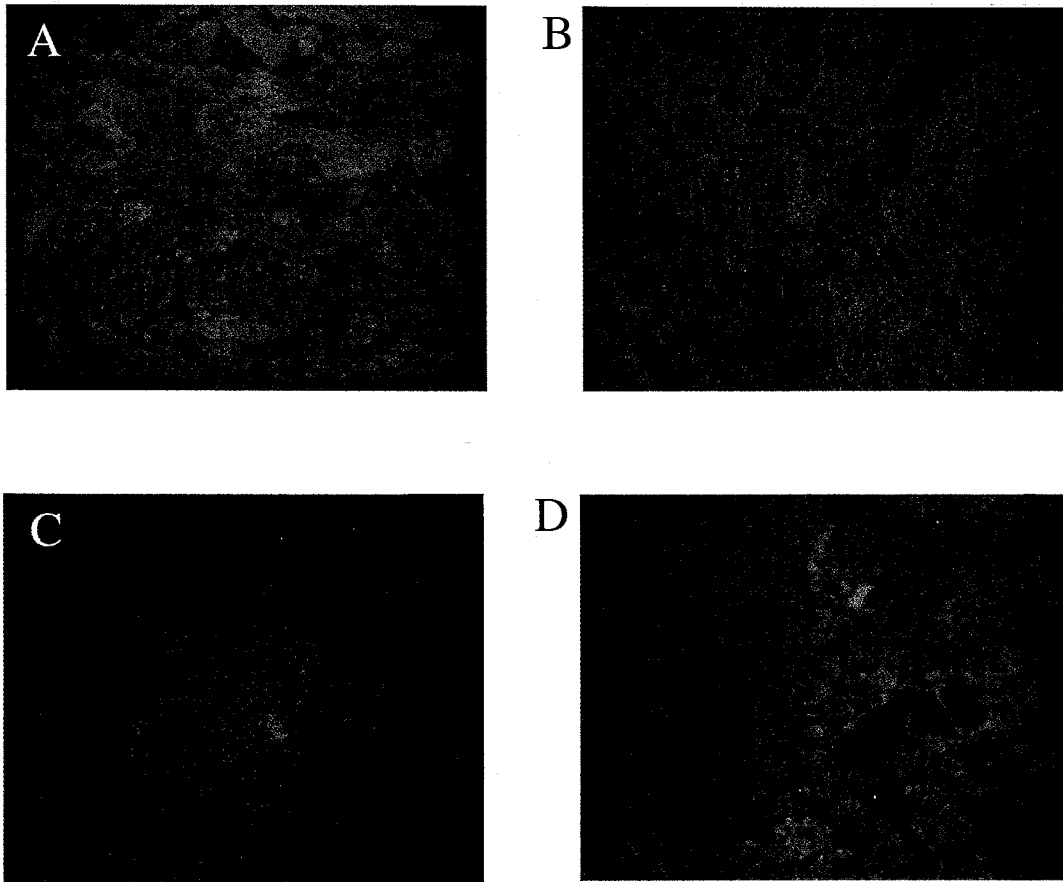


Figure 15. Stained slabs of Windy Bridge tonalite; the horizontal axis is 1.5 cm. Oligoclase is white, quartz is grey and yellow-orange stain denotes K-feldspar. Reddish stains are sericite alteration in feldspar. A. Poorly foliated, partially altered sample. About 20% of the oligoclase has been altered to K-feldspar. B. Well-foliated altered sample with up to 80% of the plagioclase replaced. C. Extensively altered tonalite in which much of the rock has been replaced by K-feldspar. Foliation is only visible as narrow quartz ribbons from top to bottom. Note shear fractures that cut foliation. D. Aplite dyke on the left of the image in contact with partially altered, nonfoliated tonalite on the right.

A partially altered sample, RP-40, and a strongly altered and brecciated sample, RP-90, were analyzed with an electron microprobe. X-ray maps show that the margins between K-feldspar and orthoclase are abrupt (Figure 16). Mineralogical and structural boundaries, such as grain boundaries or internal cracks, localize the metasomatism at the grain scale. At a larger scale, fold hinges and foliation-parallel domains of recrystallized plagioclase are typically more altered than matrix plagioclase. In a number of areas, the degree of metasomatism appears to be directly related to the intensity of foliation developed. Locally, vugs are present in the metasomatized breccias, suggesting shallow conditions that permitted dilation during brecciation.

XIII. K-FELDSPAR THERMOCHRONOLOGY

A. Multi-Diffusion Domain theory

Concepts of Multi-Diffusion Domain (MDD) theory (Lovera et al., 1989) using K-feldspar kinetic data were utilized for thermal modeling. MDD theory (Lovera et al., 1989) is a modification of the closure temperature (T_c) concept (Dodson, 1973). Closure temperature is the temperature above which a mineral diffuses appreciable argon. Below the closure temperature $^{40}\text{Ar}^*$, produced from the decay of ^{40}K , accumulates within the crystal lattice. Based on the observation that K-feldspars usually have temperature-dependent, nonlinear Arrhenius relationships, Lovera et al. (1989) suggested that K-feldspars have variable diffusion domain sizes (diffusion length scales). The domains have a range of closure temperatures since argon diffusing out of a large domain has to travel farther relative to a small domain before it reaches a diffusion boundary. K-

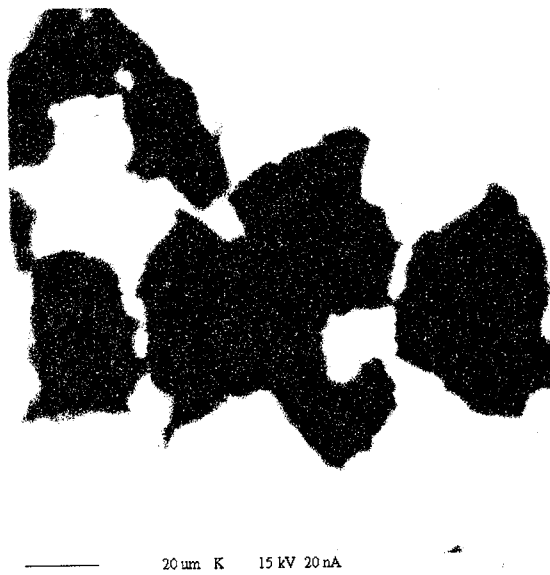
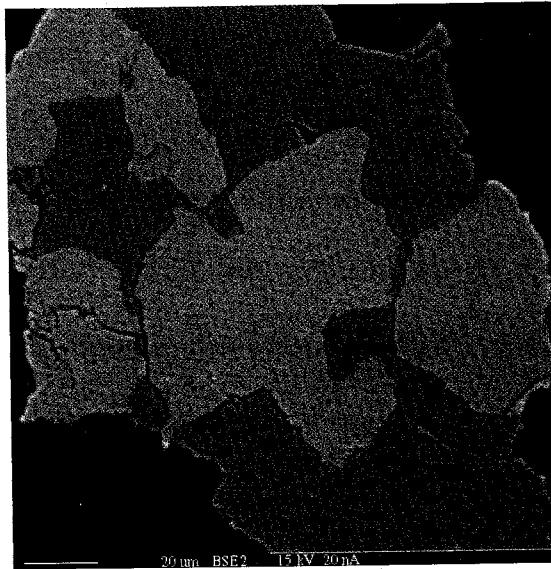


Figure 16. Back-scattered electron microprobe image and false color potassium map of RP-90, an altered Windy Bridge tonalite. Note the crisp, sharp boundaries of K-feldspar against oligoclase.

feldspars, which typically have domains with several orders of magnitude size differences, are shown to have closure temperatures from ~150 – 350°C (e.g. Lovera et al., 1997).

In order to utilize MDD theory, accurate measurements of the argon kinetic parameters and age spectra are required. The collection of meaningful diffusion data for deciphering a thermal history from K-feldspar is aided by its structural stability during incremental step-heating (McDougall and Harrison, 1999). Elucidating the thermal history depends largely on the assumption that argon loss both in the laboratory and in nature occurs by volume diffusion. Also, the release of argon from a K-feldspar crystal lattice must utilize the same pathways under both natural and laboratory conditions. Meaningful kinetic parameters, and thus thermal histories, can only be obtained if the above assumptions are true.

Current controversies over the use of MDD theory to model K-feldspar argon data center on the possible modification of the geometry, size, and boundaries of diffusion domains without a change in the $^{40}\text{Ar}^*$ concentration (e.g. Parsons et al., 1999). Possible modifying agents include diagenetic processes and/or metasomatism below the argon closure temperature, which may homogenize diffusion domains (e.g. Parsons et al., 1999). In many cases, the assumptions behind MDD theory appear to be valid, because calculated thermal histories are consistent with other thermochronometers (e.g. AFTs) and internally consistent, geologically relevant results are often obtained (e.g. Hoisch et al., 1997; Warnock and Zeitler, 1998).

Excess argon released during step heating can compromise the usefulness of K-feldspar $^{40}\text{Ar}/^{39}\text{Ar}$ thermochronology, as it results in anomalously old ages, which have

no meaning. Excess argon could be held in fluid inclusions (Harrison et al., 1993), anion vacancies in the K-feldspar crystal lattice (Harrison and McDougall, 1981) or in cation sites within large diffusion domains (Forster et al., 1990). Argon in the latter two sites is preferentially released at high temperatures during furnace heating (McDougall and Harrison, 1999), while fluid inclusions degas at low temperatures (Harrison et al., 1993).

B. Sample descriptions

The Picuris-Pecos and Pecos River faults, both of which have significant dip-slip separation, divide the study area into three structural blocks. K-feldspar samples collected across the faults were grouped considering only the shapes of their respective age spectra and minimum to maximum ages, as discussed in the following sections. It subsequently became evident that the groups corresponded to the structural blocks. Sample locations and descriptions are given from west to east in Figure 12, Table 4, and Appendix B.

Sample RP-87 was collected 100 m west of the Picuris-Pecos fault (Figure 12). Rocks near the sample locality are extensively fractured. K-feldspar crystals in the separate are also fractured, cubic, subhedral, and up to 1 mm in length. K-feldspar crystals display deformation twins in thin section. The electron microprobe revealed no alteration and only a few apatite and iron oxide inclusions.

Two samples (RP-70 and WB-6) were collected east of the Picuris-Pecos fault and west of the Pecos River within the middle structural block (Figure 12). RP-70 is a sample of megacrystic Macho Creek granite with euhedral K-feldspar crystals up to 1.5 mm in size. BSE imaging shows that grains contain iron-oxide impurities, irregular

Table 4. Sample locations and descriptions

Sample locality	Unit	UTM	Lithology
RP-87 West of P-P fault, north of Macho Creek Canyon	Macho Creek granite	3955900	433050 granite
RP-70 East of P-P fault, in Macho Creek Canyon	Macho Creek granite	3951743	433165 coarse granite
WB-6 West shore of Pecos River, south of Indian Creek Canyon	Indian Creek granite	3951153	438182 granite
RP-90 East of Pecos River	altered Windy Bridge tonalite mylonite	3952460	438920 highly metasomatized tonalite mylonite
RP-34 East of Tres Lagunas, 20m below Great Unconformity	Proterozoic pegmatite	3953100	439600 cross-cutting (?) pegmatite
RP-40 East of Tres Lagunas	Windy Bridge tonalite	3952350	439300 metasomatized tonalite

oligoclase domains up to 50 μm in largest dimension, and 20 μm wide pits. WB-6 (nonfoliated Indian Creek granite) was collected further east on the west bank of the Pecos River, 120 m below the Early Mississippian unconformity. Anhedral K-feldspar crystals appear broken along irregular fractures, and also contain albite. The feldspar separate is only 50% pure; the other half of the separate is plagioclase. K-feldspar crystals are ~ 200 μm in size and have abundant round quartz inclusions.

Three samples were collected east of the Pecos River (Figure 12). Sample RP-34 was taken 20 m below the unconformity, at an elevation of 2633 m, from a pegmatite that intruded the Windy Bridge tonalite. This sample has large, euhedral K-feldspar crystals, some of which are rimmed by albite. Only crystals 2 mm and smaller in size were dated. Samples RP-40 and RP-90 were collected from metasomatized Windy Bridge tonalite mylonite about 200 m below the Mississippian unconformity. In RP-40 K-feldspar grains are ~ 300 μm in size, anhedral, and contain no impurities. The K-feldspar separate from sample RP-40 is impure and contains up to 50% oligoclase (Figure 15a). RP-90 is more metasomatized than RP-40. Sample RP-90 is a breccia, which is compositionally heterogeneous and foliated with retrograde alteration of biotite to epidote and chlorite. K-feldspars from RP-90 are anhedral, and include two feldspar phases. BSE imaging of separated grains shows that fractured and altered grains ~ 500 μm in size have ~ 50 μm patchy K-feldspar sub-domains in sharp contact with oligoclase domains (Figure 16).

C. Age spectra and argon kinetic parameter determination

1. Age spectra

The six K-feldspar separates yield diverse age spectra (Figure 17), however all have Proterozoic apparent ages with gradients typical of Proterozoic New Mexico K-feldspars (e.g. Heizler, 1998). In detail, the degree and intervals of argon loss in these samples vary. All of the samples were step heated using the isothermal duplicate technique reported by Harrison et al. (1993), and samples RP-70, RP-34 and RP-40 gave alternating old and young ages during these isothermal heating steps. Old ages are thought to be caused by excess argon evolution from fluid inclusions, which degas during the first of the two isothermal heating steps (Harrison et al., 1993). Age corrections applied by Harrison et al. (1994) use the different amounts of $^{38}\text{Ar}_{\text{Cl}}$ (chlorine-derived ^{38}Ar) evolved between the isothermal steps to correct for excess argon believed to be in fluid inclusions (and therefore chlorine correlated). In this study, the Harrison et al. (1994) method corrected the measured ages to negative values. The over-correction of age indicates that the correlation of chlorine to excess argon is not one to one. The younger ages obtained from the duplicate heating steps are nevertheless more accurate, and better represent the true ^{40}Ar concentration gradient. Because the second isothermal steps are more accurate, the first isothermal steps were corrected to fall within the age gradient determined from the second steps for samples RP-70, RP-34 and RP-40 (e.g. Figure 18). Samples RP-87, WB-6 and RP-90 yield essentially 'climbing' ages during isothermal heating and appear not to be affected by excess argon (Figure 17). Because the results of this analysis indicate that the second isothermal step is not free of excess argon, caution was exercised

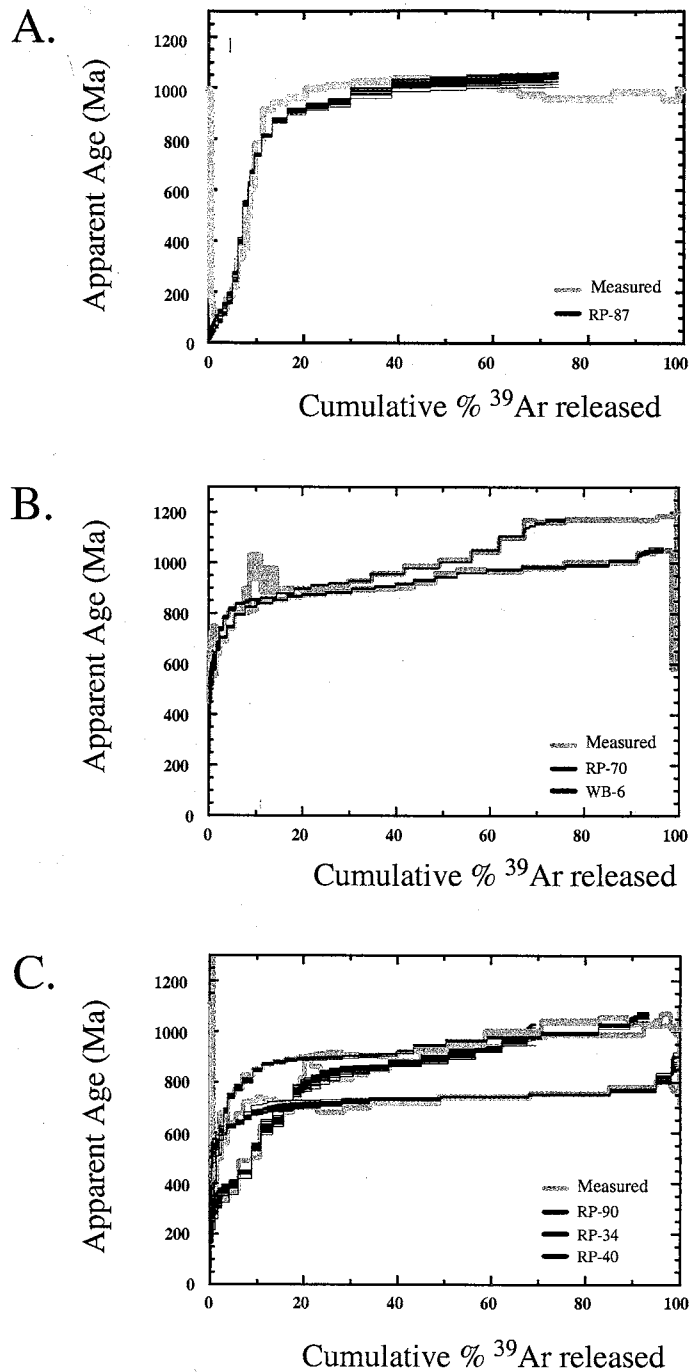


Figure 17. Compilation of feldspar age spectra (grey) and their respective modeled ages (blue, red and green). Samples are divided into three groups based on the shapes of their age profiles. A) Sample (RP-87) west of the Picuris-Pecos fault, with ages as young as ~70 Ma. B) Samples taken east of the P-P fault and west of the Pecos River, with Proterozoic ages. C) Samples taken east of the Pecos River with ages older than the Mississippian unconformity at 330 Ma.

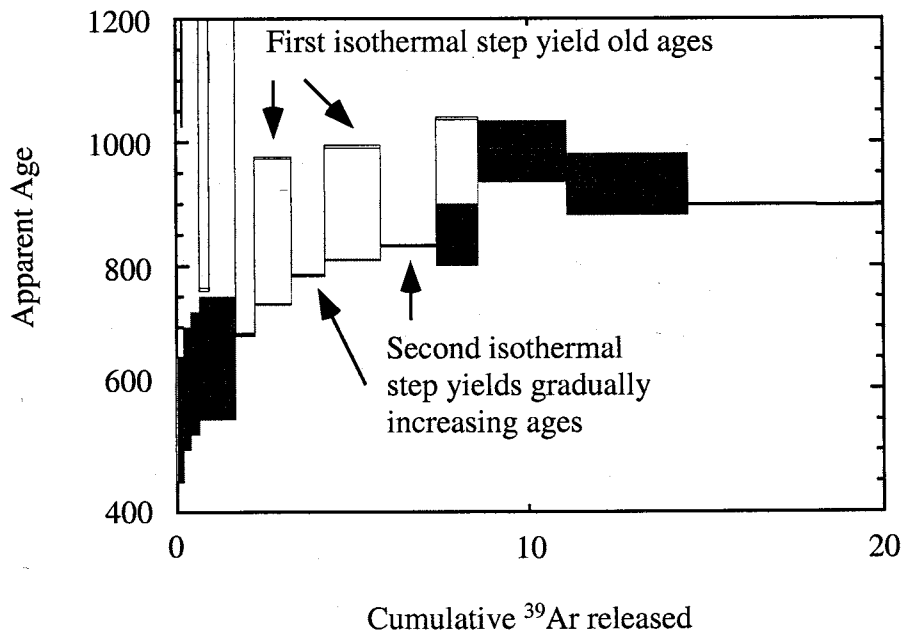


Figure 18. Corrected ages (shaded) for suspected excess argon within initial heating steps (black) of RP-70. Older ages mark all first isothermal steps. The ages in grey were chosen based on the interpretation that the ages of the first isothermal steps must lie between gradually increasing ages of the second isothermal steps.

in placing too much weight on thermal history information derived from the early heating steps.

The age spectra obtained in this study can be divided into three groups on the basis of general form. These groups are correlated to the three structural blocks defined in the study area. Age spectra are described from west to east in the following paragraphs (Figure 12). The age spectrum for sample RP-87, in the westernmost structural block, displays a complex, concave-down pattern. Late Mesozoic ages at low temperature steps rise steeply to a hump with a maximum of ~1037 Ma for the initial 20 % of the age spectrum, before falling in an undulatory manner to between 951 and 992 Ma (Figure 17a). The hump portion has more than 50% of the argon released, and is older than the highest temperature steps, perhaps indicating excess argon (cf. Foster et al., 1990).

RP-70 and WB-6 K-feldspars from the central block yield similar age spectra (Figure 17b). The majority of steps from these spectra fall on age gradients that slope gently from ca. 800 to >1000 Ma (Figure 17b). The initial age gradient is steeper (especially for WB-6) and the ages of the first of two isothermal steps for RP-70 are anomalously old for the first 10% of ^{39}Ar released (Figure 18). The second set of isothermal steps yields steadily increasing ages, as mentioned in the previous section. WB-6 reaches a maximum age of ~1025 Ma, whereas RP-70 climbs to a plateau segment of 1150 Ma over the final 25% of ^{39}Ar released (Figure 17b).

All spectra from the eastern most block (RP-90, RP-34 and RP-40) yield Phanerozoic ages during the initial heating steps (Figure 17c). For RP-34, young ages lie between 300 and 350 Ma and climb gradually to 1050 Ma, with no defined plateau (Figure 17c). Like other samples discussed previously, the first steps of isothermal duplicates give old ages.

In contrast, sample RP-40 has an age spectrum where initial ages of ~400 Ma rise steeply to > 800 Ma over the first ~10% of the argon released and essentially no excess argon is observed, as most isothermal duplicate heating steps yield overall increasing ages (Figure 17c). Following a local maximum of 920 Ma at ~25% ³⁹Ar released, the spectrum dips to ~900 Ma, before rising to a more complex section at ~1050 Ma. Sample RP-90 K-feldspar yields much younger apparent ages relative to the other two samples from this block. This K-feldspar is from the most strongly metasomatized tonalite mylonite, and yields a spectrum characterized by ages younger than 400 Ma rising abruptly to a small hump during the first 20% of ³⁹Ar released (Figure 17c). Following this hump about 75% of the gas released defines a segment of ages gently rising from ca. 680 to 810 Ma.

2. Determining the kinetic parameters

The relative domain sizes for argon diffusion were calculated from the Arrhenius parameters - diffusion coefficient (D), Temperature (T), and the frequency factor (D₀) - assuming that each domain has a single activation energy and a slab geometry (Table 5). A diffusion coefficient can be determined from the heating time and the amount of ³⁹Ar released by the sample (Giletti, 1974; Harrison, 1981). The diffusion coefficients are then plotted on an Arrhenius diagram (Figure 19), which is derived from the Arrhenius equation relating temperature to diffusion rate:

$$(1) \quad D = D_0 \exp(-E/RT)$$

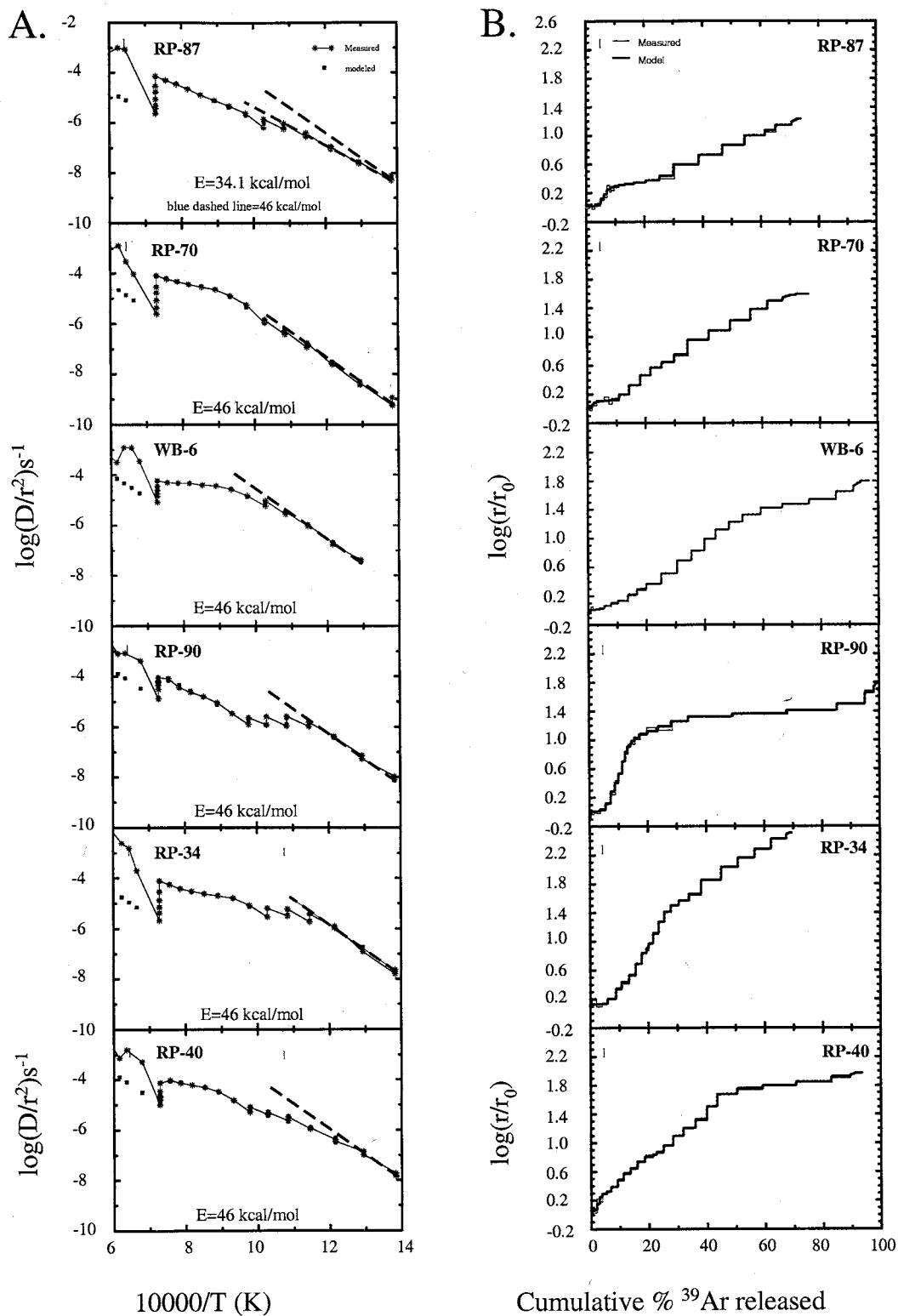


Figure 19. Arrhenius and $\log(r/r_0)$ plots for K-feldspar step-heating data. Variables defined in the text. A. The blue dashed line is the activation energy (E) used to determine the domain distribution (e.g. size and volume fraction). B. The black line is the measured fraction of ^{39}Ar released and the red line is the model diffusion domain distribution.

where \mathfrak{R} is the gas constant. The slope of a line fit through diffusion data obtained from initial heating steps on an Arrhenius plot is proportional to the activation energy (E):

$$(2) \quad -\log D = (E/2.303 \cdot \mathfrak{R})(1/T) + \log D_0.$$

The slope of the curve is defined by the initial degassing of small diffusion domains at low temperature, and decreases as larger domains dominate the higher temperature gas release.

Despite uncertainties in fitting a line through the diffusion data obtained from the initial heating steps, the activation energy calculated using Lovera's (1992) equations for five of the six samples is similar, and falls between 43.9 and 49 kcal/mol (Table 5). These results are within the range of error in activation energy calculated for 115 K-feldspars by Lovera et al. (1997): 46 ± 6 kcal/mol. I therefore have chosen a default value of $E = 46$ kcal/mol for all five samples, which is represented by the blue dashed reference line on the Arrhenius plots shown in Figure 19. Thermal histories derived from MDD modeling are sensitive to the choice of activation energy and I feel that the spread in calculated activation energy reflects analytical uncertainty rather than true deviation from the 46 kcal/mol mean. In contrast, sample RP-87 has a much shallower slope on the Arrhenius plot, which suggests that this sample has a lower activation energy than the other K-feldspars. It has a well-defined Arrhenius relationship and yields a slope proportional to 34.1 kcal/mol, which is interpreted to be accurate for this sample. Sample RP-90 has a lower age relative to other feldspars from the eastern block. This suggests that it might have a lower retentivity also, and therefore was also modeled with an

Table 5. K-feldspar kinetics and domain size distributions

RP-87 E = 34.09 kcal/mol				RP-90A E = 41 kcal/mol			
Domain	$\log D_{0\text{ cm}^2/\text{s}}$	Volume fraction	Relative domain size	Domain	$\log D_{0\text{ cm}^2/\text{s}}$	Volume %	Relative domain size
1	4.511	0.03461	0.0031	1	6.637	0.05797	0.0026
2	2.437	0.18702	0.0340	2	5.930	0.03547	0.0058
3	1.465	0.17824	0.1042	3	3.903	0.05713	0.0594
4	0.600	0.08708	0.2819	4	2.583	0.21392	0.2714
5	0.599	0.07408	0.2821	5	2.242	0.56165	0.4020
6	0.599	0.02876	0.2823	6	1.450	0.07385	1.0000
7	-0.500	0.41020	1.0000				
$\log D_0$ 2.1		slope 0.74510		$\log D_0$ 4.45		slope 0.89613	

RP-70 E = 44.8 kcal/mol				RP-34 E = 48.69 kcal/mol			
Domain	$\log D_{0\text{ cm}^2/\text{s}}$	Volume fraction	Relative domain size	Domain	$\log D_{0\text{ cm}^2/\text{s}}$	Volume %	Relative domain size
1	7.673	0.00315	0.0008	1	9.109	0.05610	0.0003
2	5.823	0.09598	0.0050	2	8.003	0.07755	0.0010
3	5.250	0.03896	0.0100	3	7.046	0.05758	0.0030
4	4.313	0.14339	0.0351	4	6.222	0.03309	0.0078
5	3.173	0.13406	0.1303	5	4.836	0.10474	0.0380
6	2.752	0.08296	0.2105	6	4.085	0.05748	0.0907
7	1.400	0.50150	1.0000	7	3.471	0.11460	0.1841
				8	2.000	0.49887	1.0000
$\log D_0$ 4.4		slope 0.97918		$\log D_0$ 7		slope 1.06421	

WB-6 E = 43.85 kcal/mol				RP-40B E = 49 kcal/mol			
Domain	$\log D_{0\text{ cm}^2/\text{s}}$	Volume fraction	Relative domain size	Domain	$\log D_{0\text{ cm}^2/\text{s}}$	Volume %	Relative domain size
1	6.668	0.07011	0.0036	1	10.091	0.01550	0.0002
2	5.664	0.13518	0.0113	2	8.394	0.04457	0.0013
3	4.941	0.07037	0.0260	3	7.422	0.05349	0.0039
4	4.632	0.06494	0.0371	4	6.388	0.11536	0.0128
5	3.912	0.05574	0.0849	5	5.399	0.03295	0.0399
6	3.489	0.05073	0.1383	6	5.323	0.09693	0.0435
7	2.519	0.32727	0.4220	7	3.271	0.41572	0.4624
8	1.770	0.22566	1.0000	8	2.600	0.22548	1.0000
$\log D_0$ 4.97		slope 0.95842		$\log D_0$ 7		slope 1.07098	

* K-feldspar is modeled with a slab geometry, where the radius (r) is equal to half the thickness of the plane sheet (McDougall and Harrison, 1999).

Table 5 (continued). Preferred K-feldspar kinetics and domain size distributions

RP-87 E = 34.09 kcal/mol				RP-90A E = 46 kcal/mol			
Domain	$\log D_0$ cm ² /s	Volume fraction	Relative domain size	Domain	$\log D_0$ cm ² /s	Volume %	Relative domain size
1	4.511	0.03461	0.0031	1	8.033	0.05538	0.0001
2	2.437	0.18702	0.0340	2	7.069	0.04476	0.0004
3	1.465	0.17824	0.1042	3	6.230	0.00766	0.0097
4	0.600	0.08708	0.2819	4	4.814	0.05480	0.0479
5	0.599	0.07408	0.2821	5	3.321	0.27299	0.2753
6	0.599	0.02876	0.2823	6	3.032	0.46096	0.3839
7	-0.500	0.41020	1.0000	7	2.651	0.05040	0.5957
				8	2.200	0.05305	1.0000
$\log D_0$ 2.1		slope 0.74510		$\log D_0$ 5.8		slope 1.00541	

RP-70 E = 46 kcal/mol				RP-34 E = 46 kcal/mol			
Domain	$\log D_0$ cm ² /s	Volume fraction	Relative domain size	Domain	$\log D_0$ cm ² /s	Volume %	Relative domain size
1	8.233	0.00442	0.0004	1	8.343	0.05644	0.0003
2	6.149	0.08150	0.0047	2	7.294	0.08123	0.0011
3	5.563	0.05529	0.0093	3	6.365	0.05183	0.0033
4	4.519	0.14024	0.0309	4	5.755	0.02895	0.0067
5	3.346	0.11842	0.1192	5	4.388	0.11073	0.0321
6	3.336	0.03706	0.1209	6	3.589	0.07726	0.0805
7	2.731	0.09008	0.2424	7	2.831	0.13867	0.1925
8	1.500	0.47298	1.0000	8	1.400	0.45489	1.0000
$\log D_0$ 4.7		slope 1.00541		$\log D_0$ 6.5		slope 1.00541	

WB-6 E = 46 kcal/mol				RP-40B E = 46 kcal/mol			
Domain	$\log D_0$ cm ² /s	Volume fraction	Relative domain size	Domain	$\log D_0$ cm ² /s	Volume %	Relative domain size
1	7.998	0.01378	0.0010	1	9.252	0.01326	0.0003
2	7.001	0.07381	0.0030	2	7.676	0.04036	0.0019
3	6.054	0.13343	0.0089	3	6.824	0.04846	0.0049
4	5.185	0.11742	0.0242	4	5.788	0.11707	0.0161
5	4.347	0.06276	0.0633	5	4.818	0.13802	0.0491
6	3.717	0.05831	0.1294	6	2.820	0.20977	0.4899
7	2.794	0.36966	0.3786	7	2.814	0.16827	0.4937
8	1.950	0.17082	1.0000	8	2.200	0.26479	1.0000
$\log D_0$ 5.55		slope 1.00541		$\log D_0$ 6.2		slope 1.00541	

* K-feldspar is modeled with a slab geometry, where the radius (r) is equal to half the thickness of the plane sheet (McDougall and Harrison, 1999).

arbitrarily chosen activation energy of 35 kcal/mol. This choice and contrasting model will be discussed further later.

Following assignment of activation energy, the fraction of ^{39}Ar released at each temperature step was used to obtain the diffusion domain distribution (Table 5). Relative domain sizes are determined by normalizing domains to the size of the largest domain, which is assigned the value of 1. A $\log(r/r_0)$ plot is constructed, which relates the volume of ^{39}Ar released to the relative size of each diffusion domain independent of the laboratory heating schedule, and regardless of the temperature plotted on the Arrhenius plot (Lovera et al., 1991). The modeled $\log r/r_0$ plot is derived by comparing the measured diffusion coefficients with those determined using the activation energy picked for each sample (the slope of the dashed line in Figure 19). The value r_0 is the diffusion length associated with the reference line, while r is the deviation from that length. For example, the first release of argon from the smallest domain size in the $\log(r/r_0)$ function is equal to zero as the deviation (r) from the linear reference line (r_0) in an Arrhenius plot is zero. The wider the range in a $\log(r/r_0)$ plot the greater the difference in size of the diffusion length scales. The model $\log r/r_0$ plot ends prior to 100% ^{39}Ar released (Figure 19) because no volume diffusion data are obtained after the sample begins to melt incongruently ($>1100^\circ\text{C}$).

D. Thermal History

The modeling of K-feldspar age spectra utilizes K-feldspar kinetics (Table 5) along with computer-input thermal histories. Modeled age spectra were matched to the measured K-feldspar age spectra of each sample. After the sizes and volume fractions for

each diffusion domain were determined, the thermal histories of the samples were evaluated. All modeled thermal histories were required to start at an initial high temperature to satisfy the mathematics presented by Dodson (1973). The thermal history results were obtained by using Arrhenius parameters and diffusion domain data in a series of computer programs, which modeled each age spectrum using a nonlinear, least squares routine following methods introduced by Quidelleur et al. (1997). Two approaches were used to fit the measured age spectra:

- a. Thermal histories were unconstrained and reheating was allowed; and
- b. continuous cooling from a high temperature (monotonic cooling, after Quidelleur et al, 1997) was prescribed.

Between 17 and 35 successful models were produced for each modeling approach. The unconstrained thermal histories are contoured in Figure 20 to identify the high probability nodes. The successful model age spectra from both approaches are plotted along with the measured spectra in Figure 17. Model age spectra correlate well with K-feldspar step-heating age spectra. For all samples, cooling below $\sim 300^{\circ}\text{C}$ began between 900 and 1000 Ma. Samples RP-70, WB-6, RP-34 and RP-40 yield models displaying approximately linear cooling from 300°C to 150°C between 750 - 850 Ma. RP-87 cooled through $\sim 300^{\circ}\text{C}$ at 1100 Ma, but in contrast to the other samples dropped below 100°C by 1000 Ma. RP-90, on the other hand, cooled relatively late, dropping from $\sim 300^{\circ}\text{C}$ at 750 Ma to 100°C by 650 Ma. The model cooling rate during the Late Proterozoic is remarkably similar for all samples ($1 - 2^{\circ}\text{C}/\text{Ma}$). Most samples record evidence of

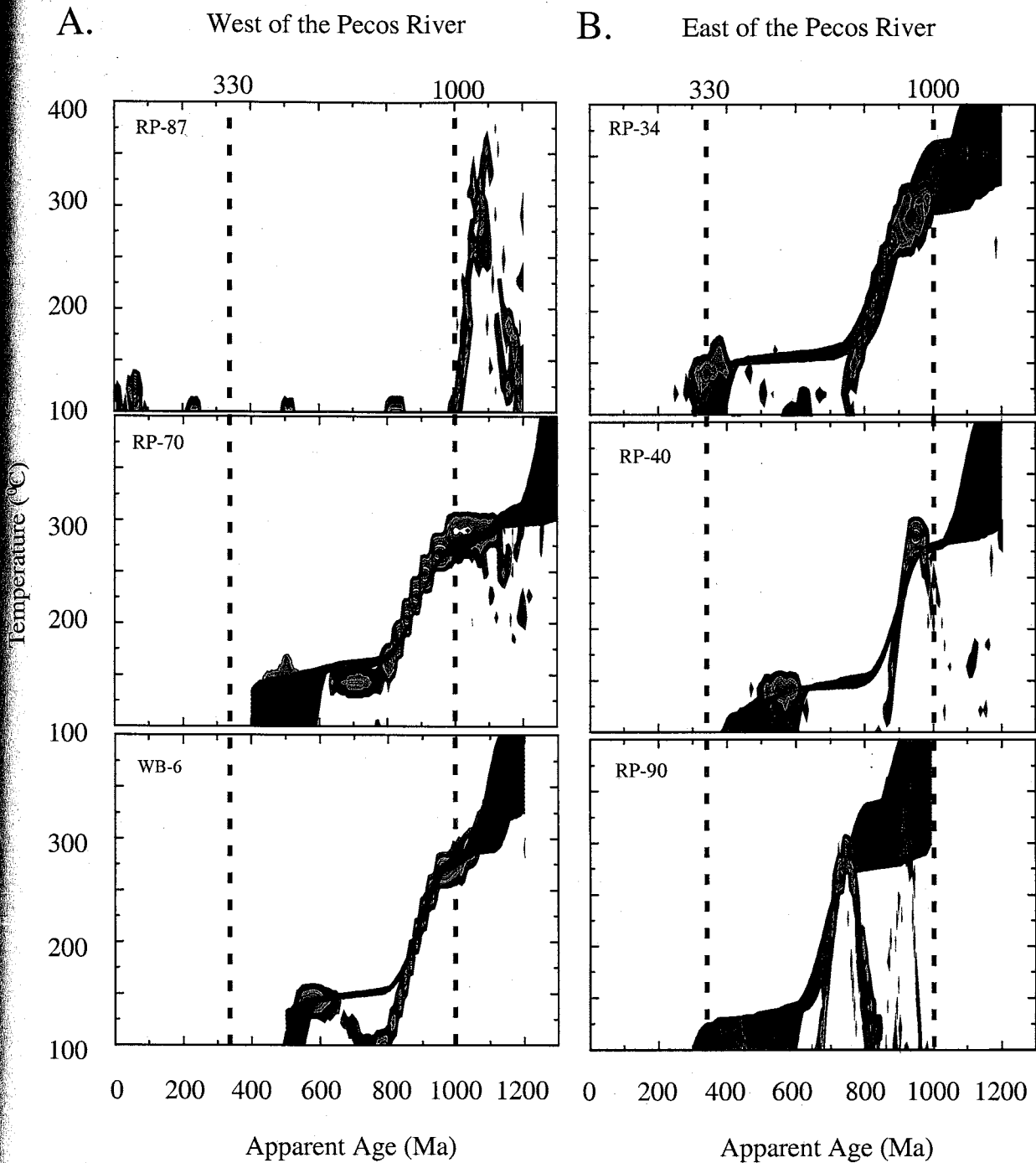


Figure 20. Cooling histories for samples in tectonic blocks. A. West of the Pecos River, including RP-87 from the western most structural block. B. East of the Pecos River. Monotonic cooling histories are shown as a blue (90% confidence) and red (66% confidence) swath, while unrestricted cooling histories are color contoured. Ages older than the oldest age recorded by the rocks are arbitrary and therefore show large errors. The black dashed reference lines mark 330 Ma (Mississippian unconformity) and 1000 Ma.

temperatures between 125° - 140°C during the Phanerozoic. Sample RP-87, for example, records a temperature of ~125°C at 70 Ma. Temperatures of ~140°C at 550 Ma were recorded by samples WB-6 and RP-40, whereas sample RP-34 records a temperature of ~140°C at 330 Ma. Sample RP-90 records temperatures of ~125°C at 425 Ma. The exception is RP-70, which cooled slowly with no reheating, and stayed at ~150°C from 800 – 450 Ma and cooled to 100°C by 400 Ma.

The monotonic cooling history solutions are not contoured, but have been combined to identify envelopes representing 90% confidence intervals for all cooling histories (shown in blue in Figure 20). Sample RP-87 has ages younger than the Mississippian unconformity, which suggest reheating of this sample since the Late Paleozoic. It was therefore not modeled with monotonic, continuous cooling. For most samples, cooling through 250 - 275°C occurred between 900 and 950 Ma. Similar cooling curves were derived for samples RP-70, WB-6, RP-34 and RP-40, all of which cooled at a rate of ~1°C/Ma to ~150°C by ~800 Ma. In order to create the measured age gradients between 800 and 600 Ma, all samples except RP-34 were held at ca. 150-170°C from 800 – 600 Ma. For RP-34, the isothermal segment of the cooling curve lasted until ~450 Ma. The Early Phanerozoic cooling history is relatively poorly constrained, reaching 100°C between 350 and 500 Ma for all samples. In agreement with the unconstrained models, the monotonic cooling approach indicates that RP-90 cooled from 275°C at 750 Ma to 150°C at 600 Ma and finally below 100°C by about 350 – 500 Ma.

In summary, both the reheating and the monotonic cooling models indicate that four out of the six samples analyzed were at 275 – 300°C at about 1000 Ma and cooled to temperatures of 150°C by 750 – 850 Ma. Sample RP-87's Proterozoic cooling history is

ambiguous, due to Late Mesozoic reheating. Sample RP-90 did cool from a high temperature of nearly 300°C at ~750 Ma to 150°C at 675 Ma, and the cooling history is anomalous compared to the other samples. Cooling rates varied from 2.0 to 0.7 °C/Ma.

XIV. DISCUSSION

A. Thermal histories

Samples with similar geologic histories have similar cooling histories and thus there is an expectation that the thermal histories obtained from K-feldspars should be consistent within each structural block in the study area. RP-87 is from the westernmost structural block, and a muscovite from that sample gave an anomalously young age (see part I). The model thermal history of RP-87 indicates cooling through ~300°C at 1100 Ma, well before the other samples. Although this thermal history may be correct, caution should be exercised due to its somewhat complex age spectrum, which reveals old ages in lower temperature steps before younger, final ages (Figure 17a). The age spectrum model algorithm tends to minimize the difference between the measured and model age spectra, and thus the measured undulatory pattern for RP-87 is averaged to yield an essentially flat segment at 950 Ma for the model age spectrum. This leads to the appearance of rapid cooling initiating at ca. 950 Ma. An alternative to averaging the undulatory pattern would be to fit the model through the youngest high temperature ages, which would yield an overall cooling history for RP-87 that is similar to the other samples. This alternative is attractive since the intermediate hump-shaped part of the spectrum may be caused by excess argon.

The temperature uncertainty in the thermal modeling can be tested using the central and eastern structural block samples. RP-70 and WB-6, from the central block, yield cooling histories that match within $\pm 10^{\circ}\text{C}$ (Figure 20), and are thus an example of good reproducibility. In contrast, samples RP-34 and RP-40, both from the easternmost structural block, yield model cooling curves which differ by 30 - 40°C at any given time. RP-34 and RP-40 have the same imposed kinetics, similar age spectra, and similarly shaped cooling curves (Figure 17). The variability of 30 - 40°C in their cooling curves is a sensible measure of confidence, considering the uncertainty in determining the slope of the initial linear segment of the Arrhenius plot. Adjusting the activation energy by 5 kcal/mol for these two samples could reconcile the modeled thermal history difference; a change of this magnitude falls within the uncertainty of 6 kcal/mol reported by Lovera et al. (1997). However, the third eastern block sample, RP-90, shows significant differences in age spectra compared to samples RP-34 and RP-40 despite the fact that they are from the same structural block (Figure 20). RP-90 predicts much younger cooling during the Late Proterozoic. This difference could be explained if the kinetic parameters (mostly activation energy) compensate to yield consistent thermal histories (cf. Heizler et al., 1988; Heizler and Harrison, 1998). To test whether RP-90 could be younger due to a lower closure temperature, it was modeled by lowering the activation energy from 46 to the previously mentioned value of 35 kcal/mol. This value is outside the 6 kcal/mol uncertainty range, but is at the low end of the variability range of activation energies reported by Lovera et al. (1997). However, even this dramatic change does not reconcile RP-90's cooling history with the one obtained from RP-34 and RP-40. Specifically, lowering the activation energy makes the large domains have a lower

closure temperature, and thus a lower minimum age, but the smallest domains become too nonretentive and require RP-90 to cool below $\sim 125^{\circ}\text{C}$ well before RP-34 and RP-40. Also, if the modeled histories of RP-34 and RP-40 were applied to RP-90 with a lower activation energy, they would result in substantial argon loss from the intermediate domains of RP-90 during the Paleozoic and this is not observed. In addition, based on the Arrhenius plot we have no a priori reason to believe that an activation energy of 46 kcal/mol is inaccurate for RP-90 (Figure 19). Several other possibilities may account for the young age of RP-90. RP-90 K-feldspar could have grown below its closure temperature at ca. 800 Ma. It then potentially dates metasomatism, a possibility which is further explored in the following section. Another explanation for the young age of RP-90 is that the boundaries controlling argon diffusion changed over time. An initial low retentivity which allowed $^{40}\text{Ar}^*$ to escape in the Proterozoic could have changed during low temperature homogenization of diffusion domains (cf. Parsons et al., 1999). Thus the measured high retentivity today may not be the same as the retentivity which determined the age distribution. If this occurred it would invalidate the MDD technique for this sample, making the modeled cooling history for RP-90 meaningless.

Some samples record Paleozoic ages and thus have the potential to address the Paleozoic history of the area. The timing of uplift for most samples is relatively unconstrained between 600 and 330 Ma; however, two samples were not perturbed during the Phanerozoic and therefore constrain the maximum allowable temperature during the Paleozoic. RP-70 and WB-6 were not affected by temperatures $>125^{\circ}\text{C}$ after about 600 Ma. Excess argon is present in most samples and the age of the second isothermal step cannot always be constrained to be too old, adding uncertainty to the

initial corrected ages. The gradients in the age spectra are also small and steep, thereby contributing substantial additional uncertainty to this portion of the thermal history. However, the Paleozoic ages suggest that some samples were reheated or stayed at temperatures high enough to lose argon during the Paleozoic. In the following paragraphs, I use geologic constraints to discriminate between continuous cooling versus reheating models of the Paleozoic thermal history of these samples.

Evidence for the possible emergence or the presence of plutonism of any age in the Proterozoic basement is important in deciding whether reheating or slow cooling is a better model to explain isothermal temperatures from 600 - 330 Ma. Cambrian alkalic intrusions in New Mexico are suggested to be the result of NNE extension in the Cambrian (McLemore et al., 1999). Elevated heat flow associated with extension could have prevented basement rocks from cooling significantly. Following the intrusion of alkalic igneous rocks, north-central New Mexico was a slight "positive area" from the Devonian through the Mississippian (Baltz and Myers, 1999), during which period there is no evidence for magmatism. Extensive carbonate deposition took place to the north and south of the area; however, sedimentary rocks of Ordovician - Devonian age might never have accumulated to great depths on top of the Transcontinental arch in north-central New Mexico (Carlson, 1999; Baltz and Myers, 1999). However, Baltz and Myers (1999) also stated that erosion in the area was not significant, because clastic sediments of Early Paleozoic age are virtually absent from New Mexico, suggesting that the "positive area" was near sea level. The age spectrum of sample RP-34 suggests that the sample was at a temperature between 100 and 125°C at 350 Ma, corresponding to a depth of 4 - 5 km with a normal geothermal gradient, and probably had resided there since the

Proterozoic. Paleozoic ages are therefore probably not the result of burial by Early Paleozoic sediments but instead record differential erosion of Proterozoic basement. The Mississippian unconformity requires that presently exposed Proterozoic basement was at the surface at 330 Ma. Because sample RP-34 has apparent age steps similar in age to this unconformity, it may have experienced fast cooling through exhumation between 350 and 330 Ma.

Most samples yielded model temperatures between $\sim 125^{\circ}$ - 150°C in the Late Cretaceous. Five of the six samples could be heated to $\sim 150^{\circ}\text{C}$ without argon loss. Only RP-87 loses argon at $\sim 125^{\circ}\text{C}$. The Cretaceous ages of RP-87 could have been achieved in one of two ways: 1) the sample was reheated to $\sim 125^{\circ}\text{C}$ (buried to a depth of 4 - 5 km), at a time when other samples were cooler or 2) Late Mesozoic burial depths were similar across the Picuris-Pecos fault, but since RP-87 has a lower retentivity it lost argon while the other samples remained unaffected. At present, there is no geologic evidence to support either model. Differential reheating and faster uplift for RP-87 is somewhat unlikely, since rocks on both sides of the Picuris-Pecos fault cooled through the AFT annealing temperature ($60 - 120^{\circ}\text{C}$) at ca. 70 Ma (Kelley, 1990; Kelley and Chapin, 1995). Similar AFT ages for rocks on either side of the Picuris-Pecos fault support concurrent uplift since the Cretaceous. Before uplift, temperatures during the Late Cretaceous were hot enough ($\sim 125^{\circ}\text{C}$) to cause argon loss from the small diffusion domains of low retentivity sample RP-87, leaving the other five more retentive samples unaffected. The cooling history of RP-87 can therefore be a result of Mesozoic burial and exhumation from depths of $\sim 4 - 5$ km since the Late Cretaceous. For the other five samples Mesozoic burial and exhumation is probable.

B. Timing of faulting, brecciation and metasomatism

Montgomery (1963) suggested that both metasomatism and brecciation occurred during the Proterozoic, but did not provide unequivocal evidence supporting this assertion. Bauer and Ralser (1995) suggested that breccia ridges parallel to the Picuris-Pecos fault are evidence of pre-Mississippian brittle deformation. Cemented breccia ridges were fault zones, since they contain angular clasts. Metasomatism was localized in the fault zones and contemporaneous with brecciation (RP-90), however, metasomatism also occurred without brecciation (RP-40). Metasomatism occurred prior to Carboniferous sedimentation, since rocks overlying the Proterozoic basement are unaffected. The timing of metasomatism, and brecciation can both be constrained by K-feldspar thermochronology.

Metasomatized, unbrecciated sample RP-40 has the older cooling age of the two samples at 1050 Ma, when modeling suggests it cooled below 300°C. Since the tonalite initially was free of K-feldspar it would have been introduced into the tonalite prior to ca. 1050 Ma. Thus the 1050 Ma age indicates a minimum age of metasomatism.

Metasomatism is localized, since mica cooling ages from similar tonalites (Chapter 1) are 1345 Ma, indicate cooling below 325°C, and are not perturbed by alteration due to fluid flux.

Metasomatized rock and breccia clasts in the fault zone are comprised of the foliated Windy Bridge tonalite, indicating that ductile deformation predated metasomatism and brecciation. Micas from these foliated tonalites (Chapter 1) yield cooling ages of 1345 Ma, and cooled below 325°C at this time. The cooling age of the micas provides a maximum age of metasomatism and brecciation. $^{40}\text{Ar}/^{39}\text{Ar}$ ages of fractured K-feldspar

from metasomatized sample RP-90 also constrain the timing of metasomatism and therefore provide a minimum age of brecciation. As mentioned previously, K-feldspar in RP-90 could have grown below its closure temperature at 800 Ma. The latter result is consistent with the observation that vugs are locally preserved in the breccia, indicating that breccias formed at shallow crustal levels.

Metasomatism thus likely occurred twice in the Proterozoic basement of the Rosilla Peak quadrangle: once before 1050 Ma and once at ~800 Ma. Two tectonic events affected northern New Mexico in this time period: the far-field effects of the Grenville Orogeny at ca. 1100 Ma (Heizler et al., 1997) and rifting associated with the break-up of Rodinia at 800 Ma (e.g. Timmons et al., in press). It is therefore suggested that each event is recognizable in the Proterozoic basement of the Rosilla Peak quadrangle.

XV. CONCLUSIONS

The Proterozoic basement of the Rosilla Peak quadrangle in the southern Sangre de Cristo Mountains experienced mostly slow cooling punctuated by two Neoproterozoic metasomatic events, at least one of which was associated with brecciation (see Figure 21). Thermochronologic data indicate that the Picuris-Pecos fault did not accommodate significant throw during Proterozoic time. Rocks east and west of the fault have similar cooling histories from the Proterozoic through the Paleozoic. Sometime prior to 1050 Ma, the Proterozoic basement, including the Windy Bridge tonalite, was locally metasomatized. This age is constrained by the oldest metasomatized tonalite. At 800 Ma, K-feldspar grew locally, as in sample RP-90 east of the Pecos River, as a result of

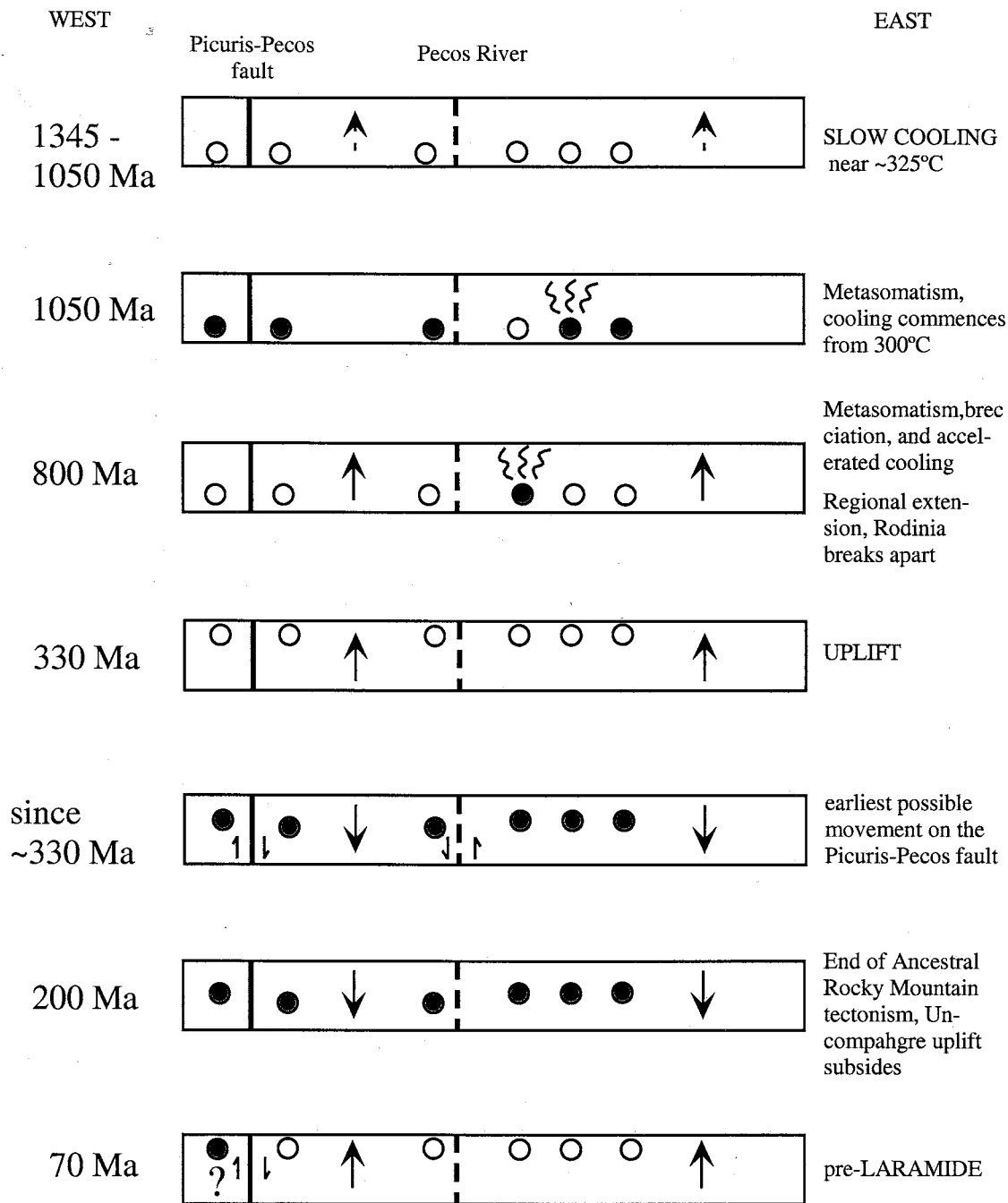


Figure 21. Schematic cross section of part of the Rosilla Peak 7.5 minute quadrangle showing sample locations (see Figure 2) in circles. Green colored circles represent burial or reheating of a sample. Red circles depict cooling of the rock. Metasomatism is indicated by wavy lines. Arrows show sense of motion on faults. Note that only the dip-slip component of faulting is shown, as strike-slip motion cannot be constrained with K-feldspar thermochronology.

renewed or diachronous metasomatism along breccia zones that parallel the Picuris-Pecos fault. In most of the area accelerated cooling occurred at 800 Ma. This is interpreted to represent a time of exhumation of the Proterozoic basement, probably related to extension during the breakup of Rodinia.

Most of the area stayed at temperatures of approximately 150°C during the Late Proterozoic, but locally could have been below 100°C by 600 Ma. Geologically relevant modeling using slow, steadily decreasing cooling implies that the hotter areas remained at elevated temperatures through the Silurian and Devonian. Most of the area shows accelerated cooling prior to Mississippian exhumation and Ancestral Rocky Mountain tectonism. Sample RP-34, east of the Pecos River, underwent extremely rapid exhumation from ~150°C to ~125°C in about 10 Ma beginning at 330 Ma.

Based on field relations, the youngest faulting on the Picuris-Pecos fault and similar N- to NNE-striking faults can at best be constrained to be post-Carboniferous. For example, a previously unidentified N-striking fault (herein named the Pecos River fault) within the Pecos River valley displaced Paleozoic strata as much as 200 m (west-down offset). The Picuris-Pecos fault also displays some component of dip-slip offset of Paleozoic strata. It is significant that the K-feldspar samples record no argon loss during the Pennsylvanian - Permian Ancestral Rocky Mountain burial and deposition, indicating maximum depths of burial of ~4-5 km. The Proterozoic basement was reheated to at least 125°C, but not above 150°C, during Late Mesozoic time, which is interpreted to record burial followed by uplift at ~70 Ma during the Laramide Orogeny. The normal-slip character of the Pecos River fault and other west-down faults could be evidence for Rio Grande rift related extension in the southern-most Sangre de Cristo Mountains.

Combined References Cited

- Anderson, J.R., 1983, Petrology of a portion of the eastern Peninsula Ranges mylonite zone, Southern California: *Contributions to Mineralogy and Petrology*, v. 84, p. 253-271.
- Apted, M.J., and Liou, J.G., 1983, Phase relations among greenschist, epidote-amphibolite, and amphibolite in a basaltic system: *American Journal of Science*, v. 283-A, p. 328-354.
- Armstrong, A.K., and Mamet, B.L., 1990, Stratigraphy, facies and paleotectonics of the Mississippian system, Sangre de Cristo Mountains, New Mexico and Colorado and adjacent areas, in Bauer, P.W., Lucas, S.G., Mawer, C.K., and McIntosh, W.C., eds., *Tectonic development of the southern Sangre de Cristo Mountains, New Mexico, Guidebook Forty-first annual field conference*, New Mexico Geological Society, p. 241-249.
- Arth, J.G., Barker, F., Peterman, Z.E., and Friedman, I., 1978, Geochemistry of the gabbro-diorite-tonalite-trondhjemite suite of southwest Finland and its implications for the origin of tonalitic and trondhjemitic magmas: *Journal of Petrology*, v. 19, part 2, p. 289-316.
- Baltz, E.H., and Myers, D.A., 1999, Stratigraphic framework of upper Paleozoic rocks, southeastern Sangre de Cristo Mountains, New Mexico, with a section on speculations and implications for regional interpretation of Ancestral Rocky Mountains paleotectonics: Socorro, NM, New Mexico Bureau of Mines and Mineral Resources, 269 p.
- Bauer, P.W., Daniel, C.G., Lucas, S.G., Barker, J.M., and Kottowski, F.E., 1995, Second-day road log, from Santa Fe to Pecos, Rowe, Bernal, Romeroville, and Mineral Hill, in Bauer, P.W., Kues, B.S., Dunbar, N.W., Karlstrom, K.E., and Harrison, B., eds., *Geology of the Santa Fe region, New Mexico, Guidebook Forty-sixth field conference*, New Mexico Geological Society, p. 29-55.
- Bauer, P.W., and Pollock, T.R., 1993, *Compilation of Precambrian isotopic ages in New Mexico*: New Mexico Bureau of Mines and Mineral Resources, Open-file Report 389, 130 pgs.
- Bauer, P.W., and Ralser, S., 1995, The Picuris-Pecos fault - Repeatedly reactivated, from Proterozoic(?) to Neogene, in Bauer, P.W., Kues, B.S., Dunbar, N.W., Karlstrom, K.E., and Harrison, B., eds., *Geology of the Santa Fe region, New Mexico, Guidebook Forty-sixth field conference*, New Mexico Geological Society, p. 111-115.
- Bauer, P.W., and Williams, M.L., 1994, The age of Proterozoic orogenesis in New Mexico, U.S.A.: *Precambrian Research*, v. 67, p. 349-356.
- Boullier, A-M., and Bouchez, J-L., 1978, Le quartz en rubans dans les mylonites: *Bulletin Société Géologique Française*, v. 7, p. 253-262.
- Bowring, S.A., and Condie, K.C., 1982, U-Pb zircon ages from northern and central New Mexico: *Geological Society of America Abstracts with Programs*, v. 14, p. 304.
- Bowring, S.A., and Karlstrom, K.E., 1990, Growth, stabilization and reactivation of Proterozoic lithosphere in the southwestern United States: *Geology*, v. 18, p. 1203-1206.

- Brown, C.L., Karlstrom, K.E., Heizler, M., and Unruh, D., 1999, Paleoproterozoic deformation, metamorphism, and $^{40}\text{Ar}/^{39}\text{Ar}$ thermal history of the 1.65 Ga Manzanita pluton, Manzanita Mountains, New Mexico, in Pazzaglia, F.J., Woodward, L.E., Lucas, S.G., Bauer, P.W., and Karlstrom, K.E., eds., *Albuquerque Geology, Guidebook Fiftieth field conference*, New Mexico Geological Society, p. 255-268.
- Carlson, M.P., 1999, Transcontinental Arch: a pattern formed by rejuvenation of local features across central North America: *Tectonophysics*, v. 305, p. 225-233.
- Cather, S.M., 1999, Implications of Jurassic, Cretaceous, and Proterozoic piercing lines for Laramide oblique-slip faulting in New Mexico and rotation of the Colorado Plateau: *GSA Bulletin*, v. 111, p. 849-868.
- Cebula, G.T., Kunk, M.J., Mehnert, H.H., Naeser, C.W., Obradovich, J.D., and Sutter, J.F., 1986, The Fish Canyon Tuff, a potential standard for the ^{40}Ar - ^{39}Ar and fission track dating methods, *Terra Cognita Abstracts*, v. 6, p. 139-140.
- Chapin, C.E., and Cather, S.M., 1981, Eocene tectonics and sedimentation in the Colorado Plateau-Rocky Mountain area: *Arizona Geological Society Digest*, v. 14, p. 173-198.
- Condie, K.C., 1982, Plate-tectonics model for Proterozoic continental accretion in the southwestern United States: *Geology*, v. 10, p. 37-42.
- Coney, P.J., 1987, Circum-Pacific tectogenesis in the North American Cordillera, in Monger, J.W.H. Francheteau, J., eds., *Circum-Pacific orogenic belts and evolution of the Pacific Ocean basin*, *Geodynamics Series 18*: Washington, D.C.: American Geophysical Union, p. 59-69.
- Cosca, M.A., and O'Nions, R.K., 1994, A re-examination of the influence of composition on argon retentivity in metamorphic calcic amphiboles: *Chemical Geology*, v. 112, p. 39-56.
- Crawford, M.L., 1966, Composition of plagioclase and associated minerals in some schists from Vermont, U.S.A., and South Westland, New Zealand, with inferences about the peristerite solvus: *Contributions to Mineralogy and Petrology*, v. 13, p. 269-294.
- Dahl, P.S., 1996, The effects of composition on retentivity of argon in hornblende and related amphiboles: A field-tested empirical model: *Geochimica et Cosmochimica Acta*, v. 60, p. 3687-3700.
- Daniel, C. G., 1995, An overview of the Proterozoic geology in the Thompson Peak - Glorieta Baldy area, Santa Fe county, New Mexico, in Bauer, P.W., Kues, B.S., Dunbar, N.W., Karlstrom, K.E., and Harrison, B., eds., *New Mexico Geological Society 46th annual field conference volume*, Santa Fe region, New Mexico, New Mexico Geological Society, p. 209-218.
- Dickerson, P.W., 1984, Structural controls on basin-margin sedimentation; Pennsylvanian Taos trough, New Mexico and contemporary Belize, Central America, in Baldrige, W.S., Dickerson, P.W., Riecker, R.E., and Zidek, J., eds., *Rio Grande Rift: Northern New Mexico*, *Guidebook Thirty-fifth annual field conference*, New Mexico Geological Society, p. 101-105.
- Dodson, M.H., 1973, Closure temperature in cooling geochronological and petrological systems: *Contributions to Mineralogy and Petrology*, v. 40, p. 259-274.

- Dunlap, W.J., and Fossen, H., 1998, Early Paleozoic orogenic collapse, tectonic stability and Late Paleozoic continental rifting revealed through thermochronology of K-feldspars, southern Norway: *Tectonics*, v. 17, p. 604-620.
- Fillipone, J.A., Yin, A., Harrison, T.M., Gehrels, G., Smith, M., and Sample, J.C., 1995, Age and magnitude of dip-slip faulting deduced from differential cooling histories: An example from the Hope Fault, northwest Montana: *Journal of Geology*, v. 103, p. 199-211.
- Forster, D.A., Harrison, T.M., Copeland, P., and Heizler, M.T., 1990, Effects of excess argon within large diffusion domains of K-feldspar age spectra: *Geochimica et Cosmochimica Acta*, v. 54, p.1699-1708.
- Fulp, M.S., 1982, Precambrian geology and mineralization of the Dalton Canyon volcanic center, Santa Fe county, New Mexico: MS Thesis, Albuquerque, University of New Mexico, 199 pgs.
- Giletti, B.J., 1974, Diffusion related to geochronology, in Hofmann, A.W., Giletti, B.J., Yoder Jr., H.S., and Yund, R.A., eds., *Geochemical transport and kinetics*, Volume Publication 634: Washington, D. C., Carnegie Institute of Washington, p. 61-76.
- Goodwin, L.B., and Renne, P.R., 1991, Effects of progressive mylonitization on Ar retention in biotites from the Santa Rosa mylonite zone, California, and thermochronologic implications: *Contributions to Mineralogy and Petrology*, v. 108, p.283-297.
- Goodwin, L.B., and Wenk, H.-R., 1990, Intracrystalline folding and cataclasis in biotite of the Santa Rosa mylonite zone: HVEM and TEM observations: *Tectonophysics*, v. 172, p. 201-214.
- Goodwin, L.B., and Williams, P.F., 1996, Deformation path partitioning within a transpressive shear zone, Marble Cove, Newfoundland: *Journal of Structural Geology*, v. 18, p. 975-990.
- Grambling, J.A., 1979, Precambrian geology of the Truchas Peaks region, north-central New Mexico, and some regional implications, in Ingersoll, R.V., editor., *New Mexico Geological Society 30th annual field conference volume*, Santa Fe country, New Mexico, New Mexico Geological Society, p. 135-143.
- Grambling, J.A., and Coddling, D.B., 1982, Stratigraphic and structural relationships of multiply deformed Precambrian metamorphic rocks in the Rio Mora area, New Mexico: *GSA Bulletin*, v. 93, p. 127-137.
- Grambling, J.A., and Dallmeyer, R.D., 1993, Tectonic evolution of Proterozoic rocks in the Cimarron Mountains, northern New Mexico: *Journal of Metamorphic Geology*, v. 11, p. 739-755.
- Grambling, J.A., Williams, M.L., and Mawer, C.K., 1988, Proterozoic tectonic assembly of New Mexico, *Geology*, v. 16, p. 724-727.
- Grambling, J.A., Williams, M.L., Smith, R.F., and Mawer, C.K., 1989, The role of crustal extension in the metamorphism of Proterozoic rocks in northern New Mexico, in Grambling, J.A., and Tewksbury, B.J., eds., *Proterozoic Geology of the southern Rocky Mountains*, Volume 235: Special Paper: Boulder, CO., Geological Society of America, p. 87-110.
- Grambling, J.A., and Ward, D.B., 1987, Thrusting of the Pecos greenstone belt over younger supracrustal rocks, Rio Mora area, New Mexico: *GSA Abstracts with Program*, v. 19, p. 278-279.

- Hames, W.E., and Bowring, S.A., 1994, An empirical evaluation of the argon diffusion geometry in muscovite: *Earth and Planetary Science Letters*, v. 124, p. 161-167.
- Hames, W.E., and Hodges, K.V., 1993, Laser $^{40}\text{Ar}/^{39}\text{Ar}$ evaluation of slow cooling and episodic loss of ^{40}Ar from a sample of polymetamorphic muscovite: *Science*, v. 261, p. 1721-1723.
- Harrison, T.M., 1981, Diffusion of ^{40}Ar in hornblende: *Contributions to Mineralogy and Petrology*, v. 78, p. 324-331.
- Harrison, T.M., and Burke, K., 1989, $^{40}\text{Ar}/^{39}\text{Ar}$ thermochronology of sedimentary basins using detrital feldspars: Examples from the San Joaquin Valley, California, Rio Grande Rift, New Mexico, and North Sea, in Naeser, N.D., and McCulloh, T.H., eds., *Thermal history of sedimentary basins: methods and case histories*: New York, Springer-Verlag, p. 141-155.
- Harrison, T.M., and Fitz Gerald, J.D., 1986, Exsolution in hornblende and its consequences for $^{40}\text{Ar}/^{39}\text{Ar}$ age spectra and closure temperature: *Geochimica et Cosmochimica Acta*, v. 50, p. 247-253.
- Harrison, T.M., Heizler, M.T., and Lovera, O.M., 1993, In vacuo crushing experiments and K-feldspar thermochronometry: *Earth and Planetary Science Letters*, v. 117, p. 169-180.
- Harrison, T.M., Heizler, M.T., Lovera, O., Wenji, C., and Grove, M., 1994, A chlorine disinfectant for excess argon released from K-feldspar during step-heating: *Earth and Planetary Science Letters*, v. 123, p. 95-104.
- Harrison, T.M., and McDougall, I., 1981, Excess ^{40}Ar in metamorphic rocks from Broken Hill, New South Wales: Implications for $^{40}\text{Ar}/^{39}\text{Ar}$ age spectra and the thermal history of the region: *Earth and Planetary Science Letters*, v. 55, p. 123-149.
- Harrison, T.M., Morgan, P., and Blackwell, D.D., 1986, Constraints on the age of heating at the Fenton Hill site, Valles Caldera, New Mexico: *Journal of Geophysical Research*, v. 91, p. 1899-1908.
- Heizler, M.T., 1998, Argon thermochronology I - The billion year thermochronological void, New Mexico Geological Society Spring conference: Socorro, NM, New Mexico Geological Society.
- Heizler, M.T., and Harrison, T.M., 1998, The thermal history of the New York basement determined from $^{40}\text{Ar}/^{39}\text{Ar}$ K-feldspar studies: *Journal of Geophysical Research*, v. 103, p. 29795-29814.
- Heizler, M.T., Lux, D.R., and Decker, E.R., 1988, The age and cooling history of the Chain of Ponds and Big Island Pond plutons and the Spider Lake granite, West-Central Maine and Quebec: *American Journal of Science*, v. 288, p. 925-952.
- Heizler, M.T., and Ralser, S., 1994, $^{40}\text{Ar}/^{39}\text{Ar}$ thermochronology of low-temperature shear zones, Manzano Mountains, New Mexico: *GSA Abstracts with Programs*, v. 26, p. A-528.
- Heizler, M.T., Ralser, S., and Karlstrom, K.E., 1997, Late Proterozoic (Grenville?) deformation in central New Mexico determined from single-crystal muscovite $^{40}\text{Ar}/^{39}\text{Ar}$ age spectra: *Precambrian Research*, v. 84, p. 1-15.
- Hirth, G., and Tullis, J., 1992, Dislocation creep regimes in quartz aggregates: *Journal of Structural Geology*, v. 14, p. 145-159.
- Hodges, K.V., Hames, W.E., and Bowring, S.A., 1994, $^{40}\text{Ar}/^{39}\text{Ar}$ age gradients in micas from a high-temperature-low-pressure metamorphic terrain: Evidence for very slow

- cooling and implications for the interpretation of age spectra: *Geology*, v. 22, p. 55-58.
- Hoisch, T.D., Heizler, M.T., and Zartman, R.E., 1997, Timing of detachment faulting in the Bullfrog Hills and Bare Mountain area, southwest Nevada: Inferences from $^{40}\text{Ar}/^{39}\text{Ar}$, K-Ar, U-Pb, and fission track thermochronology: *Journal of Geophysical Research*, v. 102, p. 2815-2833.
- Karlstrom, K.E., Cather, S.M., Kelley, S.A., Heizler, M.T., Pazzaglia, F.J., and Roy, M., 1999, Sandia Mountains and Rio Grande Rift: Ancestry of structures and history of deformation, in Pazzaglia, F.J., and Lucas, S.G., eds., *Albuquerque geology, Guidebook Fiftieth annual field conference*, New Mexico Geological Society, p. 155-165.
- Karlstrom, K.E., Dallmeyer, R.D., and Grambling, J.A., 1997, $^{40}\text{Ar}/^{39}\text{Ar}$ evidence for 1.4 Ga regional metamorphism in New Mexico: implications for thermal evolution of lithosphere in the southwestern USA: *Journal of Geology*, v. 105, p. 205-223.
- Karlstrom, K.E., and Daniel, C.G., 1993, Restoration of Laramide right-lateral strike-slip in northern New Mexico by using Proterozoic piercing points: Tectonic implications from the Proterozoic to the Cenozoic: *Geology*, v. 21, p. 1139-1142.
- Karlstrom, K.E., and Houston, R.S., 1984, The Cheyenne Belt; analysis of a Proterozoic suture in southern Wyoming: *Precambrian Research*, v. 15, n. 4, p. 415-446.
- Karlstrom, K.E., and Humphreys, E.D., 1998, Persistent influence of Proterozoic accretionary boundaries in the tectonic evolution of southwestern North America: Interaction of cratonic grain and mantle modification events: *Rocky Mountain Geology*, v. 33, p. 161-179.
- Kelley, S.A., 1990, Late Mesozoic to Cenozoic cooling history of the Sangre de Cristo Mountains, Colorado and New Mexico, in Bauer, P.W., Lucas, S.G., Mawer, C.K., and McIntosh, W.C., eds., *Tectonic development of the southern Sangre de Cristo Mountains, New Mexico, Guidebook Forty-first annual field conference*, New Mexico Geological Society, p. 123-132.
- Kelley, S.A., and Chapin, C.E., 1995, Apatite fission-track thermochronology of southern Rocky Mountain-Rio Grande Rift-western High Plains provinces, in Bauer, P.W., Kues, B.S., Dunbar, N.W., Karlstrom, K.E., and Harrison, B., eds., *Geology of the Santa Fe region, New Mexico, Guidebook Forty-sixth annual field conference*, New Mexico Geological Society, p. 87-96.
- Kelley, S.A., Chapin, C.E., and Corrigan, J., 1992, Late Mesozoic to Cenozoic cooling histories of the flanks of the northern and central Rio Grande rift, Colorado and New Mexico: Socorro, New Mexico Bureau of Mines and Mineral Resources, 39 p.
- Kirby, E., Karlstrom, K.E., Andronicos, C.L., and Dallmeyer, R.D., 1995, Tectonic setting of the Sandia pluton: An orogenic 1.4 Ga granite in New Mexico: *Tectonics*, v. 14, p. 185-201.
- Klich, I., 1983, Precambrian geology of the Elk Mountain - Spring Mountain Area, San Miguel county, New Mexico: Socorro, New Mexico Institute of Mining and Technology.
- Kluth, C.F., and Coney, P.J., 1981, Plate tectonics of the ancestral Rocky Mountains: *Geology*, v. 9, p. 10-15.
- Lanzirotti, A., Bishop, J.L., and Williams, M.L., 1996, A more vigorous approach to dating mid-crustal processes: U-Pb dating of varied major and accessory

- metamorphic minerals tied to microstructural studies: GSA Abstracts with Programs, v. 28, p. A-453.
- Lanzirotti, A., and Hanson, G.N., 1997, An assessment of the utility of staurolite in U-Pb dating of metamorphism: *Contributions to Mineralogy and Petrology*, v. 139, p. 352-365.
- Lister, G.S., Paterson, M.S., and Hobbs, B.E., 1978, The simulation of fabric development in plastic deformation and its application to quartzite: the model: *Tectonophysics*, v. 45, n. 2-3, p. 107-158.
- Lo, C-H., and Onstott, T.C., 1989, ^{39}Ar recoil artifacts in chloritized biotite: *Contributions to Mineralogy and Petrology*, v. 53, p. 2697-2711
- Loring, A.K., and Armstrong, D.G., 1980, Cambrian-Ordovician syenites of New Mexico, part of a regional alkalic intrusive episode: *Geology*, v. 8, p. 344-348.
- Lovera, O.M., 1992, Computer programs to model $^{40}\text{Ar}/^{39}\text{Ar}$ diffusion data from multidomain samples: *Computers and Geoscience*, v. 18, p. 789-813.
- Lovera, O.M., Grove, M., Harrison, T.M., and Mahon, K.I., 1997, Systematic analysis of K-feldspar $^{40}\text{Ar}/^{39}\text{Ar}$ step-heating results: Significance of activation energy determinations: *Geochimica et Cosmochimica Acta*, v. 61, p. 3171-3192.
- Lovera, O.M., Richter, F.M., and Harrison, T.M., 1989, The $^{40}\text{Ar}/^{39}\text{Ar}$ geothermometry for slowly cooled samples having a distribution of diffusion domain sizes: *Journal of Geophysical Research*, v. 94, p. 17917-17935.
- Lovera, O.M., Richter, F.M., and Harrison, T.M., 1991, Diffusion domains determined by ^{39}Ar released during step heating: *Journal of Geophysical Research*, v. 96, p. 2057-2069.
- Mahon, K.I., 1996, The "New" York regression: application of an improved statistical method to geochemistry: *International Geology Review*, v. 38, p. 293-303.
- Marcoline, J.R., 1996, Field, petrographic and $^{40}\text{Ar}/^{39}\text{Ar}$ constraints on the tectonic history of the central Manzano Mountains, central New Mexico: MS Thesis, Socorro, New Mexico Institute of Mining and Technology, 124 pgs.
- Marcoline, J.R., Heizler, M.T., Goodwin, L.B., Ralser, S., and Clark, J., 1999, Thermal, structural, and petrological evidence for 1400-Ma metamorphism and deformation in central New Mexico: *Rocky Mountain Geology*, v. 34, n. 1, p. 93-119.
- Marcoline, J.R., Ralser, S., Goodwin, L.B., 2000, Field and microstructural observations from the Capilla Peak area, Manzano Mountains, central New Mexico: *New Mexico Geology*, v. 22, n. 3, p. 57-63.
- McDougall, I., and Harrison, T. M., 1999, *Geochronology and thermochronology by the $^{40}\text{Ar}/^{39}\text{Ar}$ method*, second edition, Oxford University Press, New York.
- McLemore, V.T., McMillan, N.J., Heizler, M.T., and McKee, C., 1999, Cambrian alkaline rocks at Lobo Hill, Torrance county, New Mexico: more evidence for a Cambrian-Ordovician aulocogen, in Pazzaglia, F.J., and Lucas, S.G., eds., *Albuquerque Geology, Guidebook Fiftieth annual field conference*, New Mexico Geological Society, p. 247-253.
- McMillan, N., and McLemore, V.T., 1999, The Lobo Hill alkalic complex, Torrance county, NM: Cambrian magmatism in the New Mexico aulacogen, *New Mexico Geological Society 1999 annual spring meeting*: Socorro, p. 23.

- Melis, E.A., Harpel, C.J., Kelley, S.A., and Bauer, P.W., 2000, Latest Eocene felsic volcanic rocks from the southern Sangre de Cristo Mountains, New Mexico, New Mexico Geological Society 2000 annual spring meeting: Socorro.
- Montgomery, A., 1963, Precambrian Rocks, in Miller, J.P., Montgomery, A., and Sutherland, P.K., eds., *Geology of Part of the southern Sangre de Cristo Mountains, New Mexico*, Memoir 11: Socorro, New Mexico Bureau of Mines and Mineral Resources, p. 7-21.
- Naesar, C.W., 1979, Fission-track dating and geologic annealing of fission tracks, in Jager, E., and Hunziker, J.C., eds., *Lectures in isotope geology*: New York, Springer Verlag, P. 154-169.
- Nyman, M.W., Karlstrom, K.E., Kirby, E., and Graubard, C.M., 1994, Mesoproterozoic contractional orogeny in western North America: evidence from ca. 1.4 Ga plutons: *Geology*, v. 22, p. 901-904.
- Parsons, I., Brown, W.L., and Smith, J.V., 1999, $^{40}\text{Ar}/^{39}\text{Ar}$ thermochronology using alkali feldspars: real thermal history or mathematical mirage of microtexture?: *Contributions to Mineralogy and Petrology*, v. 136, p. 92-110.
- Passchier, C.W., and Trouw, R.A.J., 1996, *Microtectonics*: Berlin, Springer Verlag.
- Paterson, S.R., Vernon, R.H., and Tobisch, O.T., 1989, A review of criteria for the identification of magmatic and tectonic foliations in granitoids: *Journal of Structural Geology*, v. 11, n. 3, p. 349-363.
- Pedrick, J.N., Karlstrom, K.E., and Bowring, S.A., 1998, Reconciliation of conflicting tectonic models for Proterozoic rocks of northern New Mexico: *Journal of Metamorphic Geology*, v. 16, p. 687-707.
- Pollock, T.R., 1994, Evidence for the relative timing and character of Proterozoic deformation and metamorphism in the Ladron Mountains, New Mexico: Socorro, New Mexico Institute of Mining and Technology, 69 pgs.
- Pryer, L.L., 1993, Microstructures in feldspars from a major crustal thrust zone: the Grenville Front, Ontario, Canada: *Journal of Structural Geology*, v. 15, p. 21-36.
- Quidelleur, X., Grove, M., Lovera, O.M., Harrison, T.M., Yin, A., and Ryerson, F. J., 1997, Thermal evolution and slip history of the Renbu Zedong Thrust, southeastern Tibet: *Journal of Geophysical Research 'B'*, v. 102, n. 2, p. 2659-2679.
- Ralser, S., 2000, Microstructural constraints on the timing of Proterozoic deformation in central New Mexico: *Journal of Metamorphic Petrology*, v.18, p. 457-466.
- Read, A.S., Karlstrom, K.E., Grambling, J.A., Bowring, S.A., Heizler, M., and Daniel, C., 1999, A middle crustal cross-section from the Rincon Range, northern New Mexico: Evidence for 1.68-Ga, pluton-influenced tectonism and 1.4-Ga regional metamorphism: *Rocky Mountain Geology*, v. 34, p. 67-91.
- Read, C.B., and Wood Jr., G.H., 1947, Distribution and correlation of Pennsylvanian rocks in late Paleozoic sedimentary basins of northern New Mexico: *Journal of Geology*, v. 55, p. 220-236.
- Reed, J.C., Bickford, M.E., Premo, W.R., Aleinikoff, J.N., and Pallister, J.S., 1987, Evolution of the Early Proterozoic Colorado province: Constraints from U-Pb geochronology: *Geology*, v. 15, p. 861-865.
- Richter, F.M., Lovera, O.M., Harrison, T.M., and Copeland, P., 1991, Tibetan tectonics from $^{40}\text{Ar}/^{39}\text{Ar}$ analysis of a single K-feldspar sample: *Earth and Planetary Science Letters*, v. 105, p. 266-278.

- Riesmeyer, W.D., 1978, Precambrian geology and ore deposits of the Pecos mining district, San Miguel and Santa Fe counties, New Mexico: MS Thesis, Albuquerque, University of New Mexico, 215 pgs.
- Robertson, J.M., and Condie, K.C., 1989, Geology and geochemistry of early Proterozoic volcanic and subvolcanic rocks of the Pecos greenstone belt, Sangre de Cristo Mountains, New Mexico, in Grambling, J.A., and Tewksbury, B.J., eds., Proterozoic Geology of the southern Rocky Mountains, Volume 235: Special Paper: Boulder, CO., Geological Society of America, p. 119-146.
- Robertson, J.M., Grambling, J.A., Mawer, C.K., Bowring, S.A., Williams, M.L., Bauer, P.W., and Silver, L.T., 1993, Precambrian geology of New Mexico, in Reed, J.C., Bickford, M.E., Houston, R.S., Link, P.K., Rankin, D.W., Sims, P.K., and Van Schmus, W.R., eds., Precambrian: Conterminous U. S., Volume C-2: Decade of North American Geology: Boulder, Colorado, The Geological Society of America, p. 228-238.
- Robertson, J.M., and Moench, R.H., 1979, The Pecos greenstone belt: A Proterozoic volcano-sedimentary sequence in the southern Sangre de Cristo Mountains, New Mexico, New Mexico Geological Society 30th Field Conference, Volume 30, New Mexico Geological Society, p. 165-173.
- Samson, S.D., and Alexander Jr., E.C., 1987, Calibration of the interlaboratory $^{40}\text{Ar}/^{39}\text{Ar}$ dating standard, Mmhb-1: Chemical Geology, v. 66, p. 27-34.
- Silverstone, J., Hodgins, M., Shaw, C., Aleinikoff, J.N., and Fanning, C.M., 1997, Proterozoic tectonics of the northern Colorado Front Range, in Bolyard, D.W., and Sonnenberg, S.A., eds., Geologic history of the Colorado Front Range: Denver, Rocky Mountain Association of Geologists, 1997 Guidebook, p. 9-18.
- Sibson, R.H., 1977, Fault rocks and fault mechanisms: Journal of the Geological Society of London, v. 133, p. 191-213.
- Simpson, C., 1985, Deformation of granitic rocks across the brittle-ductile transition: Journal of Structural Geology, v. 7, n. 5, p. 503-511.
- Simpson, C., and Wintsch, R.P., 1989, Evidence for deformation-induced K-feldspar replacement by myrmekite: Journal of Metamorphic Geology, v. 7, p. 261-275.
- Spear, F.S., 1993, Metamorphic phase equilibria and Pressure-Temperature-Time paths: Washington, D.C., Mineralogical Society of America, 799 pgs.
- Stacey, J.S., Doe, B.R., Silver, L.T., and Zartman, R.E., 1976, Plumbotectonics IIA, Precambrian Massive Sulfide Deposits: USGS Open-File Report 76-476.
- Sutherland, P.K., 1963a, Paleozoic Rocks, in Miller, J.P., Montgomery, A., and Sutherland, P.K., eds., Geology of Part of the southern Sangre de Cristo Mountains, New Mexico, Memoir 11: Socorro, New Mexico Bureau of Mines and Mineral Resources, p. 22-46.
- Sutherland, P.K., 1963b, Laramide Orogeny, in Miller, J.P., Montgomery, A., and Sutherland, P.K., eds., Geology of Part of the southern Sangre de Cristo Mountains, New Mexico, Memoir 11: Socorro, New Mexico Bureau of Mines and Mineral Resources, p. 47-49.
- Taylor, S.R., 1982, Planetary Science: A lunar perspective: Houston, Lunar and Planetary Institute.

- Tikoff, B., and Greene, D., 1997, Stretching lineations in transpressional shear zones: an example from the Sierra Nevada Batholith, California: *Journal of Structural Geology*, v. 19, p. 29-39.
- Timmons, M.J., Karlstrom, K.E., Dehler, C.M., Geissman, J.W., and Heizler, M.T., 2000, Proterozoic multistage (1.1 and 0.8 Ga) extension in the Grand Canyon Supergroup and establishment of northwest and north-south tectonic grains in the southwestern United States: *Geological Society of America Bulletin*, in press.
- Urai, J., Means, W.D., and Lister, G.S., 1986, Dynamic recrystallization of minerals, in Heard, H.C., and Hobbs, B.E., eds., *Mineral and rock deformation: laboratory studies, the Paterson volume*, Volume 36: *Geophysical Monographs*: Washington, D. C., American Geophysical Union, p. 161-200.
- Vernon, R.H., 1991, Questions about myrmekite in deformed rocks: *Journal of Structural Geology*, v. 13, n. 9, p. 979-985.
- Vollbrecht, K.M., 1997, Constraints on the timing and character of Proterozoic deformation and metamorphism in the San Andres Mountains of south-central New Mexico: Socorro, New Mexico Institute of Mining and Technology, 74 pgs.
- Warnock, A.C., and Zeitler, P.K., 1998, $^{40}\text{Ar}/^{39}\text{Ar}$ thermochronometry of K-feldspar from the KTB borehole, Germany: *Earth and Planetary Science Letters*, v. 158, p. 67-79.
- White, S.H., 1976, The effect of strain on the microstructures, fabrics, and deformation mechanisms in quartzites: *Philosophical Transactions of the Royal Society of London A*, v. 283, p. 69-86.
- Williams, M.L., 1991, Heterogeneous deformation in a ductile fold-thrust belt: The Proterozoic structural history of the Tusas Mountains, New Mexico: *Geological Society of America Bulletin*, v. 103, n. 2, p. 171-188.
- Williams, M.L., Karlstrom, K.E., Lanzirotti, A., Read, A.S., Bishop, J.L., Lombardi, C.E., Pedrick, J.N., and Wingsted, M.B., 1999a, New Mexico middle-crustal cross sections: 1.65-Ga macroscopic geometry, 1.4-Ga thermal structure, and continued problems in understanding crustal evolution: *Rocky Mountain Geology*, v. 34, p. 53-66.
- Williams, M.L., Jercinovic, M.J., and Terry, M.P., 1999b, Age mapping and dating of monazite on the electron microprobe: Deconvoluting multistage tectonic histories: *Geology*, v. 27, p. 1023-1026.
- Williams, M.L., and Karlstrom, K.E., 1996, Looping P-T paths and high-T, low-P middle crustal metamorphism: Proterozoic evolution of the southwestern United States: *Geology*, v. 24, p. 1119-1122.
- Wingsted, M., Williams, M., and Lanzirotti, A., 1996, Timing constraints on porphyroblast growth and fabric development in the southern Picuris Range, north central New Mexico: Implications for the protracted tectonic/thermal evolution of the middle crust: *GSA Abstracts with Programs*, v. 28, p. A-495.
- Yavuz, F., 1999, A revised program for microprobe-derived amphibole analyses using IMA rules: *Computers & Geoscience*, v. 25, p. 909-927.
- Ye, H., Royden, L., Burchfiel, C., and Schuepbach, M., 1996, Late Paleozoic deformation of interior North America: The greater Ancestral Rocky Mountains: *AAPG Bulletin*, v. 80, p. 1397-1432.

APPENDIX A
THIN SECTION DESCRIPTIONS

RP-28B Pecos granodiorite

Mineral	Mode	<1mm	1-5mm	>5mm	Pre	Syn	Post	Grain shape	Comments
Plagioclase	35			x			x	Euhedral	
Quartz	25	x					x		
K-spar	15	x					x		
Biotite	15	x					x	Clusters, anhedral	Incl. Qtz, ep., ap.
Epidote	2	x-x					x		
Chlorite	3	x					x	Alteration of biotite	along cleavage
Other	5						x		

Equigranular, and granoblastic fabric in an unfoliated, slightly altered granitoid. Biotite crystals are slightly bent perpendicular to their cleavage planes.

RP-23A Quartz-tourmaline amphibolite

Mineral	Mode	<1mm	1-5mm	>5mm	Pre	Syn	Post	Grain shape	Comments
Quartz	35		x				x	Anhedral	Late
Plagioclase	30	x				x			
B-G amphibole	23	x-x				x			
Tourmaline	7		x				x	Euhedral	Incomplete crystals
Sphene	5	x				x			

Clustered rafts of amphiboles, sphene and plagioclase in an equigranular matrix of injected (?) quartz. Unaligned, the amphibole appears broken up and has undulose extinction. Big crystals consist of a aggregate of smaller crystals. Tourmaline is well dispersed, and has perfect hexagonal form.

RP-99 Windy Bridge tonalite mylonite

Mineral	Mode	<1mm	1-5mm	>5mm	Pre	Syn	Post	Grain shape	Comments
Plagioclase	35				x				
Quartz	30				x			Strongly elongate	
Biotite	15	x				x	x	Elongate	clusters not altered
Epidote	trace						x		
Tourmaline	trace						x	Euhedral, sep. as hb.	has no argon
Oxides	5	x					?		

The porphyroclasts and the quartz ribbons are outlined by biotite, which is not always parallel to the foliation. Epidote is euhedral. Plagioclase is broken perpendicular to the foliation, the break filled by biotite. Quartz in quartz ribbons has aspect ratios of 5:1 and a good shape preferred orientation. In other places the quartz is recrystallized.

RP-40 yz Altered tonalite mylonite

Mineral	Mode	<1mm	1-5mm	>5mm	Pre	Syn	Post	Grain shape	Comments
Plagioclase	30	x							
Quartz	40		x						
K-Spar	10	x						Euhedral	Rxn from Bt.
Biotite	13	x				x		Altered, anhedral	Incl. Qtz, ep., ap.
Chlorite	2	x				x		Alteration of biotite	along cleavage
Epidote	3	x			x				
Other	2								

Mylonitized tonalite with good compositional layering of honey-yellow biotite and porphyroclasts of plagioclase as well as ribbons of quartz. Inclusions of quartz are common in the biotite. Biotite is locally altered to chlorite and epidote. Chlorite is bent into the foliation. K-feldspar is a reaction product of biotite and quartz, also yielding chlorite and epidote.

RP-87 Biotite-muscovite-K-feldspar mylonite (Macho Creek granite)

Mineral	Mode	<1mm	1-5mm	>5mm	Pre	Syn	Post	Grain shape	Comments
Plagioclase	15	x			x				Fractured
Quartz	35		x		x	x		CPO, euhedral	Fractured
K-Spar	30	x			x			Euhedral	Myrmekite
Biotite	5	x				x		Euhedral	Alt. on Musc.
Chlorite	3	small						Alteration	Alt. on Bt.
Muscovite	7	x				x		Elongate	WM
Epidote	2	small						Alteration	Late
Garnet	2	x			?				
Other	1	x				?		Euhedral	Ilmenite?

Broken garnet with a reaction rim of muscovite and biotite in K-feldspar-rich two-mica granite-gneiss. Muscovite is in general reacting to biotite; both have undulose extinction and both have intergrown chlorite among cleavage planes. Spectacular subgrain development in quartz. These subgrains differ in orientation due to the near perfect hypidiomorphic granitoid grain distribution. Quartz also forms incipient myrmekites in potassium feldspars, which have no preferred orientation. K-feldspar possesses flame perthites. Muscovite and biotite are aligned parallel to and cut across the foliation.

WB-6 unfoliated Indian Creek granite

Mineral	Mode	<1mm	1-5mm	>5mm	Pre	Syn	Post	Grain shape	Comments
Plagioclase	10			x	x			subhedral	recrystallized
K-spar	40			x	x			some megacrysts	brittle fractures
Quartz	30	x			x			ribbons/subgrains	
Biotite	10	x			x			blocky; euhedral	
Epidote	5	x			x				
White mica	2	x			x				
Garnet	2	x			x				
Oxides	trace				x			square and six-sided	

Altered granite, with ratty outlines of garnet, oxides rimmed by white mica, and embayed perthitic K-feldspar. K-feldspar locally has flame perthites, neocrystals at grain edges, and brittle fractures with extension. Inclusions of biotite in recrystallized quartz. Sample is sausseritized.

RP-90

altered, Windy Bridge tonalite mylonite

Mineral	Mode	<1mm	1-5mm	>5mm	Pre	Syn	Post	Grain shape	Comments
Plagioclase	20	x					x	subhedral	altered
K-feldspar	20	x					x	impossible to tell without staining	
Quartz	40	x				x		foam texture	some elongate
Chlorite	10	x					x	euhedral	well dispersed
Epidote	5	x					x	nice hexagonal crystals	
Titanite	5	x				x		euhedral and round	
Biotite	trace	x				x		out	
Oxides	trace	x				x			

Altered, mylonitized Windy Bridge tonalite with kinked quartz ribbons and well defined compositional layering. Within these ribbons quartz has 1:5 aspect ratios. In the matrix quartz is small, pinned among feldspars and possesses a grain-shape preferred orientation. Non-aligned chlorite forms reaction rims on matrix epidote. Titanite has a reaction rim of epidote. Traces of biotite as faint smudges now pseudomorphed to chlorite. Vein epidote is pervasive; crystals are

RP-86B

Macho Creek granite mylonite

Mineral	Mode	<1mm	1-5mm	>5mm	Pre	Syn	Post	Grain shape	Comments
Plagioclase	20	x					x	euhedral	
K-spar	40	x---	x		x	x		anhedral	
Quartz	20	x					x	euhedral	recrystallized
Biotite	10	x			x			euhedral	
Muscovite	5	x			x			-	
Oxides	5					x		broken	extended

K-feldspar has a grain shape preferred orientation. Outlines of some megacrysts are recognizable, though most are mechanically broken. Plagioclase is all recrystallized, as is the quartz, having the largest grain size overall. Biotite defines irregular shearbands around the feldspar domains.

RP-83

unfoliated Macho Creek granite

Mineral	Mode	<1mm	1-5mm	>5mm	Pre	Syn	Post	Grain shape	Comments
Plagioclase	20		x		x			euhedral	sericitized
K-spar	30	x			x			anhedral	neocrystals
Quartz	30	x-	x			x		bulging	
Biotite	10	x			x			euhedral	
Muscovite	5	x			x			euhedral	
Chlorite	2						x		along Bt cleavage
Sphene	5		x				?	euhedral	
Other	sparse								

Quartz crystals have bulging grain boundaries and undulose extinction, whereas biotite is kinked, and plagioclase feldspar is sausseritized. Anhedral neocrystals of K-feldspar are locally present.

RP-17 unfoliated Indian Creek granite

Mineral	Mode	<1mm	1-5mm	>5mm	Pre	Syn	Post	Grain shape	Comments
Plagioclase	25	x			x			anhedral	subgrains present
K-feldspar	25	x			x				
Quartz	35	x			x			anhedral, bulging	elongate
Biotite	7	x			x				
Chlorite	minor	x			x				Replaces biotite
Muscovite	3	x			x				
Oxides	trace				x				

Equigranular two-mica granite, with elongate strain-free quartz.

RP-44.5 Indian Creek granite

Mineral	Mode	<1mm	1-5mm	>5mm	Pre	Syn	Post	Grain shape	Comments
Plagioclase	30		x		x			anhedral, broken	kinked albite twins
K-feldspar	15		x		x			anhedral, broken	some subgrains
Quartz	40	x			x			subgrains	
Biotite	trace	x			x			replaced by chlorite	
Chlorite	5	x					x	anhedral	
Epidote	2	x					x	anhedral	on garnet, feldspar
Muscovite	5	x					?		
Other	-								Garnet outline

Sauseritized granite containing epidote reaction rims on garnet. Evidence for deformation in sample includes undulose extinction in quartz and kinked albite twins in plagioclase.

RP-54xz Indian Creek granite mylonite

Mineral	Mode	<1mm	1-5mm	>5mm	Pre	Syn	Post	Grain shape	Comments
Plagioclase	35		x		x			all subgrains	albite twins kinked
K-feldspar	10		x		x			some subgrains	recrystallized
Quartz	35	x			x			anhedral bulging	ribbons
Biotite	5	x				x			aligned
Chlorite	10	x				x		after biotite	aligned
Muscovite	3	x					x		
Epidote	1	x					x		
Iron Oxide	1						x		

Mylonitic foliation is highlighted by brown iron staining, which roughly parallel the irregular quartz ribbons. Biotite has reaction rims of chlorite and muscovite.

RP-29xz Indian Creek granite mylonite

Mineral	Mode	<1mm	1-5mm	>5mm	Pre	Syn	Post	Grain shape	Comments
Plagioclase	15	x			x			neocrystals and elongate, old crystals	
K-feldspar	35	x			x				
Quartz	35	x			x			anhedral bulging	ribbons
Biotite	trace	x				x		anhedral	aligned
Chlorite	trace	x				x		after biotite	aligned
Muscovite	5	x				x			
Oxides	trace	x				x			

Muscovite and iron oxide are parallel to the foliation, whereas plagioclase feldspar neocrystals are recrystallized and rare elongate feldspar crystals are foliation parallel.

RP-28B unfoliated Pecos granodiorite (Intermediate rock: tonalite - granite)

Mineral	Mode	<1mm	1-5mm	>5mm	Pre	Syn	Post	Grain shape	Comments
Plagioclase	35		x		x			euhedral	concentric zoning
K-feldspar	20	x			x			small anhedral	
Quartz	25	x			x			anhedral, round	
Biotite	10	x-x			x			anhedral	embayed
Epidote	5	x					x	alteration phase	
Chlorite	trace	x					x	after biotite	
Oxides	trace	x			x				reacts to biotite
Sphene	trace	x				x			broken

Biotite is present as inclusions in plagioclase feldspar, but it also impinges on the plagioclase growth, during simultaneous igneous cooling. K-feldspar has bulging grain boundaries like quartz; the two minerals are also the same size. Biotite is not aligned and has a random distribution.

RP-98 foliated Pecos granodiorite

Mineral	Mode	<1mm	1-5mm	>5mm	Pre	Syn	Post	Grain shape	Comments
Plagioclase	30	x-x			x			elongate anhedral	altered
K-feldspar	20	x-x			x			anhedral blocky	myrmekites
Quartz	30		x		x			cusped ribbons	
Biotite	10	x			x			elongate	
Chlorite	trace	x			x				
White mica	4	x			x			alteration of feldspar	
Epidote	trace	x			x				
Oxides	minsul	x			x			six-sided	

Granodiorite mylonite with quartz ribbons and a feldspar grain shape preferred orientation. K-feldspar is blocky and the plagioclase is also locally elongate and significantly altered and overgrown. K-feldspar is poikiloblastic, and include many wormy intergrowths of quartz.

RP-73xz foliated (?) Pecos granodiorite

Mineral	Mode	<1mm	1-5mm	>5mm	Pre	Syn	Post	Grain shape	Comments
Plagioclase	30	x			x				dusty; saussuritized
K-feldspar	15		x		x			core & mantle	porphyroclasts
Quartz	30	x			x			ribbons	recrystallized
Biotite	15	x			x			kinked cleavages	in clusters
Sphene	5	x			x			euhedral	reacts to biotite
Epidote	trace	x			x			euhedral	
Oxides	-								

Quartz and the biotite define the foliation. Biotite has undulose extinction, and includes kinks at the 5 micron grain scale. Subgrains are present on the K-feldspar porphyroclasts. A strong size contrast exists between plagioclase and K-feldspar, the latter also including some myrmekites.

WB-22A 1-1 Windy Bridge tonalite mylonite

Mineral	Mode	<1mm	1-5mm	>5mm	Pre	Syn	Post	Grain shape	Comments
Plagioclase	30	x				x		subhedral	altered
Quartz	35	x				x		ribbons	
Hornblende	10-15	x-x					x	euhedral	inclusions
Chlorite	15	x					x		after hornblende
Epidote	5	x					x		
Biotite	trace	x				x		brown,	or margarite?
Sphene	trace	x				?			

The mylonite has good compositional layering, with small grains of plagioclase and quartz. Chlorite appears late in the plagioclase-rich domains only, and replaces biotite in those domains. Epidote veins cross-cut the foliation. Distinct oblique foliation defined by plagioclase SPO. Some quartz ribbons are isoclinally folded into recumbent folds parallel to the main foliation.

WB-22B 1-2 Windy Bridge tonalite mylonite

Mineral	Mode	<1mm	1-5mm	>5mm	Pre	Syn	Post	Grain shape	Comments
Plagioclase	50	x				x		subhedral	altered, v. dirty
Quartz	20	x				x		elongate	highly strained
Hornblende	15	x					x	euhedral, small	inclusions
Biotite	10	x					x		after hb/epidote
Epidote	5	x					x		late alteration
Chlorite	trace	x					x		

Mylonite with folded mafic layers, which contain up to 20% amphiboles. Felsic parts are dominated by quartz ribbons, with a slight asymmetry. Individual quartz grains have undulose extinction. The amphibole is small in this rock.

WB-22C 1-1 Windy Bridge tonalite

Mineral	Mode	<1mm	1-5mm	>5mm	Pre	Syn	Post	Grain shape	Comments
Plagioclase	45	x				x		subhedral	sausseritized
Quartz	35	x				x		euhedral	
Hornblende	5	x-x					x	euhedral	
Biotite	10	x					x		
Epidote	trace	x				x		reacts to biotite	
Chlorite	trace	x					x		

Metamorphic reaction of epidote to amphibole and to biotite.

WB-23 1-1 Windy Bridge tonalite mylonite

Mineral	Mode	<1mm	1-5mm	>5mm	Pre	Syn	Post	Grain shape	Comments
Plagioclase	45	x				x		subhedral	
Quartz	40	x				x		euhedral	
Biotite	10	x					x		
Epidote	5	x				x		reacts to biotite	
Oxides	trace	x				x			

Compositional banding, with plagioclase feldspar grain SPO at a 30° angle to the main foliation. Kinematic indicators in this rock point to dextral strike slip shear. Biotite and feldspar grains share the oblique foliation, and epidote has reacted to biotite.

WB-28 A nonfoliated Windy Bridge tonalite

Mineral	Mode	<1mm	1-5mm	>5mm	Pre	Syn	Post	Grain shape	Comments
Plagioclase	40	x	x		x			euhedral	neocrystals
Quartz	40		x		x			anhedral	bulging grain edges
Biotite	10	x			x				clusters
Epidote	5	x			x				alteration
Oxides	5				x				

Recrystallized mostly coarse-grained sample with undulose extinction and bulging grain boundaries in quartz. Plagioclase has recrystallized to small crystals locally.

WB-2 nonfoliated Windy Bridge tonalite

Mineral	Mode	<1mm	1-5mm	>5mm	Pre	Syn	Post	Grain shape	Comments
Plagioclase	40	x- x			x			euohedral	igneous zoning
Quartz	40	x- x			x			anhedral	bulging grain edges
Biotite	10		x		x			euohedral	clusters
Epidote	5	x			x			euohedral, small	alteration of fldspr
Hornblende	trace		x		x				no rxn texture
Oxides	trace				x				

Hornblende (strikingly blue-green) and biotite are both present, but have a low total modal percent.

WB-5 Windy Bridge tonalite mylonite

Mineral	Mode	<1mm	1-5mm	>5mm	Pre	Syn	Post	Grain shape	Comments
Plagioclase	40	x			x				
Quartz	35	x			x			euohedral	segregated domains
Hornblende	5								
Biotite	10	x					x	euohedral	clusters
Chlorite	10	x					x	replacing Hb.	honey-brown
Epidote	trace	x				x			

Mylonite with an oblique foliation defined by plagioclase SPO. Folia defined by continuous domains of recrystallized quartz.

RP-03 nonfoliated Windy Bridge tonalite

Mineral	Mode	<1mm	1-5mm	>5mm	Pre	Syn	Post	Grain shape	Comments
Plagioclase	35	x			x			anhedral, zoned	dusty and altered
Quartz	45	x			x			recrystallized	shape pref. orient.
Amphibole	-								
Biotite	5	x			x			euohedral	random
Chlorite	5	x			x				massive
Epidote	5	x			x				unstable
White mica	2	x					x	alteration	on plagioclase
Garnet	trace	x			x				
Titanite	2	x			x				

Tonalite with a low total mafic mineral percentage, and small percentage of subgrain formation in feldspar. There is also an unspecified amount of K-feldspar.

RP-67 recrystallized Windy Bridge tonalite

Mineral	Mode	<1mm	1-5mm	>5mm	Pre	Syn	Post	Grain shape	Comments
Plagioclase	40	x			x				altered
Quartz	35	x			x			polygonal	clusters
Biotite	10	x					x		
Epidote	5	x					x	euohedral	reacts to biotite
Chlorite	trace	x					x	along bt cleavage	alteration
White mica	trace	x					x		on plagioclase

Euhedral epidote reacts to biotite, which in turn reacts to chlorite. Quartz grains are larger than plagioclase, and clusters could be recrystallized polycrystalline ribbons. Muscovite and chlorite domains along with quartz clusters have a vein-like appearance.

RP-68 foliated Windy Bridge tonalite

Mineral	Mode	<1mm	1-5mm	>5mm	Pre	Syn	Post	Grain shape	Comments
Plagioclase	40	x			x			subgrains forming	neocrystals too
Quartz	40	x			x			foam texture	veins present
Amphibole	10					x			foliation parallel
Epidote	5	x					x		alteration
Oxides	5	x			x				
Biotite	trace	x					x		
Chlorite	trace	x					x		
Garnet	trace	x					x	euohedral, pristine	in epidote clusters

Feldspar and quartz in this sample are equigranular, though there are some poikilitic plagioclase porphyroclast left. Amphibole is foliation parallel.

RP-12 Windy Bridge tonalite-gneiss

Mineral	Mode	<1mm	1-5mm	>5mm	Pre	Syn	Post	Grain shape	Comments
Plagioclase	45			x	x			anhedral, porphs	saussuritized
Quartz	25		x		x			subgrains forming	undulose extinction
Amphibole	20	x			x			tiny acicular crystals	foliation parallel
Biotite	5		x				x		alteration
Epidote	minor	x			x				
oxides	trace	x					x		

Biotite and plagioclase are present as reaction products of the retrogression of amphibole. Acicular needles outline larger amphibole crystals, and go extinct all at once.

RP-19B

Windy Bridge tonalite-gneiss

Mineral	Mode	<1mm	1-5mm	>5mm	Pre	Syn	Post	Grain shape	Comments
Plagioclase	35	x				x		neocrystals from porphs, altered	
Quartz	50	x			x			preferred orientation	
Biotite	10	x					x	euhedral, in clusters	
Chlorite	minor	x					x		
Epidote	trace	x					x		
White mica	2	x					x	alteration of feldspar	
Titanite	2		x				x	large, euhedral	
Garnet	trace	x				?		as inclusion in plagioclase porph.	

Ratty plagioclase reacting to white mica. Lots of oriented quartz is in this rock, along with large, elongate biotite clusters (up to 0.5 mm).

RP-101

altered Windy Bridge tonalite gneiss

Mineral	Mode	<1mm	1-5mm	>5mm	Pre	Syn	Post	Grain shape	Comments
Plagioclase	40	x				x		aligned, large grains	altered
Quartz	30	x					x	subhedral, recrystallized	
Chlorite	10	x					x	aligned	
Epidote	10	x					x	blocky	
Biotite	trace	x					x	faint remnants in chlorite	
Oxide	trace	x				x			extended
Titanite	trace	x				x		elongate	extended

Altered plagioclase contain inclusions of euhedral epidote. Quartz has aspect ratios of 1:4, very few subgrains and almost no undulose extinction. Biotite has all reacted to chlorite. Sphene and oxides are extended parallel to the foliation, with rifts filled by epidote. One fracture filled by epidote cross cuts the foliation.

RP-02

Windy Bridge tonalite-gneiss

Mineral	Mode	<1mm	1-5mm	>5mm	Pre	Syn	Post	Grain shape	Comments
Plagioclase	45	x			x			bulging grain boundaries	
Quartz	35	x					x	equant	
Biotite	10	x				x		bimodal grainsizes	
Amphibole	5	x				x		pristine	inclusion trails
Epidote	3	x					x		
Chlorite	trace	x					x		
Garnet	trace	x				?			

Plagioclase porphyroclasts are sausseritized. Elongate quartz inclusions in feldspar: myrmekites (?). The amphibole reacts to biotite, also involving epidote, but amphibole also grows on biotite. Epidote reacts to biotite, which in turn alters to hematite. Garnet reacts to epidote and biotite.

RP-23A Windy Bridge tonalite

Mineral	Mode	<1mm	1-5mm	>5mm	Pre	Syn	Post	Grain shape	Comments
Plagioclase	40		x				x	phenos - perthitic	altered
Quartz	30		x				x	anhedral	clusters
Amphibole	20	x					x	multi-crystal aggregates	
Tourmaline	8		x				x	sieve texture	reaction to amph.
White mica	trace	x					x	tiny	
Oxides	trace	x					x		
Zircon	a few	x					x		

Clusters of large recrystallized quartz containing crystals with undulose extinction. Plagioclase is extensively altered by white mica. Amphiboles with good cleavage are in radiating crystal clusters around some tourmalines. White mica also as reaction rim on the oxide phase.

RP-92 Windy Bridge tonalite mylonite

Mineral	Mode	<1mm	1-5mm	>5mm	Pre	Syn	Post	Grain shape	Comments
Plagioclase	40	x		x			x	rare porphyroclasts	recrystallized
K-feldspar	minor				x	?			tartan twinning
Quartz	30	x					x	foam texture	some ribbons
Biotite	10	x					x		clusters
Amphibole	5	x					x	multi-crystal aggregates	
Epidote	minor	x					x	euhedral	
Chlorite	5		x				x	sieve texture	reaction to amph.
Oxides	trace	x			x			squares	

Good SPO in recrystallized plagioclase feldspar. Large remnant porphyroclasts show brittle extension parallel to the foliation. K-feldspar is distinct; and are perthitic. Quartz ribbons are kinked. Amphiboles appear distinctly in the plagioclase feldspar domains but are randomly oriented. Minor reaction rims of chlorite on amphibole. Amphibole has tiny needles of biotite as inclusions. The epidote - biotite assemblage is stable.

RP-49-2 Windy Bridge tonalite-gneiss

Mineral	Mode	<1mm	1-5mm	>5mm	Pre	Syn	Post	Grain shape	Comments
Plagioclase	65	x					x		recrystallized
K-feldspar	trace	x					x	some bigger crystals	recrystallized
Quartz	25	x					x	foam texture	few ribbons
Biotite	5	x					x	blocky and elongate	clusters
White mica	trace	x					x		alteration
Epidote	trace	x					x	euhedral	
Titanite	trace	x					x	anhedral	deformed

Thin section has wavy foliation (folds), defined by fractured quartz ribbons. Biotite orientation is random and biotite is present as inclusions in some of the recrystallized quartz. Epidote reaction rims are present on titanite.

RP-99

Windy Bridge tonalite mylonite

Mineral	Mode	<1mm	1-5mm	>5mm	Pre	Syn	Post	Grain shape	Comments
Plagioclase	40	x	x			x		anhedral porphs.	with subgrains
Quartz	40	x				x		foam texture	recrystallized
Biotite	10	x				x		elongate	clusters with plag
Epidote	5	x					x	euhedral	sausseritization
Chlorite	minor	x					x	along folia	alteration on biotite
Oxides	trace	x					x	cubic, hexagonal too	
Zircon	trace	x			x				

Good core and mantle structures are present in, now sausseritized, feldspars. Minor chlorite replacement on biotite. Well developed S-C structures give a dextral shear sense. SPO in quartz (S-surfaces), whereas biotite defines the C-surfaces (main foliation).

RP-4

Windy Bridge tonalite mylonite

Mineral	Mode	<1mm	1-5mm	>5mm	Pre	Syn	Post	Grain shape	Comments
Plagioclase	35	x				x		anhedral	recrystallized
Quartz	45	x				x		anhedral, deformed	ribbons
Biotite	10	x				x		defines foliation	fine grained
Amphibole	3	x					x	euhedral	sieve texture
Epidote	2	x					x		
Chlorite	2	x					x		
Garnet	trace	x				?			

Amphibole, with inclusions of quartz, reacts to chlorite and epidote. Epidote inclusions are present in plagioclase feldspar. Biotite has intragrain cataclasis as observed by brown-yellow thick lines along cleavage planes. Section has interfolial folds and transposed fold noses.

RP-11

Windy Bridge tonalite mylonite

Mineral	Mode	<1mm	1-5mm	>5mm	Pre	Syn	Post	Grain shape	Comments
Plagioclase	50	x				x		anhedral, some cores	recrystallized
Quartz	30	x					x	elongate	recrystallized
Biotite	10	x				x		elongate	
Chlorite	5	x				x		long, undulose	deformed
White mica	2	x					x	subhedral	in plagioclase
Epidote	2	x				x		euhedral, broken	
Titanite	trace	x				x		elongate	
Garnet	trace				x			anhedral	segmented, pristine
Oxides	trace	x			x			square	react to bt./chl.

Sphene has a reaction rim of epidote, which in turn has a reaction rim of biotite. Locally biotite is replaced by chlorite. Some feldspar is brittlely deformed. Dextral kinematic indicators are present, e.g. recrystallized quartz around a feldspar porphyroclast. Foliation is defined by biotite flakes. This sample has good examples of feldspar cores surrounded by recrystallized subgrains.

RP-55

amphibolite

Mineral	Mode	<1mm	1-5mm	>5mm	Pre	Syn	Post	Grain shape	Comments
Plagioclase	50	x			x			anhedral	igneous zoning
Quartz	10	x			x			blocky	
Amphibole	15		x		x			euhedral, prismatic	in clusters
Biotite	10	x			x			elongate	random orientation
Epidote	5	x					x	on plag/titanite	alteration
Titanite	5	x			x			globular/anhedral	
Oxides	trace								

Plagioclase has been sausseritized and preserves igneous zoning. Some amphiboles have their cleavage planes occupied by biotite. In places the titanite is pristine in others it appears broken and is partially replaced by biotite or epidote.

RP-93

amphibolite mylonite

Mineral	Mode	<1mm	1-5mm	>5mm	Pre	Syn	Post	Grain shape	Comments
Plagioclase	25	x					x	blocky	some subgrains
Quartz	10	x					x	foam texture	in clusters
Amphibole	40	x				x		acicular	
Biotite	5	x				x		blocky	not aligned
Epidote	5	x					x	irregular	alteration
Chlorite	10	x				x		radiating/elongate	
Oxides	trace				x			irregular	
Garnet	trace		x		x			euhedral	poikilitic

Foliation is defined by thick, tightly interwoven aggregates of acicular amphiboles. Quartz occurs in sometimes sinuous veins or clusters. Epidote veins crosscut all foliation. Garnet grows in clusters in the feldspar-rich domains and reacts to chlorite. Conjugate shearbands in the chlorite are well developed. Oxides are common in the amphibole domains.

WB-10

amphibolite mylonite

Mineral	Mode	<1mm	1-5mm	>5mm	Pre	Syn	Post	Grain shape	Comments
Plagioclase	40		x			x		blocky	recrystallized
Quartz	30		x			x		elongate	
Amphibole	25		x			x		acicular	
White mica	trace						x	blocky	not aligned
Oxides	trace				x			irregular	alteration

Compositional layering defined by alternating quartz-plagioclase domains and amphibole domains. Plagioclase is very dusty and has altered to white mica. Megacrystic, relict, albite twins have hypidiomorphic, interlocking textures. Quartz has a strong CPO at 25° to the angle of the main foliation. Randomly oriented quartz inclusions are present in the amphiboles.

RP-105 amphibolite mylonite

Mineral	Mode	<1mm	1-5mm	>5mm	Pre	Syn	Post	Grain shape	Comments
Plagioclase	20	x				x		small blocky	recrystallized
Quartz	30	x				x		anhedral, folded	1:10 aspect ratios
Amphibole	35	x				x		largest, acicular	
Biotite	5	x				x			
Chlorite	5	x					x	irregular	alteration on biotite
Epidote	trace	x					x	massive and acicular	
Oxides	trace	x			x				

Compositional banding defined by one amphibole domain. Most acicular amphiboles are found in the isoclinal fold the length of the thin section. Amphiboles are smaller in the quartz-feldspathic domains. Quartz has bulging grain boundaries.

RP-69 chlorite schist

Mineral	Mode	<1mm	1-5mm	>5mm	Pre	Syn	Post	Grain shape	Comments
Quartz	50	x				x	x	undulose, irregular	full of inclusions
Chlorite	40	x				x		elongate, radial	alteration of biotite
Biotite	5	x				x		small, tabular	titaniferous clusters
Epidote	trace	x					x		with vein quartz
Oxides	trace	x							

Biotite has reaction rims of chlorite. The rest and most of the thin-section is chlorite and quartz.

RP-88 chlorite schist

Mineral	Mode	<1mm	1-5mm	>5mm	Pre	Syn	Post	Grain shape	Comments
Quartz	55	x				x		amoeboid/ anhedral	undulose
Chlorite	15	x				x		elongate	
Muscovite	15	x			x				few
Biotite	5	x				x		euhedral	pristine
Andalusite	5			x	x	x			parallel inclusions
Oxides	5	x			x				

Very small biotite present as small inclusions in andalusite, which is breaking down to biotite and quartz. Quartz grain size and shape is determined by interspersed phyllosilicates.

RP-80

Muscovite-biotite-quartz-plagioclase mylonite

Mineral	Mode	<1mm	1-5mm	>5mm	Pre	Syn	Post	Grain shape	Comments
Plagioclase	45	x				x			recrystallized
Quartz	20	x				x		elongate/anhedral	
Biotite	15	x				x		elongate	strained
Muscovite	15	x				x		clusters	strained
Chlorite	trace	x				x			alteration
Garnet	trace	x			x				strained
Oxides	5	x			x				

Mylonite with a well developed compositional layering is now defined by biotite and muscovite populations parallel to the foliation. Q-F domains fill in the interstices, where feldspar forms the S-surfaces. One mantled, orthorhombic porphyroclast of plagioclase is remaining. The rest of the feldspar is recrystallized. Some recrystallized quartz ribbons have rims of biotite. Biotite forms some reaction rims on muscovite. Muscovite is preferentially present in feldspar domains (original heterogeneity?) and parallels the S-surfaces. Some recrystallized quartz ribbons have rims of biotite. Internal foliation in garnet is seemingly concordant to exterior foliation.

RP-86A

Quartz-chlorite schist

Mineral	Mode	<1mm	1-5mm	>5mm	Pre	Syn	Post	Grain shape	Comments
Quartz	65	x				x		good preferred shape	
Chlorite	15	x				x		aligned/clusters	alteration on biotite
Muscovite	10	x				x		elongate fish	two populations?
Biotite	5	x				x		broken, altered	with rutile needles
K-feldspar	trace	x				x		with quartz included	reacts to muscovite
Oxides	trace	x			x				iron oxide, red stain

Quartz is locally large, but amoeboid and mostly fine-grained and recrystallized. Chlorite shows shear band foliation, and has undulose extinction. Muscovite mica fish show dextral sense of shear.

APPENDIX B. ⁴⁰Ar/³⁹Ar DATA

ID	Temp (°C)	⁴⁰ Ar/ ³⁹ Ar	³⁷ Ar/ ³⁹ Ar	³⁶ Ar/ ³⁹ Ar (x 10 ⁻³)	³⁹ Ar _K (x 10 ⁻¹⁵ mol)	K/Ca	Cl/K (x 10 ⁻³)	⁴⁰ Ar* (%)	³⁹ Ar (%)	Age (Ma)	±1s (Ma)
----	--------------	------------------------------------	------------------------------------	---	--	------	-------------------------------	--------------------------	-------------------------	-------------	-------------

WB 10 Hornblende, wt. = 0.74 mg, J=0.008106, NM-84, Lab#=8841-01

A	635	76.21	1.228	248.1	0.995	0.42	561.1	3.9	11.6	43	21						
B	710	43.30	1.201	97.68	0.219	0.42	487.7	33.5	14.2	201	65						
C	760	50.69	1.077	137.5	0.119	0.47	348.5	20.0	15.6	142	120						
D	860	56.17	3.070	89.08	0.538	0.17	180.6	53.5	21.8	394	24						
E	930	105.8	9.261	31.81	0.633	0.055	175.8	91.8	29.2	1054	14						
F	990	128.6	10.99	11.55	1.74	0.046	127.3	98.0	49.6	1277.9	5.9						
G	1030	126.1	10.46	20.98	0.947	0.049	144.8	95.8	60.6	1238.8	9.4						
H	1070	131.0	10.70	44.91	0.623	0.048	5254.9	90.5	67.9	1222	13						
I	1110	132.0	12.05	8.144	1.69	0.042	210.1	98.9	87.6	1310.9	5.2						
J	1210	136.0	11.91	23.68	0.988	0.043	288.3	95.6	99.2	1306.7	8.5						
K	1310	199.1	11.41	272.6	0.071	0.045	999.2	60.0	100.0	1229	114						
total gas age										n=11	8.57	0.11	1020	14			
plateau										MSWD=0.33	n=3	steps I-K	8.57	0.11	100.0	1309.6	5.1*

WB 23 Hornblende, wt. = 2.15 mg, J=0.008105, NM-84, Lab#=8842-01

A	510	78.40	1.746	241.2	0.607	0.29	719.0	9.2	2.5	103	28						
B	635	56.71	1.591	75.30	0.289	0.32	653.2	60.9	3.7	446	39						
C	710	76.72	1.857	71.76	0.135	0.27	554.9	72.5	4.3	672	73						
D	760	88.19	2.524	102.0	0.159	0.20	389.0	66.0	4.9	698	62						
E	860	103.4	5.097	44.39	0.519	0.10	189.5	87.7	7.1	997	17						
F	930	134.0	6.904	9.283	1.97	0.074	83.0	98.4	15.2	1316.1	4.8						
G	990	141.6	6.597	5.960	7.19	0.077	44.5	99.1	45.0	1375.7	2.6						
H	1030	138.8	6.779	8.782	3.07	0.075	50.3	98.5	57.7	1350.8	3.6						
I	1070	132.5	5.802	25.51	0.617	0.088	5735.9	94.7	60.2	1269	13						
J	1110	141.9	6.674	6.632	6.35	0.076	105.8	99.0	86.5	1376.5	2.2						
K	1210	143.5	7.396	7.778	3.25	0.069	60.5	98.8	100.0	1385.7	3.3						
total gas age										n=11	24.2	0.086	1306.9	5.2			
plateau										MSWD=18.9	n=4	steps G,H,J,K	24.2	0.086	100.0	1374	12

WB 15B Hornblende, wt. = 0.77 mg, J=0.008102, NM-84, Lab#=8844-01

D	760	192.3	11.81	473.8	0.023	0.043	46.6	27.7	0.4	653	503						
E	860	93.42	13.38	37.72	0.084	0.038	50.7	89.2	1.8	939	109						
F	930	131.8	14.67	58.40	0.204	0.035	61.4	87.8	5.2	1203	41						
G	990	140.3	14.86	8.330	3.09	0.034	89.7	99.1	56.6	1372.4	3.8						
H	1030	142.0	13.78	26.24	0.442	0.037	87.1	95.3	63.9	1345	19						
I	1070	138.8	15.31	17.03	0.339	0.033	86.4	97.3	69.5	1345	24						
J	1110	144.6	15.04	18.82	0.510	0.034	94.8	97.0	78.0	1381	17						
K	1210	142.9	14.97	13.51	1.21	0.034	93.6	98.1	98.2	1379.5	7.8						
L	1310	166.1	17.47	53.63	0.110	0.029	124.9	91.3	100.0	1459	74						
total gas age										n=9	6.01	0.034	1358	14			
plateau										MSWD=1.15	n=6	steps G-L	6.01	0.034	100.0	1371.4	6.5*

RP-36B Biotite, wt. = 0.30 mg, J=0.01545, NM-102, Lab#=50025-01

A	600	55.95	0.5825	150.5	0.611	0.88	220.9	20.6	0.8	295	69						
B	700	21.13	0.0787	9.212	9.36	6.5	63.9	87.0	13.2	451.2	3.5						
C	800	68.85	0.0257	8.647	5.20	19.8	21.6	96.3	20.1	1272.1	5.0						
D	870	75.29	0.0272	5.616	7.62	18.7	31.3	97.8	30.2	1370.4	3.8						
E	950	77.40	0.1060	6.289	6.84	4.8	38.8	97.6	39.3	1395.3	4.0						
F	1025	79.75	0.0649	5.726	11.5	7.9	26.5	97.9	54.5	1427.2	3.2						
G	1060	80.66	0.0229	7.383	10.2	22.2	21.2	97.3	68.0	1432.6	3.4						
H	1130	78.24	0.0245	4.728	15.7	20.8	634.3	98.2	88.8	1411.8	2.8						
I	1160	82.40	0.0726	15.87	4.37	7.0	129.8	94.3	94.6	1422.9	5.8						
J	1200	78.08	0.2624	23.32	3.31	1.9	19.0	91.2	99.0	1338.7	7.6						
K	1250	103.6	0.4137	91.53	0.743	1.2	11.4	73.9	100.0	1409	37						
total gas age										n=11	75.4	13.6	1270.8	4.5			
plateau										MSWD=8.63	n=4	steps F-I	75.4	13.6	100.0	1422	10*

ID	Temp (°C)	⁴⁰ Ar/ ³⁹ Ar	³⁷ Ar/ ³⁹ Ar	³⁶ Ar/ ³⁹ Ar (x 10 ⁻³)	³⁹ Ar _K (x 10 ⁻¹⁵ mol)	K/Ca	Cl/K (x 10 ⁻³)	⁴⁰ Ar* (%)	³⁹ Ar (%)	Age (Ma)	±1s (Ma)
----	--------------	------------------------------------	------------------------------------	---	--	------	-------------------------------	--------------------------	-------------------------	-------------	-------------

RP-28B Biotite, wt. = 0.64 mg, J=0.01543, NM-102, Lab#=50027-01

A	600	35.14	0.8062	24.02	4.00	0.63	157.1	79.9	1.9	649.7	7.1
B	700	60.43	0.1309	5.108	11.9	3.9	43.1	97.5	7.7	1166.2	2.7
C	800	70.76	0.0223	1.442	30.0	22.8	17.7	99.4	22.2	1325.2	2.1
D	870	71.90	0.0218	0.7106	35.0	23.4	16.7	99.7	39.1	1343.2	2.2
E	950	72.04	0.0269	1.182	26.4	19.0	20.3	99.5	51.9	1343.3	2.1
F	1025	72.30	0.0183	1.611	40.0	27.8	15.3	99.3	71.3	1345.0	2.2
G	1060	71.36	0.0193	2.027	21.3	26.4	16.8	99.1	81.5	1330.9	2.7
H	1130	71.89	0.0688	1.469	26.2	7.4	436.7	99.4	94.2	1340.2	2.1
I	1160	73.13	0.4570	3.659	7.86	1.1	298.7	98.5	98.0	1348.8	3.6
J	1200	76.18	1.176	15.76	2.19	0.43	71.0	94.0	99.1	1343	10
K	1250	77.40	0.4898	20.51	1.94	1.0	32.4	92.2	100.0	1339	12
total gas age			n=11		206.7	19.0				1315.9	2.4
plateau		MSWD=2.95	n=9	steps C-K	206.7	19.0			100.0	1341.8	3.3*

RP-87 Muscovite, wt. = 0.80 mg, J=0.01550, NM-102, Lab#=50028-02

B	600	25.44	1.206	29.83	0.932	0.42	269.1	65.6	0.2	416	30
C	650	42.70	0.5211	-15.0311	0.103	0.98	223.3	110.4	0.3	990	209
D	725	59.07	0.1755	14.36	4.72	2.9	86.8	92.8	1.5	1109.5	5.3
E	775	61.62	0.0178	2.479	8.47	28.7	14.9	98.8	3.7	1198.6	3.3
F	825	61.49	0.0091	1.584	16.0	56.0	6.3	99.2	7.7	1200.5	2.4
G	850	61.36	0.0049	0.9055	19.5	105.0	4.9	99.5	12.7	1201.5	2.5
H	875	61.58	0.0032	0.7140	12.7	159.0	4.5	99.6	16.0	1205.4	2.7
I	925	64.57	0.0022	0.3954	80.3	232.2	1.7	99.8	36.6	1249.1	2.5
J	960	62.16	0.0027	0.4703	52.7	185.9	2.8	99.7	50.1	1214.7	2.2
K	1000	62.69	0.0024	0.5126	43.5	216.0	3.6	99.7	61.3	1222.1	2.5
L	1060	64.88	0.0025	0.2567	63.4	204.1	2.0	99.8	77.5	1254.0	2.6
M	1150	65.92	0.0038	0.6317	40.6	135.9	208.7	99.7	88.0	1266.9	2.2
N	1250	64.43	0.0155	2.259	12.9	33.0	15.5	98.9	91.3	1239.4	2.8
O	1600	65.03	0.0646	3.461	34.0	7.9	2.2	98.4	100.0	1243.0	2.2
total gas age			n=14		389.7	159.6				1232.6	2.5
plateau		MSWD=97.71	n=11	steps E-O	389.7	159.6			100.0	1229	15*

RP-34 Muscovite, wt. = 0.80 mg, J=0.01540, NM-102, Lab#=50030-01

B	600	76.52	0.2338	28.59	1.59	2.2	116.3	89.0	0.4	1294	15
C	650	75.16	0.0586	12.65	1.96	8.7	52.9	95.0	0.8	1338	12
D	725	74.48	0.0242	4.592	10.7	21.1	16.8	98.1	3.2	1360.8	3.0
E	775	73.05	0.0098	1.604	19.1	52.1	6.2	99.3	7.5	1353.6	2.7
F	825	72.32	0.0049	0.7402	33.2	104.3	3.7	99.7	15.0	1347.4	2.4
G	850	72.09	0.0035	0.4020	35.4	144.6	3.1	99.8	23.0	1345.6	2.3
H	875	72.20	0.0033	0.3625	35.6	155.5	2.8	99.8	31.1	1347.3	2.3
I	925	72.12	0.0023	0.2172	79.7	221.1	1.6	99.9	49.0	1346.8	2.5
J	960	71.62	0.0025	0.2855	56.4	207.7	2.4	99.8	61.8	1339.9	3.0
K	1000	72.09	0.0018	0.2790	49.8	280.9	2.1	99.8	73.0	1346.1	2.2
L	1060	71.92	0.0017	0.3575	64.3	304.0	1.3	99.8	87.5	1343.5	2.4
M	1150	71.92	0.0042	0.4914	49.7	121.7	176.3	99.8	98.7	1343.1	2.4
N	1250	57.85	0.0370	3.916	5.59	13.8	14.7	98.0	100.0	1132.1	4.7
total gas age			n=13		443.1	190.4				1342.6	2.4
plateau		MSWD=0.93	n=8	steps F-M	443.1	190.4			100.0	1345.2	1.7*

Isotopic ratios corrected for blank, radioactive decay, and mass discrimination, not corrected for interfering reactions.

Individual analyses show analytical error only; mean age errors also include error in J and irradiation parameters.

n = number of heating steps

K/Ca = molar ratio calculated from reactor produced ³⁹Ar_K/³⁷Ar_{Ca}

Correction factors:

$$(^{39}\text{Ar}/^{37}\text{Ar})_{\text{Ca}} = 0.00077 \pm 0.00002$$

$$(^{36}\text{Ar}/^{37}\text{Ar})_{\text{Ca}} = 0.00028 \pm 0.00000$$

$$(^{38}\text{Ar}/^{39}\text{Ar})_{\text{K}} = 0.0119$$

$$(^{40}\text{Ar}/^{39}\text{Ar})_{\text{K}} = 0.0262 \pm 0.0001$$

* = includes error at the 95% confidence level

ID	Temp (°C)	⁴⁰ Ar/ ³⁹ Ar	³⁷ Ar/ ³⁹ Ar	³⁶ Ar/ ³⁹ Ar (x 10 ⁻³)	³⁹ Ar _K (x 10 ⁻¹⁵ mol)	K/Ca	⁴⁰ Ar* (%)	³⁹ Ar (%)	Age (Ma)	±1s (Ma)
RP-87 K-feldspar, wt. = 1.80 mg, J=0.01533, NM-102, Lab#=50039-02										
A	450	68.93	0.0069	71.68	3.71	74.1	69.2	0.4	990.5	5.5
B	450	10.68	0.0045	12.46	1.32	114.1	65.3	0.5	183.2	5.7
C	500	6.846	0.0072	2.528	2.22	70.4	88.7	0.8	160.6	3.1
D	500	4.732	0.0060	2.939	2.32	85.3	81.1	1.0	103.2	3.2
E	550	4.953	0.0000	0.7097	4.28	-	95.2	1.5	126.0	1.5
F	550	4.001	0.0004	1.525	4.59	1368.4	88.1	2.0	94.9	1.4
G	600	4.470	0.0017	0.7009	8.86	295.1	94.8	2.9	113.53	0.81
H	600	5.228	0.0021	2.147	7.77	242.6	87.4	3.7	122.1	1.0
I	650	7.061	0.0026	1.180	11.4	193.4	94.7	4.9	176.05	0.76
J	650	8.675	0.0042	1.094	9.40	120.7	96.0	5.9	216.71	0.87
K	700	13.38	0.0041	0.9750	11.8	124.6	97.7	7.2	329.37	0.92
L	700	15.12	0.0050	1.984	7.90	101.3	96.0	8.0	362.4	1.2
M	750	20.69	0.0034	1.003	5.09	148.6	98.4	8.6	490.3	1.7
N	800	26.52	0.0056	1.805	10.1	91.8	97.9	9.7	604.4	1.5
O	850	35.48	0.0068	0.4932	15.1	75.1	99.5	11.3	780.4	1.6
P	900	43.22	0.0083	0.4377	20.5	61.7	99.6	13.5	914.6	1.5
Q	950	44.80	0.0072	0.3165	28.8	70.5	99.7	16.5	941.3	1.9
R	1000	46.07	0.0076	0.3476	35.7	67.5	99.7	20.3	961.8	1.7
S	1050	48.19	0.0033	0.1752	42.2	155.6	99.8	24.8	996.7	1.8
T	1100	48.92	0.0035	0.2241	52.7	146.6	99.8	30.4	1008.1	2.4
U	1100	49.88	0.0027	0.2827	75.3	189.3	99.8	38.4	1023.0	2.0
V	1100	50.84	0.0027	0.5959	80.1	189.1	99.6	46.9	1036.5	1.7
W	1100	50.35	0.0029	1.181	69.7	177.4	99.3	54.3	1026.2	1.9
X	1100	50.02	0.0045	2.223	65.6	113.0	98.6	61.3	1016.2	1.9
Y	1100	48.90	0.0024	3.591	37.8	216.2	97.8	65.3	992.0	2.0
Z	1100	48.22	0.0018	5.732	49.9	280.2	96.4	70.6	970.8	1.8
ZA	1280	45.63	0.0011	0.2350	137.0	476.8	99.8	85.2	955.2	2.4
ZB	1330	47.34	0.0010	0.2884	77.4	503.0	99.8	93.5	982.7	2.2
ZC	1430	47.43	0.0010	0.8679	21.2	518.2	99.4	95.7	981.3	1.7
ZD	1530	45.61	0.0013	1.155	29.6	383.2	99.2	98.9	950.5	1.6
ZE	1650	49.37	0.0021	5.209	10.7	240.5	96.8	100.0	991.8	2.0
total gas age			n=31		940.3	257.0			919.7	1.8
plateau			n=31	steps A-ZE	940.3	257.0		100.0	503	69

ID	Temp (°C)	⁴⁰ Ar/ ³⁹ Ar	³⁷ Ar/ ³⁹ Ar	³⁶ Ar/ ³⁹ Ar (x 10 ⁻³)	³⁹ Ar _K (x 10 ⁻¹⁵ mol)	K/Ca	⁴⁰ Ar* (%)	³⁹ Ar (%)	Age (Ma)	±1s (Ma)
RP-70 K-feldspar, wt. = 1.70 mg, J=0.01537, NM-102, Lab#=50041-01										
A	450	748.0	0.0218	56.63	1.93	23.4	97.8	0.1	4518.0	10.9
B	450	59.86	0.0095	31.14	0.559	53.6	84.6	0.2	1038.2	13.2
C	500	243.9	0.0217	18.04	1.31	23.5	97.8	0.3	2778.8	8.5
D	500	65.04	0.0078	7.791	1.34	65.3	96.4	0.4	1217.3	6.0
E	550	271.9	0.0076	11.06	3.24	67.2	98.8	0.6	2948.7	6.1
F	550	34.95	0.0050	2.419	3.75	101.4	97.9	0.9	762.0	2.7
G	600	108.6	0.0075	4.171	9.53	68.1	98.8	1.7	1757.4	3.2
H	600	30.73	0.0066	1.584	7.19	76.8	98.4	2.2	688.4	1.9
I	650	46.99	0.0067	1.085	13.6	75.7	99.3	3.3	974.9	1.8
J	650	35.82	0.0058	1.194	12.4	87.4	98.9	4.2	784.4	1.6
K	700	48.07	0.0058	0.9263	20.7	88.5	99.4	5.8	993.0	1.9
L	700	38.48	0.0053	0.9344	20.6	95.7	99.2	7.4	832.8	1.9
M	750	51.02	0.0061	1.157	15.8	83.5	99.3	8.6	1038.5	1.9
N	800	47.47	0.0058	0.5884	32.6	87.5	99.6	11.1	985.0	1.6
O	850	44.08	0.0049	0.1749	44.8	103.4	99.8	14.5	931.7	1.7
P	900	42.11	0.0052	0.2390	46.8	98.1	99.8	18.1	898.6	1.7
Q	950	42.03	0.0051	0.1946	47.4	99.6	99.8	21.8	897.5	1.4
R	1000	42.25	0.0057	0.2875	50.3	89.0	99.7	25.6	900.6	1.5
S	1050	42.92	0.0056	0.2517	53.2	90.4	99.8	29.7	912.1	1.5
T	1100	43.93	0.0063	0.3550	65.3	81.5	99.7	34.7	928.3	1.6
U	1100	45.76	0.0044	0.5181	90.3	114.7	99.6	41.6	957.7	2.2
V	1100	47.65	0.0057	0.7827	99.1	89.6	99.5	49.2	987.0	2.1
W	1100	49.38	0.0053	1.325	88.4	97.1	99.2	56.0	1012.0	2.1
X	1100	51.74	0.0040	2.182	77.3	127.1	98.7	62.0	1045.0	1.8
Y	1100	55.61	0.0029	3.303	69.0	176.7	98.2	67.3	1099.2	1.9
Z	1230	59.59	0.0111	0.4997	31.2	45.8	99.7	69.7	1170.2	1.8
ZA	1280	59.01	0.0042	0.2841	85.5	121.8	99.8	76.2	1162.7	2.4
ZB	1330	59.68	0.0019	0.2437	199.0	269.2	99.8	91.5	1172.5	2.6
ZC	1430	59.51	0.0020	0.3853	51.3	258.3	99.8	95.4	1169.5	2.0
ZD	1530	60.69	0.0019	0.4782	51.4	264.6	99.7	99.4	1186.2	2.0
ZE	1650	63.91	0.0018	7.641	8.28	285.0	96.4	100.0	1201.9	2.4
total gas age			n=31		1303.1	142.0			1050.7	1.9
plateau			n=31	steps A-ZE	1303.1	142.0		100.0	1000	44

ID	Temp (°C)	⁴⁰ Ar/ ³⁹ Ar	³⁷ Ar/ ³⁹ Ar	³⁶ Ar/ ³⁹ Ar (x 10 ⁻³)	³⁹ Ar _K (x 10 ⁻¹⁵ mol)	K/Ca	⁴⁰ Ar* (%)	³⁹ Ar (%)	Age (Ma)	±1s (Ma)
WB-6 K-feldspar, wt. = 3.48 mg, J=0.008099, NM-84, Lab#=8847-01										
A	500	419.6	0.0145	77.31	5.91	35.2	94.5	0.5	2594.6	3.7
B	500	52.49	0.0073	6.701	4.61	70.0	96.2	1.0	618.4	1.8
C	550	63.05	0.0073	3.244	6.24	70.0	98.4	1.6	734.6	1.7
D	550	53.31	0.0072	2.615	8.74	71.3	98.5	2.4	639.3	1.4
E	600	64.50	0.0073	1.727	16.6	70.4	99.2	3.9	753.0	1.8
F	600	62.99	0.0059	1.287	16.2	85.8	99.4	5.4	739.7	1.2
G	650	69.52	0.0069	1.101	26.6	73.8	99.5	7.9	802.5	1.0
H	650	70.42	0.0062	1.041	25.3	81.7	99.5	10.2	811.0	1.5
I	700	74.50	0.0071	0.7880	38.5	72.3	99.7	13.8	849.3	1.7
J	700	74.89	0.0061	0.6868	31.6	83.2	99.7	16.7	853.1	1.6
K	750	76.18	0.0075	0.5216	36.0	67.9	99.8	20.0	865.3	1.6
L	800	77.47	0.0093	0.6095	54.2	54.7	99.7	25.0	876.8	1.7
M	850	78.41	0.0117	0.4982	60.2	43.4	99.8	30.6	885.5	1.7
N	900	79.74	0.0126	0.5677	54.2	40.4	99.8	35.6	897.2	1.7
O	950	80.16	0.0122	0.5240	47.1	41.8	99.8	40.0	900.9	1.9
P	1000	80.29	0.0119	0.8496	42.4	42.7	99.7	43.9	901.3	1.8
Q	1050	82.81	0.0174	1.409	50.2	29.4	99.5	48.6	922.1	1.7
R	1100	87.37	0.0263	2.292	50.6	19.4	99.2	53.2	959.4	1.5
S	1100	89.19	0.0312	3.265	66.9	16.4	98.9	59.4	972.4	1.7
T	1100	88.38	0.0218	2.886	83.6	23.4	99.0	67.2	966.5	1.7
U	1100	90.28	0.0127	3.087	97.8	40.1	99.0	76.2	982.1	2.1
V	1100	92.83	0.0063	3.930	104.4	81.2	98.7	85.9	1001.5	2.0
W	1100	93.93	0.0025	6.820	63.2	201.5	97.8	91.7	1003.6	1.5
X	1200	96.78	0.0015	1.613	40.6	346.5	99.5	95.5	1040.0	1.5
Y	1250	98.25	0.0014	2.000	37.6	363.0	99.4	98.9	1051.1	1.7
Z	1300	47.76	0.0027	2.205	11.4	190.9	98.6	100.0	582.8	1.2
total gas age			n=26		1080.7	81.5			933.4	1.7
plateau			n=26	steps A-Z	1080.7	81.5		100.0	865	41

ID	Temp (°C)	$^{40}\text{Ar}/^{39}\text{Ar}$	$^{37}\text{Ar}/^{39}\text{Ar}$	$^{36}\text{Ar}/^{39}\text{Ar}$ ($\times 10^{-3}$)	$^{39}\text{Ar}_k$ ($\times 10^{-15}$ mol)	K/Ca	$^{40}\text{Ar}^*$ (%)	^{39}Ar (%)	Age (Ma)	$\pm 1\sigma$ (Ma)
RP-90 K-feldspar, wt. = 1.30 mg, J=0.01533, NM-102, Lab#=50035-01										
A	450	42.9762	0.0070	77.6209	2.124	72.93	46.6	0.3	482.8	8.0
B	450	18.2834	0.0000	16.3059	1.581	-	73.5	0.5	338.0	4.8
C	500	16.8260	0.0000	6.8719	2.669	-	87.8	0.9	368.2	2.6
D	500	17.3488	0.0000	4.4805	3.832	-	92.2	1.5	395.8	2.0
E	550	21.4474	0.0044	2.5422	7.213	115.99	96.4	2.5	496.7	1.3
F	550	24.1664	0.0014	2.1262	8.380	373.24	97.3	3.8	555.4	1.3
G	600	28.2614	0.0075	1.5813	12.343	67.69	98.3	5.6	639.9	1.2
H	600	30.1981	0.0049	1.6555	10.590	104.80	98.3	7.1	676.7	1.4
I	650	32.6451	0.0067	1.5610	12.261	75.76	98.5	8.9	723.1	1.3
J	650	32.9197	0.0052	1.7246	7.258	97.96	98.4	10.0	727.3	1.5
K	700	33.5588	0.0166	1.6846	9.187	30.67	98.4	11.3	739.3	1.4
L	700	33.4945	0.0082	2.4252	6.656	62.58	97.8	12.3	734.1	1.6
M	750	33.0774	0.0139	2.1221	7.033	36.83	98.0	13.3	728.1	1.4
N	750	33.3320	0.0114	2.7120	5.866	44.69	97.5	14.2	729.5	2.0
O	800	32.9738	0.0125	3.0659	3.023	40.82	97.2	14.6	721.0	2.6
P	850	32.9958	0.0500	3.0119	7.755	10.20	97.2	15.7	721.8	1.5
Q	900	32.6923	0.0789	1.8305	12.287	6.46	98.3	17.5	722.7	1.3
R	950	32.0035	0.0515	1.6017	15.692	9.91	98.5	19.8	711.1	1.2
S	1000	31.4276	0.0222	1.7932	20.861	22.99	98.2	22.9	699.2	1.3
T	1050	30.7528	0.0246	2.7843	39.965	20.75	97.2	28.7	680.9	1.3
U	1100	31.9793	0.0377	3.7410	37.747	13.55	96.5	34.2	698.8	1.6
V	1100	32.8599	0.0358	3.1437	100.625	14.27	97.1	48.9	718.5	1.7
W	1100	33.6540	0.0191	1.8044	132.929	26.72	98.3	68.3	740.4	3.8
X	1100	34.4740	0.0086	1.8163	115.403	59.08	98.4	85.1	755.3	1.6
Y	1100	36.3769	0.0061	3.1414	67.720	83.13	97.4	95.0	782.6	1.6
Z	1100	41.1635	1.1255	14.8384	19.589	0.45	89.5	97.9	808.5	2.6
ZA	1200	36.5984	0.0000	3.5520	3.880	-	97.1	98.5	784.4	2.5
ZB	1300	35.5746	0.0000	3.5745	5.201	-	97.0	99.2	765.9	2.0
ZC	1350	35.9738	0.0000	6.9229	2.626	-	94.2	99.6	755.1	2.8
ZD	1400	38.8756	0.0000	13.3459	2.223	-	89.8	99.9	773.3	3.8
ZE	1650	796.1337	0.0000	2550.8700	0.503	-	5.3	100.0	902	187
total gas age			n=31		685.023	42.28			724.77	2.14
plateau			n=31	steps A-ZE	685.023	42.28		100.0	685	16

ID	Temp (°C)	⁴⁰ Ar/ ³⁹ Ar	³⁷ Ar/ ³⁹ Ar	³⁶ Ar/ ³⁹ Ar (x 10 ⁻³)	³⁹ Ar _K (x 10 ⁻¹⁵ mol)	K/Ca	⁴⁰ Ar* (%)	³⁹ Ar (%)	Age (Ma)	±1s (Ma)
RP-34 K-feldspar, wt. = 2.00 mg, J=0.01539, NM-102, Lab#=50033-01										
A	450	85.14	0.0019	45.54	9.85	272.8	84.2	0.7	1340.9	3.1
B	450	21.57	0.0017	12.17	3.65	295.2	83.2	0.9	440.0	2.8
C	500	21.30	0.0010	2.715	7.89	533.3	96.1	1.5	494.2	1.4
D	500	12.74	0.0012	1.797	8.97	416.8	95.6	2.1	310.1	1.1
E	550	26.91	0.0013	1.392	28.4	385.3	98.4	4.1	616.6	1.3
F	550	14.98	0.0012	0.3451	28.2	415.3	99.1	6.0	371.46	0.73
G	600	20.41	0.0014	0.3676	41.1	352.0	99.3	8.9	490.06	0.92
H	600	20.94	0.0008	0.5498	25.6	669.9	99.1	10.6	500.0	1.0
I	650	27.18	0.0013	0.6986	40.2	407.3	99.1	13.4	625.9	1.2
J	650	27.84	0.0008	0.3161	30.2	606.2	99.6	15.5	641.0	1.3
K	700	34.79	0.0014	0.8838	31.9	370.7	99.2	17.7	768.5	1.6
L	700	32.37	0.0003	0.7642	21.7	1494.1	99.2	19.2	724.7	1.4
M	750	37.61	0.0017	1.146	11.7	307.2	99.0	20.0	817.5	1.7
N	800	41.68	0.0023	1.618	22.7	225.5	98.8	21.6	885.6	1.5
O	850	40.42	0.0022	1.748	26.3	228.3	98.7	23.4	863.3	1.5
P	900	37.53	0.0028	1.219	29.3	185.4	99.0	25.5	815.6	1.6
Q	950	37.12	0.0028	1.493	33.9	184.5	98.7	27.8	806.9	1.3
R	1000	37.15	0.0029	1.100	37.3	173.1	99.1	30.4	809.6	1.5
S	1050	38.28	0.0029	0.6715	48.2	173.4	99.4	33.7	831.7	1.7
T	1100	39.36	0.0029	0.9219	64.8	176.4	99.2	38.2	849.2	2.1
U	1100	41.52	0.0024	0.9599	95.8	213.8	99.3	44.9	886.2	1.5
V	1100	42.84	0.0024	1.064	87.4	210.3	99.2	50.9	907.8	1.9
W	1100	43.75	0.0022	1.500	78.4	231.6	98.9	56.4	920.9	2.2
X	1100	45.22	0.0017	2.222	86.1	301.5	98.5	62.3	941.8	1.7
Y	1100	46.70	0.0011	4.133	73.9	459.4	97.3	67.4	956.8	2.1
Z	1230	47.24	0.0015	0.9604	62.8	336.9	99.3	71.8	980.8	2.2
ZA	1280	47.73	0.0014	0.9314	295.8	363.7	99.4	92.3	988.8	1.7
ZB	1330	49.93	0.0014	0.9799	96.5	354.9	99.4	99.0	1023.6	1.7
ZC	1430	48.18	0.0033	2.313	14.6	153.6	98.5	100.0	989.5	2.0
total gas age			n=29		1443.2	332.4			867.3	1.6
plateau			n=29	steps A-ZC	1443.2	332.4		100.0	676	42

ID	Temp (°C)	⁴⁰ Ar/ ³⁹ Ar	³⁷ Ar/ ³⁹ Ar	³⁶ Ar/ ³⁹ Ar (x 10 ⁻³)	³⁹ Ar _K (x 10 ⁻¹⁵ mol)	K/Ca	⁴⁰ Ar* (%)	³⁹ Ar (%)	Age (Ma)	±1σ (Ma)
RP-40B K-feldspar, wt. = 1.34 mg, J=0.01531, NM-102, Lab#=50036-01										
AA	450	76.7474	0.0441	72.6079	4.621	11.57	72.0	0.4	1106.0	4.4
BB	450	19.9880	0.0246	9.6761	3.105	20.72	85.6	0.7	419.6	3.0
CC	500	22.3366	0.0172	3.0672	5.771	29.65	95.8	1.3	511.3	1.7
D	500	22.3185	0.0137	1.6310	8.072	37.20	97.7	2.0	519.8	1.5
E	550	30.4429	0.0196	2.1079	7.867	25.97	97.9	2.8	677.9	1.6
F	550	28.7866	0.0159	1.3652	12.035	32.18	98.5	3.9	650.4	1.3
G	600	33.9670	0.0163	1.2247	14.881	31.28	98.9	5.3	748.3	1.7
H	600	35.1913	0.0181	0.8360	17.591	28.14	99.2	7.0	772.6	1.3
I	650	38.1870	0.0165	0.6590	23.241	30.93	99.4	9.1	826.6	1.9
J	650	39.6526	0.0159	0.7365	22.108	32.01	99.4	11.2	851.6	1.4
K	700	40.6648	0.0162	0.4766	24.091	31.51	99.6	13.5	870.3	1.4
L	700	41.2684	0.0131	0.8626	27.233	38.94	99.3	16.1	878.6	1.4
M	750	41.8919	0.0159	0.4456	28.041	32.05	99.6	18.7	891.2	1.5
N	750	42.4056	0.0170	0.5742	26.046	29.98	99.5	21.1	899.2	1.4
O	800	42.6601	0.0248	0.3092	14.062	20.55	99.7	22.5	904.8	2.1
P	850	43.0329	0.0213	0.2401	27.222	23.91	99.8	25.0	911.4	1.3
Q	900	43.3640	0.0232	0.2305	34.352	22.03	99.8	28.3	916.9	1.7
R	950	42.9697	0.0184	0.3099	37.619	27.77	99.7	31.8	910.0	1.3
S	1000	42.7231	0.0164	0.3061	42.596	31.14	99.7	35.8	905.9	1.8
T	1050	42.5731	0.0263	0.5846	45.148	19.40	99.5	40.1	902.0	1.8
U	1100	43.7629	0.0391	1.1122	37.533	13.06	99.2	43.6	919.3	1.5
V	1100	44.1109	0.0345	0.9920	74.153	14.80	99.3	50.6	925.6	2.1
W	1100	45.4955	0.0228	1.0524	85.604	22.38	99.3	58.6	948.1	1.5
X	1100	48.5755	0.0084	0.9784	128.189	61.04	99.4	70.7	998.0	5.7
Y	1100	51.3519	0.0053	1.3785	131.814	95.58	99.2	83.1	1039.7	5.3
Z	1100	52.8334	0.0042	2.4500	62.784	120.62	98.6	89.0	1057.7	1.8
ZA	1200	50.4576	0.0104	0.8550	15.161	49.03	99.4	90.4	1028.2	2.0
ZB	1300	50.7112	0.0046	0.9356	45.425	110.04	99.4	94.7	1031.8	2.0
ZC	1350	51.5888	0.0088	1.5328	14.138	57.72	99.1	96.0	1042.7	1.7
ZD	1400	53.3675	0.0088	1.2986	21.271	57.79	99.2	98.0	1071.1	1.7
ZE	1650	54.4643	0.0064	18.1632	20.869	79.82	90.1	100.0	1010.8	2.0
total gas age			n=31		1062.641	49.84			943.0	2.5
plateau			n=31	steps AA-ZE	1062.641	49.84		100.0	863	26

Isotopic ratios corrected for blank, radioactive decay, and mass discrimination, not corrected for interfering reactions.
 Individual analyses show analytical error only; mean age errors also include error in J and irradiation parameters.
 n = number of heating steps
 K/Ca = molar ratio calculated from reactor produced ³⁹Ar/³⁷Ar_{Ca}

Correction factors:

$$(^{39}\text{Ar}/^{37}\text{Ar})_{\text{Ca}} = 0.00077 \pm 0.00002$$

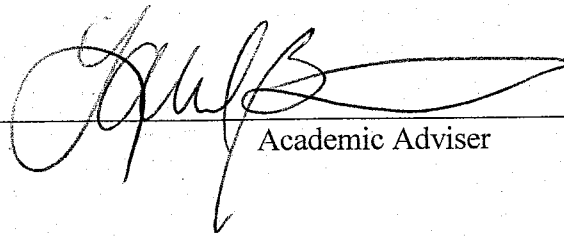
$$(^{36}\text{Ar}/^{37}\text{Ar})_{\text{Ca}} = 0.00028 \pm 0.00000$$

$$(^{38}\text{Ar}/^{39}\text{Ar})_{\text{K}} = 0.0119$$

$$(^{40}\text{Ar}/^{39}\text{Ar})_{\text{K}} = 0.0262 \pm 0.0001$$

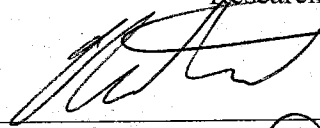
Committee
sign off
sheet

This Thesis is accepted on behalf of the faculty
of the Institute by the following committee:

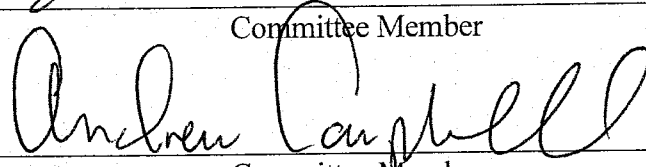


Academic Adviser

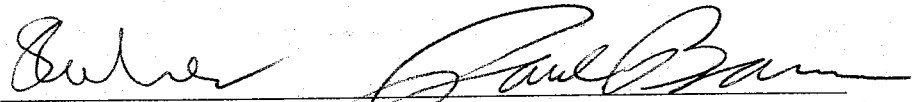
Research Advisor



Committee Member



Committee Member



Committee Member

December 12, 2000

Date